UNIVERSIDADE DE ÉVORA

ESCOLA DE CIÊNCIAS E TECNOLOGIA

DEPARTAMENTO DE QUÍMICA

Reductive dechlorination of TCE and *cis*-DCE by zero-valent iron and iron-based bimetallic reductants

Sofia Margarida Pires Ribeiro

Orientação: Doutor Martin Elsner

Co-orientação: Prof. Doutor António Teixeira

Mestrado em Química

Área de especialização: *Química Orgânica*

Dissertação

Évora, 2016

UNIVERSIDADE DE ÉVORA

ESCOLA DE CIÊNCIAS E TECNOLOGIA

DEPARTAMENTO DE QUÍMICA

Reductive dechlorination of TCE and *cis*-DCE by zero-valent iron and iron-based bimetallic reductants

Sofia Margarida Pires Ribeiro

Orientação: Doutor Martin Elsner

Co-orientação: Prof. Doutor António Teixeira

Mestrado em Química

Área de especialização: *Química Orgânica*

Dissertação

Évora, 2016

Acknowledgement

First of all, I would like to thank to the Helmholtz Zentrum München and especially to Doutor Martin Elsner, supervisor of this work, for accepting me to work at the Institute of Groundwater Ecology, providing me essential materials and equipment for the realization of this study. I would like also to thank to Doutor Martin Elsner for allowing me to be a part of his group, for the trust, support and knowledge imparted. Also thanks to Benjamin Heckel for all the help, support, dedication and effort that put in me and for the knowledge imparted.

Thanks to Prof. Doutor António Teixeira, also supervisor of this work, for the dedication, support and availability given during the course of the work, especially when I was abroad.

Thanks to Prof. Doutora Manuela Carrott for the support along all the process of the mobility.

Thanks to all my colleagues for availability given and somehow helped and supported me.

Thanks to my grandparents, parents and brother for the support, at all levels.

Also thanks to my friends for helping me somehow, for the friendship, the big support, company and complicity, especially to Joana Candeias, and Alexandre Brito, Ana Mourato, Inês Mavioso and Maria Cordeiro.

Table of contents

List of figures

List of tables

Abstract

CEs are the most frequently detected pollutants in groundwater. Several studies have been shown iron-based bimetallic reductants as a good method toward to chlorinated ethylenes degradation. However, many fundamental issues surrounding the chemistry of this phenomena remains elusive.

In this study, kinetics and compound specific isotope analysis for reductive dechlorination of TCE and *cis*-DCE by unamended iron and iron-based bimetal reductants was evaluated. Generally, all the bimetals reductants tested revealed to increase the reactivity of the degradation, in which palladium and nickel were the additional metals more reactive. Ethene and ethane were the major products of TCE degradation.

It is supported the simultaneous hydrogenolysis and β-elimination reaction hypothesis, however, the first step of TCE degradation by Au/Fe undergoes preferably by β-elimination, while by unamended iron, Pt/Fe and Co/Fe goes preferably by hydrogenolysis. No apparent elucidation was obtained to explain the high reactivity on bimetals systems.

Keywords: Chlorinated ethylenes, reductive dechlorination, bimetallic reductant, zero-valent iron, 2D-CSIA.

Degradação do TCE e *cis*-DCE por ferro de valência zero e redutores bimetálicos à base de ferro

Resumo

Etilenos clorados são os poluentes mais frequentemente detetados na água subterrânea. Vários estudos têm mostrado que redutores bimetálicos à base de ferro são um bom método para a degradação dos etilenos clorados. Porém, muitas questões fundamentais acerca da química deste fenómeno permanecem elusivas.

Neste estudo foi avaliada a cinética e a análise isotópica de compostos específicos para a degradação do TCE e *cis*-DCE por ferro e redutores bimetálicos à base de ferro. Genericamente, os redutores bimetálicos mostraram aumentar a reatividade da degradação, sendo paládio e níquel os metais adicionais mais reativos. Os produtos principais da degradação do TCE foram eteno e etano.

É apoiada a hipótese da simultaneidade de hidrogenólise e β-eliminação, porém, o primeiro passo da degradação do TCE por Au/Fe é realizada preferencialmente por β-eliminação, enquanto por ferro, Pt/Fe e Co/Fe é realizada preferencialmente por hidrogenólise. Não houve uma elucidação aparente para explicar a reatividade nos sistemas bimetálicos.

Palavras-chave: Etilenos clorados, descloração redutiva, redutores bimetálicos, ferro de valência zero, 2D-CSIA.

Acronyms and Abbreviations

AAS - Atomic Absorption Spectroscopy

AES - Auger Electron Spectroscopy

AKIE – Apparent Kinetic Isotope Effect

BET - Brunauer–Emmett–Teller

CE – Chlorinated ethylenes

CERCLA – Comprehensive Environmental Response and Compensation Liability Act

CSIA – Compound Specific Isotope Analysis

DCE – Dichloroethylene

DCM - Dichloromethane

DNAPL – Dense Non-Aqueous Phase Liquid

EPA – Environmental Protection Agency

Eq. – equation

FID - Flame Ionization Detector

GC – Gas Chromatography

GCxGC - two dimensional Gas Chromatography

HPLC - High Performance Liquid Chromatography

HTC – High Temperature Conversion

IRMS – Isotope Ratio Mass Spectrometer

KIE – Kinetic Isotope Effect

LC – Liquid Chromatography

MS - Mass Spectrometer

nZVI – nano Zero Valent Iron

P&T – Purge and Trap

PCE – Perchloroethylene

PRB – Permeable Reactive Barriers

RPC - Reversed Phase Chromatography

SEM-EDS - Scanning Electron Microscopy in conjunction with Energy Dispersive X-ray Spectroscopy

TCA - Trichloroethane

TCE – Trichloroethylene

TEM - Transmission Electron Microscopy

VC – Vinyl Chloride

WHO – World Health Organization

XPS - X-ray Photoelectron Spectroscopy

ZVI – Zero Valent Iron

ZVM – Zero Valent Metal

1. Introduction

1.1. Environmental problems

In the last decades, environmental problems have become a matter of great concern. Throughout history, after the industrialization and urbanization, concerns over air and water pollution started being faced as significant problems that could be sprawled over other conditions (as deforestation, pesticide contamination, declining animal populations and species) [1].

Nowadays the environmental problems are globalized as a result of the socioeconomic forces and the existence and impact that were responsible to cause them [1]. Some of the global issues that have been highlighted over the recent years are: acid deposition, air pollution, climate change, drinking water pollution, environmental effects and toxicology, global warming and the greenhouse effect, groundwater pollution, ozone depletion and heavy metals and their toxicology [2]. In this study the focus will be on the groundwater pollution.

1.1.1. Groundwater pollution

Groundwater pollution is one of the biggest issues of concern since groundwater play three major roles in the environment: i) it is an important source of drinking water and can be used for industrial, irrigation and spraying purposes, especially when water supplies are not available, ii) it is responsible to keep the river water quality through dilution sewage and other effluents, and iii) it maintain the base flow that preserves most rivers flowing along all the year. Groundwater is a natural reservoir of high-quality water due to the purification properties of the soils and when polluted can restrict and/or prevent the normal use of the groundwater [3, 4].

Usually, the groundwater pollution is owing to: industrial, domestic, agricultural and environmental pollution [4, 5]. In industrial pollution, it is due to waters that have in its constitution trace elements and chemical compounds, also rain infiltrating through waste disposals and storage tanks that can have chemicals or other pollutants that over the time develop leaks. Relatively to domestic pollution, the septic systems used can lead to problems since it can dropout contaminants when handled improperly, and also due to uncontrolled

hazardous waste sites, wherein rain infiltrating through sanitary landfills play a big role. In agricultural pollution, owing to the irrigation water that transfer the fertilizers, minerals, salts, pesticides and herbicides in the soil which eventually ends up in the water. Finally, in environmental pollution, and as the groundwater also belongs to the hydrologic cycle, contaminants present in the atmosphere can be transferred into groundwater supplies and also due to seawater intrusion in coastal aquifers [4, 5] (figure 1).

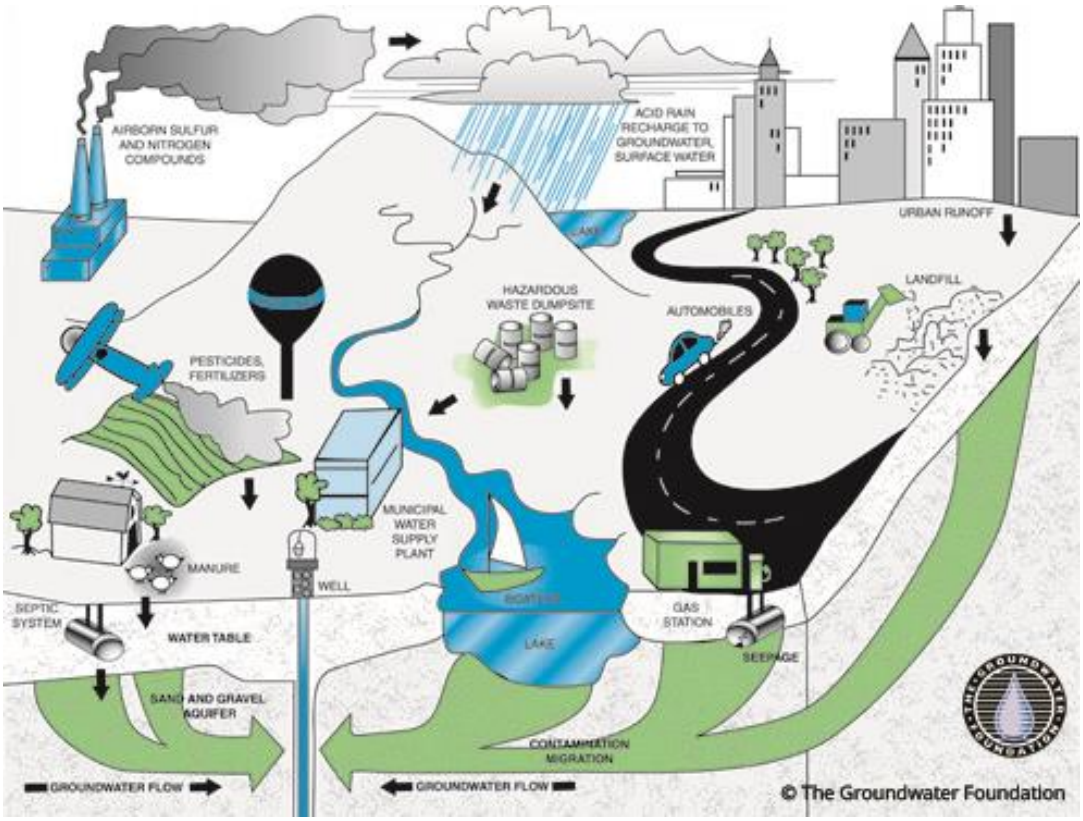

Figure 1: Schematics of groundwater contamination sources [5].

1.1.2. Groundwater and Pollutants

Besides the groundwater pollutants that, nowadays, concern the most of human health, it can be divided in some categories: microbiological, nutrients, pesticides, fuel-related chemicals, industrial chemicals, heavy metals and novel pollutants [3].

Microbiological pollutants are originated from human and animal faeces through sewer leaks, manure disposal and septic tanks which are the source of bacterial and viral diseases

(*e.g. cholera*) and can be the cause of severe human health and sometimes death. For that reason they are the groundwater pollutants of human health most concern. Relatively to nutrients pollutants, the concern is focused on nitrate pollution. Mostly diffused by agriculture wherein it is used in various forms of nitrogen, as inorganic and organic fertilizers, it is responsible to cause changes related to aquatic ecosystems (*as eutrophication*) [3]. Pesticides, such as atrazine, bentazone and isoproturon, have been detected at trace concentrations for a considerable period. The biggest problem are the pesticide metabolites and reaction products formed that are biologically active, which may also be toxic and are detected in higher concentrations than the parent compounds. Due to its greatest threat to the environment, many of them are now banned and were also gradually withdrawn [6].

As reported above, areas where a diverse array of chemicals, i.e., fuel-related chemicals (*petroleum hydrocarbons*), industrials chemicals (*chlorinated solvents*), heavy chemicals (*As, Zn, Pb, Cr)* and novel pollutants (*pharmaceutical and personal care products*) are processed by society, the groundwater becomes contaminated in greater or lesser extent. Therefore, pollutants environmental fate and potential toxicity have become subject of a big interest in the past decades [7]. The most common pollutants detected, in these cases, are mobile and do not attenuate in the surface, like petroleum hydrocarbons (*such as benzene and toluene*) and chlorinated hydrocarbons (*e.g. TCE*), and are also detected owing to some degradation products formed [3, 6]. Consequently, these compounds are classed as priority pollutants [6].

So far regulations have been implemented maximum allowable concentrations of pollutants in water. The World Health Organization (WHO) is responsible to produce international norms in the form of guidelines for water quality and human health [8]. In the USA the maximum allowable concentrations are regulated by the Environmental Protection Agency (EPA) and it has 125 contaminants in drinking water, where chlorinated ethylenes are included in a priority list of pollutants [6, 9]. In Europe, drinking water is regulated under Drinking Water Directive that sets limits for a small number of organic micropollutants (*e. g. aromatic hydrocarbons and chlorinated solvents*) and the groundwater quality is regulated under the Water Framework Directive and the Groundwater Daughter Directive [6]. The Priority Substances Directive lay down a number of Priority Substances, where in the Comprehensive Environmental Response and Compensation Liability Act of 2007 (CERCLA), vinyl chloride ranks on 3rd, TCE ranks on 16th and PCE on 33rd priority list of hazardous compounds [10 - 12] (table 1).

However, there is no evidence of enough political effects to tackle the long-term conflicts between groundwater and land, which makes necessary to develop and adopt a management approach [3]. Nevertheless, understanding the degradation mechanism is essential to develop efficient dechlorination processes to degrade these compounds and implement environmental remediation. In this study the effort is on the degradation of chlorinated ethylenes by zero valent iron (ZVI or Fe^0) and by iron-based bimetals reductants.

1.2. Chlorinated ethylenes

Chlorinated ethylenes (CEs) such tetrachloroethylene (PCE), trichloroethylene (TCE) and dichloroethylene (DCE) are the most frequently detected pollutants in groundwater due to their low solubility [13]. They have been introduced since 20th century into the environment and every year millions of tons of chlorinated ethylenes are produced [14]. Chlorinated ethylenes are frequently used in commercial and industrial applications, like industrial solvents, and are present in many household and consumer products as degreasing and cleaning agents [15]. For example, vinyl chloride is mostly used for the production of PVC (polyvinyl chloride) by polymerization and to produce 1,1,1-trichloroethane. In the case of dichloroethylenes, these compounds are used as an intermediate in captive organic chemical synthesis and to form other chlorinated solvents and compounds. As an end-product it can be used to extract oils from animal material and, at low temperature, in extraction of organics materials. Likewise, 1,1,1-trichloroethane can be used as well as an industrial solvent, metal degreaser, chemical intermediate in the production of other chlorinated compounds and as consumer products like adhesives aerosol cans [16].

The released in the environment of chlorinated compounds is typically done by the air [16]. Most of these compounds are highly toxic, mutagenic and carcinogenic, and are linked to some human diseases such as liver, nervous system and lung damage [17, 18].

Chlorinated ethylenes also have low boiling points and much greater density than water. These physicochemical parameters allows to the formation of plumes of dense non-aqueous phase liquid (DNAPL) due to the migration of these compounds downwards by the saturated zone until they achieve a confining layer, forming pools [19]. In fact, solubility and density is higher in highly chlorinated ethenes and ethanes (table 1) [8], of which PCE and TCE are the most frequently compounds spotted in urban area wells [19].

Table 1: Physicochemical parameters of chlorinated ethenes and ethanes [8, 20].

Name	Acronym	Boiling point (°C)	Solubility in water as 25°C (mg/L)	Density at 20°C (g/cm^3)	EPA maximum contaminant levels (µg/L)	WHO guideline values (µg/L)
Chloroethane	CA	12.3	5,700	0.89	-	-
1,1-Dichloroethane	1,1-DCA	57.3	5,060	1.18	-	-
1,2-Dichloroethane	1,1-DCA	85.3	8,600	1.25	5	30
***cis*-Dichloroethene**	c-DCE	60.1	3,500	1.28	70	50
1,1-Dichloroethene	1,1-DCE	31.6	2,250	1.21	7	30
***trans*-Dicloroethene**	t-DCE	48.7	6,260	1.26	100	50
Tetrachloroethene	PCE	121.3	200	1.62	5	40
Trichloroethene	TCE	88	1,000	1.46	5	70
1,1,1,2-Tetrachloroethane	1,1,1,2-TeCa	130.2	1,100	1.54	-	-
1,1,2,2-Tetrachloroethane	1,1,2,2-TeCA	145.2	2,850	1.59	-	-
1,1,1-Trichloroethane	1,1,1-TCA	74	1,490	1.34	200	-
1,1,2-Trichloroethane	1,1,2-TCA	112.8	4,390	1.44	5	-
Vinyl chloride	VC	-13.9	2,700	0.91	2	0.3

Another problem is that the degradation of CEs can lead to *cis*-DCE and vinyl chloride (VC). These intermediates are more hazardous and toxic than their parent compound (PCE) [13] and a successful remediation implies that the toxic daughter products may be avoid [21].

1.2.1. Chlorinated compounds degradation

The degradation of chlorinated ethylenes in the environment strongly depends on the environmental conditions where they are. Therefore, the geochemical, microbiological conditions and co-contaminant patterns play a very important role in their degradation. In the environment can occur both abiotic and biotic degradation. Microbial degradation is faster under anaerobic conditions, although in cases in which the concentration of reactive minerals and/or the activity of reduction by the bacteria is different, it may be crucial to change the reaction time [8]. In fact, reductive dechlorination is able to occur through an element of natural attenuation or stimulated by the addition of dechlorinating culture (e.g. *Dehalococcoides* (Dhc)) and/or electron donor [21]. However, there are some organisms that are not completely able to conduct the reduction of these compounds and the degradation, resulted from sequentially replacement of the chlorine substituents by hydrogen, often stops at the stage of *cis*-DCE or VC. As a result, it leads to accumulation of these toxic products and the biggest problem is that they are more hazardous and toxic than their parent compound [13, 22].

Investigations have been done before using a broad set of approaches, including the use of purified dehalogenases (*cobaloxime and cyanocobalamin*), pure microorganisms, enrichment cultures and chemical model reactants, such as zero valent iron (ZVI) [22, 23].

Generally, in aqueous solutions and in the absence of strong oxidants (*as carbonate, sulfate and nitrate ions when used zero valent iron*), the reductive dechlorination of TCE consists of multisteps reaction pathways. As a result, depending on the predominant pathway are produced more or less chlorinated daughter products (figure 2) [13].

Hydrogenolysis is a reductive reaction wherein a carbon-chorine bond is broken and hydrogen replaces chlorine. Simultaneously, the addition of two electrons to the molecule occurs [24]:

eq. 1 $ClHC = CCl_2 + H^+ + 2e^- \rightarrow ClHC = CHCl + Cl^-$ [25]

Hydrogenolysis can result in a sequential replacement of chloro-substituents with H atom, releasing chloride ions. Thereby, it leads to the formation and accumulation of more toxic and recalcitrant byproducts such as dichloroethylene and vinyl chloride (TCE → *cis*-DCE → VC→ ethene → ethane). However, this reaction corresponds to the microbial anaerobic reductive dechlorination and concurs with the other pathway during abiotic reductive dehalogenation [19].

The other pathway is vicinal β-dichloroelimination, i.e., vicinal reduction, β-elimination or α-elimination [8]. This is the dominant pathway involved in the reductive dechlorination of chlorinated ethylenes by zero valent iron and it is also the thermodynamically more favorable reaction [26, 27]. This reaction involves two-electron transfer to the target molecule and the elimination of either two chlorine atoms or one chlorine and a hydrogen atom with simultaneous formation of a triple bond (equation 2) [28]:

eq. 2 $ClHC = CCl_2 + 2e^- \rightarrow HC \equiv CCl + 2Cl^-$ [25]

As in this reaction is increased bond order, it does not allow to accumulate toxic intermediates [13, 15]. It produces chloroacetylene from TCE and acetylene from *cis*-DCE**.** In turn, the degradation from chloroacetylene to acetylene is through hydrogenolysis reaction [19].

Lastly, the formation of ethane from acetylene is a hydrogenation reaction, which involves the reduction of the triple bond to double bonds by H_2 (figure 2) [19, 27]. The upper pathway shows abiotic dehalogenation β-dichloroelimination and the lower pathway shows sequential hydrogenolysis to ethene [13].

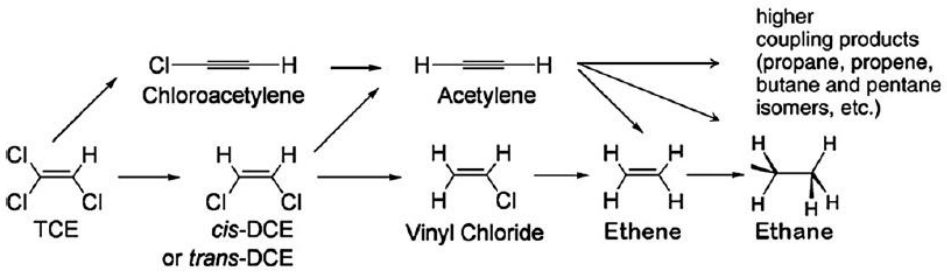

Figure 2: Reductive dechlorination of TCE [13].

1.2.2. Reactivity of chlorinated ethylenes with metals

Arnold and Roberts 2000 suggested that the reactivity trends of the chlorinated ethylenes decreases with increasing halogenation, which is consistent with the slower reduction rates of DCE and VC since they are poorer electron acceptors than TCE. However, it is often assumed that reactivity should increase with increase reduction potential [29] (table 2).

Table 2: Standard redox potentials (E^0) in aqueous solution at 25°C [25] (adapted).

Aqueous solution	Half reactions	E^0(V)
Tetrachloroethylene	$Cl_2C=CHCl_2 + H^+ + 2e^- \leftrightarrow Cl_2C=CHCl + Cl^-$	0.57
Trichloroethylene	$Cl_2C=CHCl + H^+ + 2e^- \leftrightarrow Cl_2C=CH_2 + Cl^-$	0.53
Vinyl chloride	$ClHC=CH_2 + H^+ + 2e^- \leftrightarrow H_2C=CH_2 + Cl^-$	0.45
1,1-Dichloroethene	$Cl_2C=CH_2 + H^+ + 2e^- \leftrightarrow ClHC=CH_2 + Cl^-$	0.42

For example, Arnold and Roberts 1998 reported greater reactivity of higher chlorinated ethylenes when used Zn(0) [27]. The same result was acquired when used vitamin B_{12} [26], ZVI and iron-bearing soil minerals (*biotite, magnetite and green rust*) [30]. On the other hand, when used iron sulfide, palladium and palladium iron bimetallic reductant, it was reported the opposite trend of reactivity [26, 30].

The reactivity trend of chlorinated ethylenes can depend on several factors such solutions conditions, the type of nanoparticle used and by the properties of the particles [25, 26, 31].

1.2.3. Reactivity with ZVI

Numerous reports have shown that Fe^0 particles quickly aggregate due to their high surface energy and intrinsic magnetic interactions [32], decreasing surface area for reaction and limiting mobility [25]. Another example is when it is used different methods to produce ZVI nanoparticles, may be expected to exhibit diversify properties, as solution chemistry and overtime [33].

Likewise, pH strongly influences the redox reactions occurring at the ZVI surface. At low pH the corrosion is accelerated due to greater availability of electrons from the Fe^0 core that rapidly dissolved of the surrounding oxide layer [31]. However, at high pH this leads to formation of iron hydro(oxides). As mentioned before, the oxidation of Fe^0 in aqueous systems releases OH^- ions, increasing the pH over the time in batch reactors of the system, and iron

reactivity decreases with pH increasing [25], howsoever, at some point it is achieved a meta-stable equilibrium between the oxide and the solution [34]. Besides, at neutral pH conditions, the iron oxide shell is insoluble and may protect the iron core from the rapid oxidation [33].

Furthermore, Cwiertny *et al.* 2007 noticed that the rate of *cis*-DCE reduction by unamended iron with identical experimental conditions compared with Arnold and Roberts 2000 was slower [26, 35]. They suggested that it was due to compositional variations in the granular iron used that was less reactive than the lot of iron used by Arnold and Roberts 2000 [21], which means that the composition of iron may depend on fabrication processes [33].

It is believed that the reduction process by zero valent iron consists on (i) adsorption of substrates to reactive sites at the surface of the iron, (ii) reduction at the surface, and (iii) desorption of the products [26]. The ZVI particles are composed of a Fe^0 core surrounded by an iron oxide shell [31]. This core-shell of the iron act as an electron source for reductive immobilization, i. e., implies facile electron transfer across the thin oxide shell. Also the oxide shell provides adsorptive sites and the initial surface of precipitation and mineralization render ZVI to be a truly multifunctional remediation agent [24].

Therefore, the reactivity of the iron is determined by the corrosion of Fe^0 with water that consumes dissolved oxygen and protons. As the result is produced molecular hydrogen and hydroxide ions, generating the pH enhancement over the time (figure 3) [36].

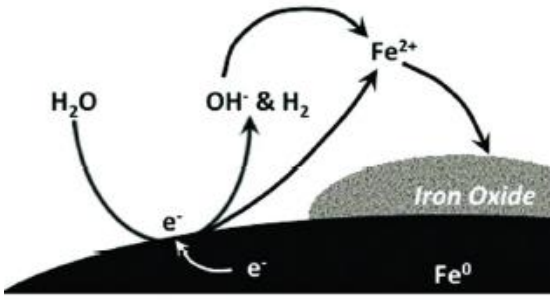

Figure 3: Schematic of the corrosion of Fe^0 [37] (adapted).

In fact, Fe^0 can be a very effective electron donner, i.e., reductant. Iron have a very low standard reduction potential of which is lower than chlorinated ethylenes, for example, and for that reason these compounds are disposed to be reduced [33].

More specifically, Arnold and Roberts 2000 hypothesized that initially a π-bonded surface species is formed (figure 4). The π-bonded intermediate forms a di-σ-bonded surface-adsorbed species. This step involves conversion of the π system to a σ bond of the ethylenes. In this hypothesis, the di-σ-bonded species can undergo two successive fast halide ion elimination steps to form first a mono-σ-bonded vinyl surface-adsorbed species and then acetylene (*β-elimination*). Or, on the other hand, a rapid reaction with adsorbed hydrogen followed by rapid halide ion elimination that gives the hydrogenolysis product (*hydrogenolysis*) [26] (figure 4). The source of the hydrogen atoms is most likely protons reduced by the iron. Audí-Miró *et al.* 2013 indicated that the rate-determining step in TCE and *cis*-DCE transformation by ZVI is a C–Cl bond breakage (that involve an electron transfer to a π* LUMO) [13, 26].

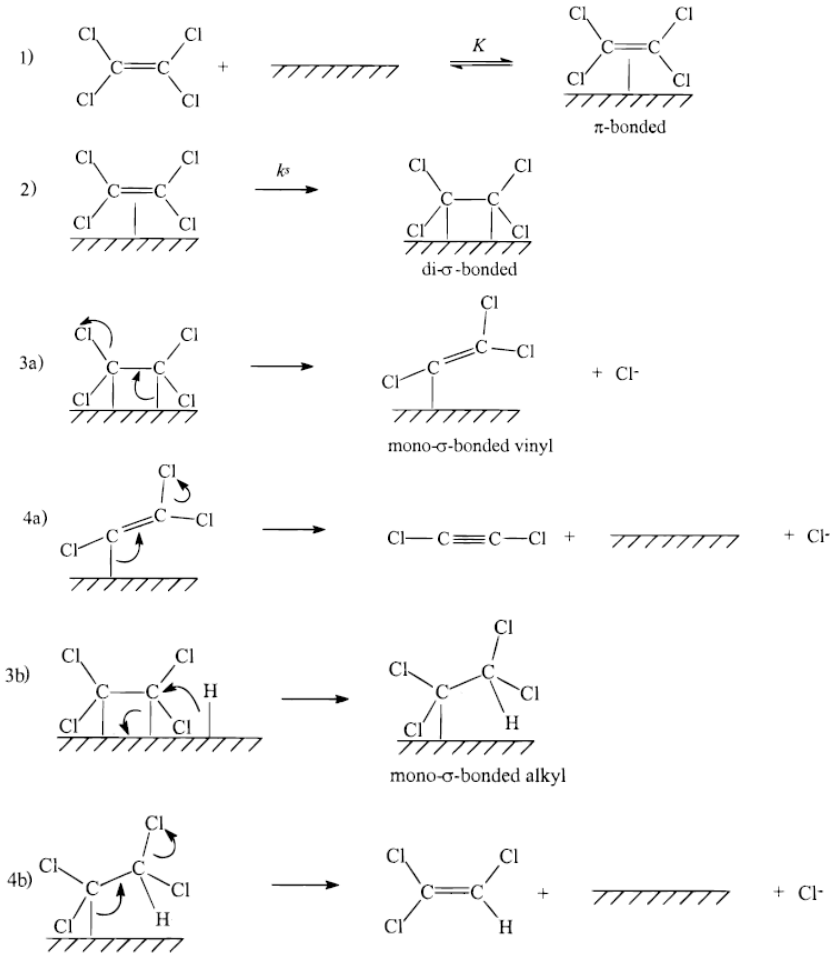

Figure 4: Mechanism for reaction of PCE with iron particles [26].

1.3. Remediation techniques

Remediation techniques to degrade persistent organic contaminants in the environment can be divided into three major categories: containment, removal and degradation. In the first category the contaminants are restricted to a specific domain to prevent further spreading, in the second one, the pollutants are transferred from an open to a controlled environment and, in the last one, the targets are converted into nonhazardous substances. This last category is the only one that directly destroys the contaminant and eliminates its toxicity over non-destructive techniques [19, 38].

More specifically, to treat groundwater are used two types of remediation methods: *in-situ* and *ex-situ* remediation. In *ex-situ* remediation, the treatment proceeds on the surface, which requires to pump the water to the surface. This type of remediation brings more concerns

insofar as it is required engineering equipment and higher costs. In that point of view, *in-situ* remediation is advantageous since it brings cost savings and minimization of potential cross-contamination at the surface because the treatment is directly applied into the aquifer [19].

In-situ treatment technologies include thermal treatment (for example steam-enhanced extraction, electrical resistive heating or thermal conductive heating), chemical oxidation, surfactant co-solvent flushing, bioremediation and, the common type, permeable reactive barrier (PRB) [39].

1.3.1. Permeable Reactive Barrier and the use of (nano)Zero-Valent Iron

In 1991 the first field application of ZVI in permeable reactive barrier, for *in-situ* remediation of groundwater contaminated by TCE and PCE showed 95% and 91% of removal rates for these compounds, respectively. Owing to the success of this treatment, it has attained much attention and were presented as one of the most promising alternative technology to the *ex situ* pump-and-treat method [19, 40].

In fact, in the past 20 years, research have been done focused on the reduction of chlorinated ethylenes by zero valent metals (ZVMs), such ZVI [40] and remediation strategies have been developed to address these problems [41] due to their capacity to rapidly transform contaminants [40] and also due to an enhanced reactivity that includes higher density of reactive surface sites and greater intrinsic reactivity of surface site [42].

Metals with higher reduction potentials have greater ability for degrading chlorinated contaminants in water (table 3). However, the use of metals such zinc and aluminum can bring some concerns over the environmental impact insofar as the water contamination by Zn^{2+} and Al^{3+}, and the reduction of zero valent zinc reactivity by passivation and for the insolubility of aluminum oxide layers between 4 to 9 pH range [43].

Table 3: Standard electrode reduction potential values in aqueous solution at 25°C [43] (adapted).

Metal	Half Reaction	Standard Electrode Reduction Potential (E^{0}) V
Fe	$Fe^{2+} + 2e^{-} \leftrightarrow Fe$	-0.440
Zn	$Zn^{2+} + 2e^{-} \leftrightarrow Zn$	-0.763
Si	$SiO_2 + 4H^{+} + 4e^{-} \leftrightarrow Si + 2H_2O$	-0.909
Al	$Al^{3+} + 3e^{-} \leftrightarrow Al$	-1.676
Mg	$Mg^{2+} + 2e^{-} \leftrightarrow Mg$	-2.356

Permeable reactive barrier treatment consists on the installation of an iron surface permeable reactive barrier. This reactive material is placed in the surface where a plume of contaminated groundwater moves (figure 5). Upon the contact of the water with the iron surface, pollutants are chemically transformed or immobilized [44, 45].

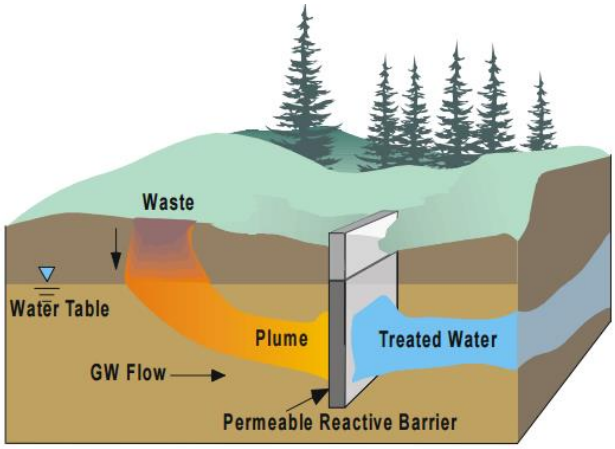

Figure 5: Schematic of a field-scale permeable reactive barrier [45].

In addition to the chlorinated ethylenes, this type of remediation technology have been also applied for the treatment of groundwater with halogenated organics, nitroaromatics, dyes, phenolic compounds, heavy metals (*Cr, U, As and Hg*) [19] and oxyanions [40]. Other advantage of the Fe(0) is its low cost, environmental acceptable and readily available [8, 46]. However,

chlorinated organic compounds such as dichloromethane (DCM), chloromethane, 1,2-dichloroethane and chloroethane are not able to be treated by ZVI [19].

Nevertheless, it must be also taken into consideration higher uncertainties such as variability in aquifer characteristics as geologic, hydrogeologic, subsurface conditions and geochemical proprieties (pH, ionic strength, dissolved oxygen, oxidation-reduction potentials and concentrations of nitrate, nitrite and sulfate) and, therefore, the homogeneity of the treatment [39]. Limitations associated with PRB have been reported, such as losses of reactivity and permeability and adverse hydraulic changes [39, 47]. In order to address key to these limitations, nanoscale iron (nZVI) can be regarded as an extension of the ZVI technology. Nanoscale iron can be used to treat pollutant source zones or plumes too deep in the surface since it can be delivered into the subsurface area at a specific location [33, 44] (figure 6). Furthermore, nanoparticles are able to pervade very small spaces in the subsurface and remain suspended in groundwater, permitting the particles to travel farther and achieve wider distribution. Although, in practice, it has been shown that they do not move so far from their injection point [39].

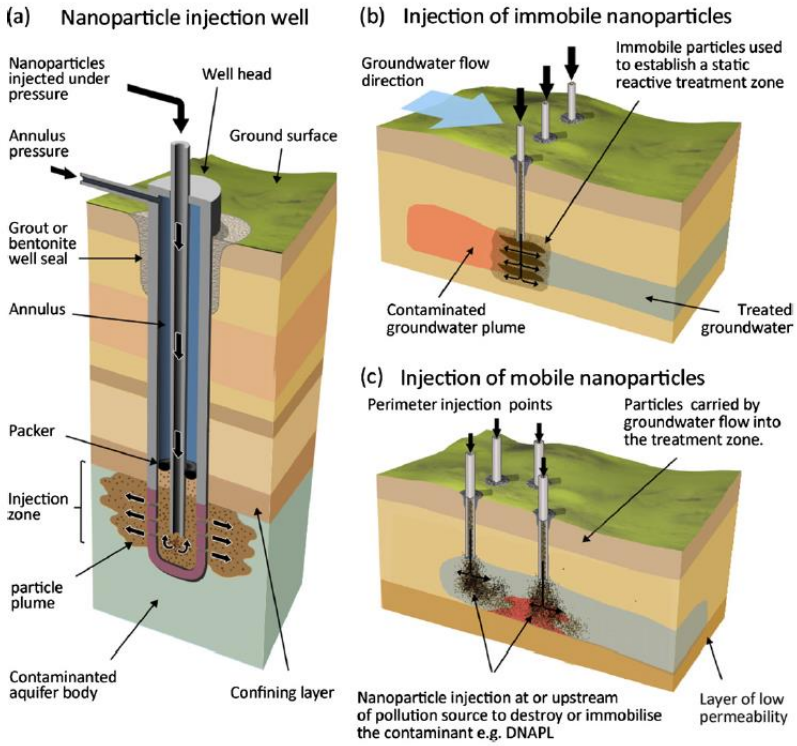

Figure 6: Schematic of subsurface injection of nanoparticle injection well [48].

Likewise, besides of nanoparticles of iron could serve as a substitute of iron PRBs, in some cases, it can also complement the fixed PRBs. Due to the small size of the nanoparticles, they can be injected under pressure and even by gravity flow to the contaminated area, continuing in suspension and flow with water for a long period of time [33]. On the other hand, as the dechlorination reaction of halogenated contaminants is surface-mediated, it is possible to increase the rate of the reduction of chlorinated ethylenes by increasing the surface area of the iron [29]. Thus, these particles provide large specific surface area and, as a result, more sites on which reactions occur [25].

Iron oxide nanoparticles have been shown to bind arsenic irreversibly, and based on their super-paramagnetic proprieties, it is possible to remove the iron bound to arsenic from the water with a magnetic field [39].

1.4. Iron-based bimetallic reductant

Metals that exhibit catalytic properties and have the oxidized form in solution can be used to create bimetallic nanoparticles [25]. When used bimetallic particles in system, the reaction rate of the degradations is increased due to the presence of these additional metals that allows to reduce the activation energy and also to occur more interactions between the compounds [25, 49].

ZVM technology have been extensively studied, including the use of bimetals for remediation, for example, Pd/Fe, Ni/Fe, Fe/Al, Cu/Al, Pd/Al and as well as trimetals such Pd/Ni/Fe, Pd/Fe/Al and Pd/Cu /Fe [9].

However, the molecular-level phenomena responsible for the enhanced reactivity of bimetallic reductants, is not clear yet, but several plausible explanations have been proposed. One of those is the formation of a galvanic cell between the additive metal, such as palladium, and the metal base (*e.g. iron*), which creates a large electrochemical potential difference. Here, the iron function as an anode by oxidation of Fe^0 to Fe^{2+} and palladium function as a cathode allowing the reduction of the pollutant. The other explanation proposed is the surface coverage of the additive metal on the reductive metal by making the first metal work as hydrogenation catalyst, in which adsorbed or absorbed atomic hydrogen species associated are accountable of the pollutant transformation [44, 50, 51].

The biggest advantage of the use of bimetals seems to be their propensity to generate completely dehalogenated hydrocarbons, and, therefore, not allowing the formation and accumulation of more toxic and recalcitrant intermediates such as vinyl chloride [24, 52]. It is believed that these effects results from a combination of factors, namely, higher rates of Fe^0 oxidation and release of electrons, the capacity of the additive metal to generate and store active hydrogen species and also the strong interactions between the bimetals particles and contaminants [52]. In fact, merely small amounts of those additive metals applied on the surface of Fe^0 are enough to cause an increased reactivity and also provides good protection against passivation [53] (figure 7).

1.4.1. Synthesis of bimetals

Numerous methods to synthesize bimetallic nanoparticles have been reported recently. Bimetallic nanoparticles can be synthesized in solution, gas phase, in a matrix or supported on a substrate [54]. Accordingly, these methods can be classified as physical or chemical methods. Physical methods permit the preparation of bimetals by using different compositions and sizes, at room temperature, without requiring toxic reducing agents, for example radiolysis and mechanical alloying methods. From that point of view, it is an advantage. Nevertheless, these methods involves complicated equipment and it is difficult to control the morphology of the particles. Thus, when compared with chemical methods, these are more commonly used since those problems are overcome and they are easier to perform. However, in these methods are needed toxic solvents and reducing agents and they are also time and energy consuming. The chemical methods usually used are thermal decomposition of metal complexes, chemical reduction and electrochemical synthesis [55].

Chemical reduction is the most common method used to this purpose. Typically, are used metal salts in a solution and, afterwards, they are reduced by the appropriate reducing agent ($NaBH_4$ and N_2H_4 for example). During the reduction process, the metal with higher redox potential is reduced first and leads to the formation of the core where the other metal species (with lower reduction potential) is deposited as a shell [54]. In fact, it is possible to change the order of the core-shell structure, i.e., when used a reducing agent that strongly bond with higher redox potential metal, the structure of the nanoparticles can be reverse. For example, reduction of Ag and Pd usually leads to $Pd_{core}Ag_{shell}$ since palladium have higher redox potential. However, when used ammonia as a reducing agent, due to the stronger blinding

to Pd than Ag, it is formed $Ag_{core}Pd_{shell}$ [54]. For that reason it is suggest to select the proper reducing agent and reaction system [55].

In the case of the iron, as it has a relatively low standard reduction potential when compared to other metals (Ni, Pd, Pt, for example), it makes possible to reduce the other metals by using iron itself [33], acting as an electron donor [55]. Therefore, irrespectively of the method of synthesis applied, the additional metal is reduced by the iron and the metal deposits onto the iron surface [25], for example:

eq. 3 $Pd^{2+} + Fe^{0} \rightarrow Pd^{0}\downarrow + Fe^{2+}$ [25]

where the resulting nanoparticle is composed by a thin discontinuous layer of the additional metals on top of the Fe^0 surface (figure 7) [25].

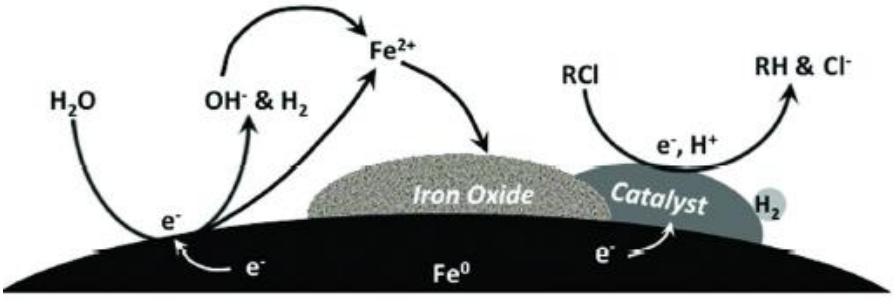

Figure 7: Schematic of treatment of chlorinated compounds by bimetallic nanoparticles [37].

1.4.2. Reactivity of chlorinated ethylenes towards bimetals reductants

As mentioned above, nZVI reactivity and also the reactivity of chlorinated compounds and metals can be influenced by several factors [25]. In this case, the factors include mass loadings of the metal additive, their chemical states and physical distribution onto the base metal, as well as the size and morphology of the base metal [52]. Here, the composition of bimetals nanoparticles is an important factor since it can change the properties of the iron, i.e., if the additional metal has a different content, it may lead to different atomic distribution on the surface, the morphology and size of the nanoparticles, for example [55].

Also, strong acid and alkaline conditions in the system are disadvantageous, although a higher pH can stimulate the enhancement of the electron transfer, at low pH it can promote the reduction of H^+ to form H_2 and, therefore, can act as a reductant, after the activation of the additional metal [55]. Moreover, the increase of the pH over the time in batch reactors of the system is a behavior that can influence the magnitude of the rate enhancement or inhibition for each metal [56]. Cwiertny *et al.* 2006 observed that, with 1,1,1-trichloroethane, the pH in Ni/Fe, Cu/Fe and Au/Fe systems increased but did not vary as a function of these additives' loadings. Besides, the increase of pH in Pt/Fe and Pd/Fe systems were greater and tended to increase with Pt and Pd loading [56].

In bimetallic systems, the enhanced rates of iron oxidation may not play a very important role at the increase rates of the reduction [35] since the formation of Fe-rich or Pd-rich surfaces, for example, formed by insufficient or excessive coating can lower the catalytic efficiency [57]. The high loading of the second metal may lead to the aggregation of fine catalytic nanoparticles into large ones [51]. Therefore, determining the optimum ratio of the additional metal to iron nanoparticles is critical to obtain maximum reactive sites [57]. Cwiertny 2005 suggested that, relatively to alkyl polyhalides, the most cost-efficient additive loading in terms of optimizing reductant reactivity is one monolayer equivalent, since the surface coverage of the additive metal on iron was maximized [44].

On the other hand, it was suggested that the iron and the additive metal need to be in electronic contact to maximize the reduction of the compounds. The degradation rate of TCE toward Ni/Fe co-precipitate by a physical mixture of nano-scale iron was much faster than during TCE degradation with nano-scale nickel precipitated by individual reduction of the salt in aqueous solution [57].

However, it was also shown that using catalytic metals on Fe^0 not always enhanced rate degradation. For example, Kim and Carraway 2000 reported slower removal rates when used Pd/Fe, Pt/Fe, Ni/Fe and Cu/Fe for the degradation of pentachlorophenol (PCP) comparing with unamended iron [58]. Cwiertny 2005 reported that Pt/Fe inhibited 1,1,1-TCA reductive dechlorination but the same bimetal enhanced the rates of *cis*-DCE reduction [44]. They suggested that reactivity may depend on the compound to be dechlorinated [58]. Moreover, Cwiertny 2005 reported that vinyl halides are more likely to be reduced by iron-based bimetals than alkyl polyhalides, suggesting that the metal additives' role is not the same for vinyl polyhalide systems and for alkly polyhalides, in which different active reductants may be

involved in each case and, therefore, dechlorination is influenced by the identity of the electron acceptor [35, 44].

Conversely, several studies have demonstrated that iron-based bimetallic reductants can achieve biggest degradation rates, when compared with unamended iron, and prevent or reduce the formation of toxic byproducts [59]. For example, it was shown in PCE degradation that acid-treated and untreated iron was less effective than Ni-plated on iron [60], similar for the degradation of TCE when used Ni/Fe particles, which were faster than monometallic nZVI [25]. Cwiertny 2005 reported that Pd/Fe was more reactive than Ni/Fe and all the other bimetals toward *cis*-DCE, i.e., Pt/Fe, Cu/Fe, Co/Fe and Au/Fe, where Pt/Fe was the fastest of those [44]. When tested all of those same bimetals toward 1,1,1-trichloroethane dechlorination, Cwiertny *et al.* 2006, found somewhat different trend: Ni/Fe ≈ Pd/Fe > Cu/Fe > Co/Fe > Au/Fe ≈ Fe > Pt/Fe [56]. Analogous, Doong and Lai 2006 reported enhanced dechlorination efficiency and rate of PCE, when used bimetals, with the bimetallic trend: Ni(II) > Cu(II) > Co(II) (61). Kim and Carraway 2003, also studied the degradation of TCE using iron and zinc bimetals and found that all the iron bimetals used were faster than zinc bimetals, following the trend: Pd/Fe > Pd/Zn > Ni/Fe > Cu/Fe > Ni/Zn > Cu/Zn > Fe > Zn [46].

Some authors investigated also the trend of reactivity of the degradation of chlorinated ethylenes. For example, Zhang *et al.* 1998 reported the trend consistent with the redox potential: PCE > TCE > *cis*-DCE > VC, for both nanoscale iron and Pd/Fe particles [49].

Furthermore, it was also found that the product partitioning is different in bimetallic systems. The reaction products may depend upon the metal additive employed because additive properties resulting in enhanced bimetal reactivity, which may be responsible for favorably altering reduction product partitioning [44]. For example, when used Pd/Fe nanoparticles on TCE degradation, the major end products found were ethene and ethane, but in the case of nZVI, the major end product was only ethene [62]. On the other hand, if it is compared the end products of the degradation of PCE and TCE using Pd/Fe, it was observed that PCE produced ethane whereas TCE formed ethane and ethene [25]. Cwiertny 2005 also suggested that the cumulative concentration of reduction products increased with the additive loading in the system when used Cu/Fe, Co/Fe, Au/Fe and Pt/Fe [44].

In this study were chosen six metal additives, namely, Pd/Fe, Ni/Fe, Cu/Fe, Co/Fe, Pt/Fe and Au/Fe, because they are often encountered for chemical transformations catalyzed by transition metals and due to the physical and electrochemical properties. Pd, Pt, Au and Cu

have large, positive reduction potentials versus standard electrode, as well the thermodynamic driving force for deposition, in contrast with Ni and Co, that have negative reduction potentials [56] (table 4).

Table 4: Standard reduction potentials of metallic reductants [37, 63] (adapted).

Half Reaction	Standard Electrode Reduction Potential (E^{θ}) V
$Au^{3+} + 3e^- \rightarrow Au^0$	1.52
$Pt^{2+} + 2e^- \rightarrow Pt^0$	1.2
$Pd^{2+} + 2e^- \rightarrow Pd^0$	0.99
$Cu^{2+} + 2e^- \rightarrow Cu^0$	0.34
$Ni^{2+} + 2e^- \rightarrow Ni^0$	-0.25
$Co^{2+} + 2e^- \rightarrow Co^0$	-0.28

1.5. Methods and techniques used during chlorinated ethylenes degradation

As mentioned above, reductive dechlorination of chlorinated ethylenes using zero valent iron and iron-based bimetallic reductants have been extensive studied. Depending on the aim of each study they are used different techniques.

The technique that normally is used to determine aqueous concentrations of target compounds and/or reaction products is gas chromatography. It allows, for example, the study of reaction kinetics and understand the degradation mechanism [13, 26, 44, 50]. Usually, a surface-area-normalized kinetic model is applied toward organohalide reduction in iron batch systems, where the iron specific surface area is determined by N_2- or Kr-BET (Brunauer–Emmett–Teller) adsorption. Most of these studies are applied as representative comparison of the iron reactivity and as a tool to understand the role of the iron through the degradation [64]. Iron concentrations can be measured using the 1,10-phenanthroline method [50].

In the case of the bimetals reductants, atomic absorption spectroscopy (AAS) or inductively coupled plasma mass spectrometry are techniques commonly used to determine the

mass of additive metals onto the metal-base surface, to understand the role of each bimetal on the degradation and the location at which the compounds-target reduction occurs on the bimetallic particles [50, 56, 65]. The use of scanning electron microscopy in conjunction with energy dispersive X-ray spectroscopy (SEM-EDS), X-ray photoelectron spectroscopy (XPS) and/or Auger electron spectroscopy (AES) can be applied to characterize the deposition, composition and structure of the additional metal onto the iron surface. More precisely, AES allows to acquire the quantitative measure of two-dimensional additive metal and XPS allows to obtain the oxidation state information [65]. To examine the morphology of bimetallic particles can be used transmission electron microscopy (TEM) on one parameter that influence the reactivity of the particles, for example, aging [50].

Nonetheless, many fundamental issues surrounding the chemistry behind of the reductive dechlorination remains unclear. Thus, one of the purpose of this study is try to make the bridge between what have been described in the literature.

1.5.1. Chemical kinetics

The reaction mechanisms of chemical processes can be accomplished by chemical kinetics through the rates of chemical reactions and factors that may influence on the rates. In chemical kinetics are examined the rate of concentration changes of products or reactants and the time variable. As a consequence, it allows the quantitative determination of chemical reactions rate and the effect of different factors that the rates may depend, for example temperature, pH, catalyst effect, concentration [66].

Thus, to obtain the chemical kinetic of a reaction is necessary to determine the concentration of the reactant or the product as a function of time. Here, the method used to determine the concentration may be faster than the reaction rate. Therefore, when it is used a reaction in gaseous phase, it is required the determination of the partial pressure in place of the concentration. However, when used reactions in solution, it is required withdraw aliquots of the reaction through the means of suitable means and, afterwards, proceed with the analysis [66].

In the case of chlorinated compounds in contact with highly pure Fe^0 in a closed, well-mixed and anaerobic batch system the degradation reaction is effectively described by the pseudo-first-order rate model:

eq. 4 $$-\frac{dC_w}{dt} = k_{obs} \times C_w$$ [67]

where C_w is the concentration of contaminants in the aqueous phase, t is the reaction time (time), and k_{obs} is the observed rate constant (time^{-1}) [67].

Therefore, data referred to the rates and products of TCE and *cis*-DCE reduction (determined from batch studies), allows relationships between deposited additive metal mass, and, as a result, its surface coverage onto iron surface, and reductant reactivity to be developed [65].

1.5.2. Chromatography

Chromatography is a series of techniques that allows the separation of components present on a mixture as a result of their partitioning, i.e., differential sorption, between two different phases: a mobile phase, which is in contact with the stationary phase that has a large surface [68].

The separation process of the compounds can be accomplished by gas, liquid or solid analytes and it requires interaction of the compounds present in the sample between the stationary phase and the mobile phase [68, 69].

There are many types of chromatographic techniques, ranging from highly sophisticated and expensive to simple and inexpensive such as: affinity chromatography, reversed phase chromatography (RPC), gas chromatography (GC), two dimensional gas chromatography (GCxGC), liquid chromatography (LC), high performance liquid chromatography (HPLC), and others [70].

Gas chromatography is mainly use to analyze volatile substances in the gas phase. The separation is due to distinct migration rates of the compound that interact in a different ways with the stationary phase and are carried through the mobile phase inside the column. Mobile phase is responsible to carry the molecules of the analyte over the heated column [71]. Therefore, must be chosen a column that expresses the strength of the intermolecular forces between the analyte and the stationary phase, as well as the carrier gas, to certificate the properly separation of all components present in the sample [68, 69].

Chromatography is a versatile and unique technique and can be applied to a wide range of purposes besides analytical separation, namely, the determination of physicochemical constants, preparation of pure substances, structural investigations on the molecular scale and study of the kinetics reactions as well the mechanism reactions [68].

As an analytical technique, it must be coupled to a detector for product identification and also to provide a quantitative measurement of the components. Typically the detectors more used in chromatography are Flame Ionization Detector (FID) and Mass Spectrometer (MS) [68].

MS is usually applicable for any type of sample and is the most powerful. In GC-MS is used an electron-impact ion source that is responsible to ionize and fragment the sample. Once it is bombarded, the molecule becomes ionized and, afterwards, loose an electron owing to electrostatic repulsion. After new bombardment, the ions are forced to fragment and are passed through the mass analyzer [71].

The FID is more used to measure hydrocarbons, however, it is the most broadly applicable detectors due to be highly sensitive and low noise. In GC-FID, the sample goes through an air-hydrogen flame after leaving the column, where is pyrolized or chemical decomposed. Here, the pyrolized analyte releases ions and electrons carrying current and, afterwards, this current is measured to monitor the sample's elution [71].

Therefore, gas chromatography is used as a potent instrument in several studies (for example, [19, 26, 44]) and also herein, to the extent that when used an appropriate method and column toward reductive dechlorination, it is able to detect the target chlorinated compound, as well as their lower chlorinated intermediates and non-chlorinated end products simultaneously [72]. Also, gas chromatography allows further determination of compounds concentration, designate degradation products and obtain product partitioning, wherein these kind of studies, the analysis of TCE and/or DCE is necessary, the biggest advantages is the common use of FID or MS as detector and the fact that it allows to determine analytes from sample headspace [72].

1.5.3. Isotope analysis

Compound specific isotope analysis (CSIA) is a powerful tool that allows to separate organic analytes from complex mixtures and to determine their individual stable isotope ratios of the target element at natural isotopic abundances.

In the late 1930s, Nier and Gulbrasen observed for the first time carbon isotope composition in nature. Thereafter, natural changes were attributed to isotope fraction processes and it was realized that this could be a new approach to follow complex geochemical and biological processes and climate change studies. Subsequent developments leaded to the multiple Faraday collector cups which were able to continuous recording all isotope masses at the same time, with better amplifications electronic and also differential pumping systems [73]. As a result, to accommodate the experimental data was introduced the delta notation:

eq. 5 $$\delta^{h}E_{comp} = \frac{R({}^{h}E/{}^{l}E)_{comp} - R({}^{h}E/{}^{l}E)_{std}}{R({}^{h}E/{}^{l}E)_{std}} = \frac{R({}^{h}E/{}^{l}E)_{comp}}{R({}^{h}E/{}^{l}E)_{std}} - 1$$ [74]

where $\delta^{h}E_{comp}$ represents the relative difference between the isotope ratio of a sample $R({}^{h}E/{}^{l}E)_{comp}$ (e.g., $R({}^{13}C/{}^{12}C)$) and of an internationally accepted reference standard $R({}^{h}E/{}^{l}E)_{std}$. The positive and negative δ values express enrichment and depletion of the heavier isotope in a sample relative to the reference material, respectively [73].

Later developments in the technique brought a rapidly increase of studies published in CSIA. Nowadays, carbon isotope measurements are the most commonly applied. However, it is also possible to obtain isotope fractionation of other elements such as hydrogen, chlorine, oxygen and nitrogen [73, 74].

Table 5: Parameters for CSIA of elements typically present in organic contaminants [73] (adapted).

Element	Minor isotope	Natural abundance (%)	Analyzed gas (M)
Hydrogen	^{2}H	0.01557	H_2
Carbon	^{13}C	1.1056	CO_2
Nitrogen	^{15}N	0.3663	N_2
Oxygen	^{18}O	0.20004	O_2
Chlorine	^{37}Cl	24.221	$C_xH_yCl_z$ or HCl

Thus, the accomplishment by the direct coupling of gas chromatography (GC) or liquid chromatography (LC) makes possible the separation of the different compounds to an isotope ratio mass spectrometer (IRMS). Briefly, initially the continuous carrier flow with the baseline-separated analyte peaks is directed into a chemical conversion interface, where the individual analytes are converted into a measurement gas M, which is appropriate for isotope analysis. As a result, the M peaks are transferred in a He carrier stream into the IRMS [73] (figure 8).

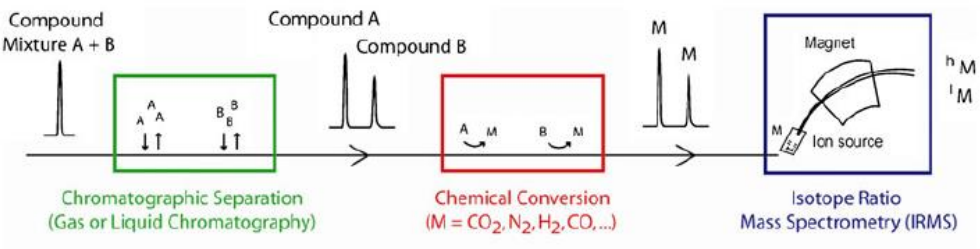

Figure 8: Scheme of general principle of compound specific isotope analysis by chromatography-IRMS [73].

The combustion interface it is normally constituted by a few oxidized copper and/or nickel metal wires threaded through a narrow ceramic reactor tube, maintaining the peak separation [73]. In the case of carbon isotope analysis is used a combustion interface that converts the carbon atoms to CO_2 (GC-C-IRMS) [19] (figure 9).

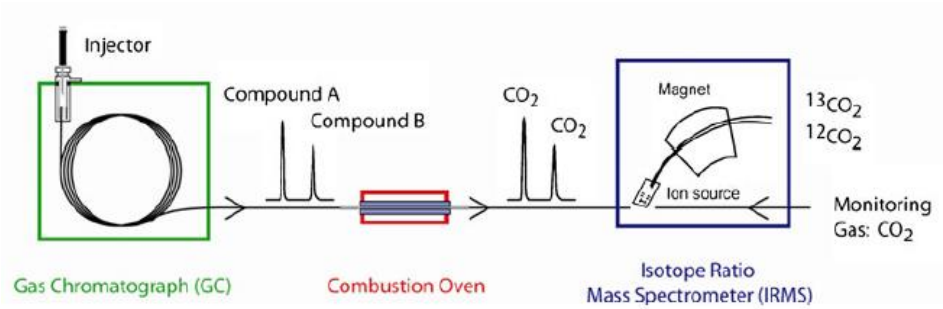

Figure 9: General instrumentation scheme for carbon-isotope analysis by GC-IRMS [73].

For chlorine isotope analysis, in spite of the difficulty of create a simple chlorine-containing gas in a continuous He carrier flow, which could be problematic, it is used another approach. This approach entails the direct analysis of the isotopologues containing multiple chlorine substituents (e.g. $C_2H_2{}^{37}Cl^{35}Cl$ or $C_2H_2{}^{35}Cl_2$) and thus, in turn, it is not necessary to convert the target molecules [73] (figure 10).

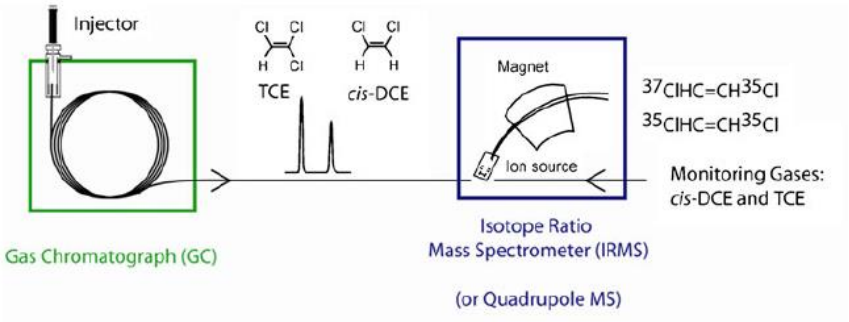

Figure 10: General instrumentation scheme for compound-specific chlorine-isotope analysis [73].

Hence, the evaluation can be done based on fragment ions, molecular ions or combination of both. Thereby, it is necessary to apply a calibration method to preserve the accuracy of isotope measurements for each target compound, using a chemical identically isotope reference material with known isotopic composition. In this study is used two different isotope standards chemically identical to the analyte and with different ^{37}Cl abundance [73].

In the case of compound-specific hydrogen isotope analysis, it is fairly challenging. First, for chlorine-, nitrogen- and sulfur-containing organics it leads to the formation of

hydrogen-containing byproducts such as HCl, for example. To overcome this question it is used a ceramic reactor tube packed with chromium as a high temperature conversion (HTC) which allows the conversion of organic hydrogen to H_2 and reduces the formation of hydrogen-containing byproducts [75] (figure 11).

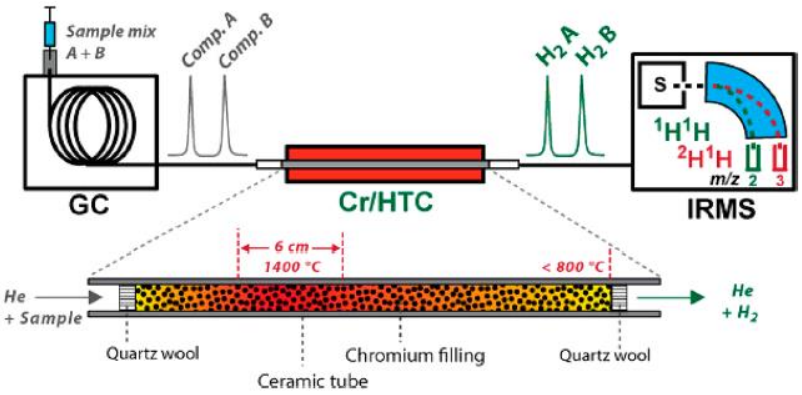

Figure 11: General instrumentation scheme for hydrogen-isotope analysis by GC-HTC-IRMS [75].

Moreover, conventional concentration analysis usually just measures the most abundance isotope and the natural abundance of ^2H, when compared with the natural abundance of other compounds, which is very low (0.0156 atom %), and so it is not so easy to create a sufficient strong deuterium-containing ion current [73]. To address key to this question, some methods can be used to pre-concentrate the analytes, namely, Purge and Trap (P&T) method. Briefly, in this method, the compounds are sorbed in a trap after the aqueous sample be sparged by a gas stream. Subsequently, they are released by heating and are transported to the injection port of the GC by He stream [73].

Accordingly, CSIA provides evidences of ongoing degradation of the parent contaminants and the intermediates due to isotope fractionation. Isotope fractionation factors reflect the average behavior of isotopes in a molecule. During abiotic and biotic reactions, the lighter isotopes are transferred from the reactant to the product pool and, as a consequence, the residual reactant becomes increasingly enriched in the heavy isotope with the ongoing reaction [73]. This trend is described by the Rayleigh equation:

eq. 6

$$\frac{\left({}^{h}E/{}^{l}E\right)}{\left({}^{h}E/{}^{l}E\right)_{0}} = \frac{\delta^{h}E+1}{\delta^{h}E_{0}+1} = f^{\alpha_E - 1} \approx f^{\varepsilon_E}$$

$$\ln\frac{\delta^{h}E+1}{\delta^{h}E_{0}+1} = (\alpha_E - 1)\cdot \ln f \approx \varepsilon_E \cdot \ln f$$

[73]

where $({}^{h}E/{}^{l}E)_0$ is the average isotope ratio of element E in the substrate (irrespective of its position), $({}^{h}E/{}^{l}E)$ is the isotope ratio reached once degradation has proceeded to a residual fraction of the substrate f, α_E is the isotope fractionation factor and ε_E is the isotope enrichment factor which reflects the extent of isotope fractionation per increment of transformation.

Kinetic isotope effect (*KIE*) is the most fundamental parameter to characterize isotope fractionation [76]. Depending on the order and manner of chemical bond is broken or formed, *KIE* express the reaction rate of heavy and light isotopes, defined by:

eq. 7

$$KIE_E = \frac{{}^{l}k}{{}^{h}k}$$

[74]

where ${}^{l}k$ and ${}^{h}k$ are the rate constants for molecules with a light and heavy isotope, respectively. Since it is expected isotopes from the same element have the same behavior due to their chemical proprieties (for example number of electrons), if they have different rates it is owing to the fact of the presence of additional neutrons, responsible to change atomic motions, and to the magnetic moment or nuclear volume of atomic nuclei [74].

The observable (apparent) kinetic isotope effect (*AKIE*), is related by a mathematical approach that takes into account that the isotopes may be present at positions that do not participate in the reaction. Also, is considered the multiple reacting positions that can occur in a molecule wherein, only one of these reacts [73]. Therefore, typical isotope effects in the reacting bond can be followed by the equation:

eq. 8

$$KIE_E = \frac{1}{n \cdot \varepsilon_{E,compound\ average} + 1}$$

$$\varepsilon_{E,compound\ average} = \frac{1}{n} \cdot \left(\frac{1}{KIE_E} - 1 \right)$$

[74]

where *n* is the number of atoms of element *E* in a molecule. Hence, for an increased in *n*, the observable isotope fractionation is reduced and leads to an upper limit of the number of atoms of *E* for which isotope fractionation may still be measured [73].

As reported above, compound-specific isotope effects can be measured for multiple elements (C, Cl and H). This can give additional information about the reaction mechanism when changes in compound specific isotope values are visualized in dual element isotope plots. As a result, the given slopes are linked to compound-specific isotope effects which are related to the respective mechanism. Thus, it can provide the bridge between similar isotope fractions among different transformation pathways [21].

On the other hand, when steps become rate-determining, masking effects can occur. When used one element isotope plots, the effect can be intense but if it is used dual element isotope plots, the slopes often remain constant due to the decrease in the same proportion of *KIE* values for both elements. Consequently, the observable kinetic isotope effect decrease but with dual element isotope representations, the slopes are insensitive toward masking effects [22].

For example, according to Audí-Miró *et al.* 2015, for biodegradation experiments, values of the enrichment factor for carbon are ranging from -2.5 to -16.0‰ [77], while for TCE abiotic degradation by zero valent iron, Schüth *et al.* 2003 reported the average enrichment factor value of -10.1‰ with iron samples toward PRBs in batch experiments [78], Elsner *et al.* 2008 reported -23.5‰ with Fe^{BH} (produced by reduction of dissolved Fe^{II} by $NaBH_4$) and from -20.9‰ to -26.5‰ with Fe^{H2} (by goethite and hematite reduction with H_2 gas at 200-600˚C) [79] and, using cast iron and autoclaved electronic iron, Slater *et al.* 2002 reported an enrichment factor of -16.7‰ [80]. Thus, as the ε_C overlap, may not be possible to distinguish the different types of degradation using only carbon isotope effects [77].

Also, Cretnik *et al.* 2013 were able to compare TCE reductive dechlorination by cobalamine and cobaloxime to dehalogenating bacteria (*Geobacter lovleyi* strain SZ and *Desulfitobacterium hafniense* Y51) using dual element isotope analysis, where they found that

dual element isotope slopes ($m = \Delta\delta^{13}C/\Delta\delta^{37}Cl$) of cobaloxime strongly disagrees with the slopes of cobalamin and natural dechlorination systems biotransformations, suggesting a different mechanism with cobaloxime [22].

Even though a big set of studies have been reporting isotopic enrichment factors during biotic and abiotic degradation and aerobic biodegradation of chlorinated ethylenes [21, 77], compound specific isotope effects during reductive dechlorination of TCE by iron-based bimetallic reductants have not been clearly delineated.

2. Problem

In the last years, the environmental problems has been increasing the interest due to the impact of contaminants over the environment throughout the history [81]. CEs (*for example, PCE, TCE, DCE and VC*) have been extremely used and released to the environment since 20th century, due to poor waste management, and every year continue to be produced millions of tons [14]. As these compounds are denser than water allows to the formation of pools and, therefore, they are the most frequently detected pollutants in groundwater [13]. As CEs are highly toxic, they can be responsible for causing liver and nervous system damage as well for developing cancerous problems in the human being [17, 18].

Under anoxic conditions CEs can be degraded by microorganisms or by zero valent iron. However, these organisms are not able to completely conduct the reduction of these compounds, leading to accumulation of toxic products. The biggest problem is that these toxic products are intermediates, that resulted from sequentially replaces of the chlorine substituents by hydrogen (for example *cis*-DCE and VC), and are more hazardous and toxic than their parent compound [13, 22].

One of subsurface remediation that has received attention is the use of nanometals, such zero-valent iron (ZVI), due to their capacity to rapidly transform contaminants by the large specific surface area provided, which offers more sites where reactions can occur [25]. Also, they have an enhanced reactivity due to their higher density of reactive surface sites and greater intrinsic reactivity of surface site. Several studies have shown that the ability to increase the rates of organohalide reduction and the production of more fully dehalogenated reaction products is greater achieved with iron-based bimetallic reductants [25, 46, 56, 62].

Although many fundamental issues surrounding the chemistry behind CEs dechlorination have become clearer, still necessary try to make the bridge and understand better the degradation mechanism to develop efficient dechlorination processes to degrade these compounds and implement remediation processes. Therefore, the aim of this study is to evaluate the kinetic and compound specific isotope effects during CEs reductive dechlorination by zero-valent iron and iron-based bimetallic reductants.

3. Objectives

The general aim of this study is to evaluate the reductive dechlorination of TCE and *cis*-DCE by zero-valent iron and iron-based bimetallic reductants in anaerobic conditions.

In order to achieve the general aim it will be:

- Evaluated the kinetics of TCE and *cis*-DCE reduction in the systems with different additive loadings;
- Determined the generalized bimetallic trend;
- Determined the mechanism, intermediates and products partitioning toward TCE transformation;
- Investigated 2D compound specific isotope effects (^{13}C, ^{37}Cl, ^{2}H) during dechlorination by zero-valent iron and iron-based bimetallic reductants.

4. Results and Discussion

4.1. Kinetics

As reported above, the rate constants relating to compounds reduction allows relationships between surface coverage onto iron by additive metals and reductant reactivity to be developed. Kinetic batch experiments were performed in order to evaluate the reactivity of different iron-based bimetallic reductants (Pd/Fe, Ni/Fe, Au/Fe, Pt/Fe, Cu/Fe and Co/Fe) during TCE and *cis*-DCE degradation. For this purpose, different sets of reactions were prepared and tested toward i) influence of unamended iron loading at pH 7, to verify the reactivity trend and to compare, afterwards, the rate constant reaction with the rate constant obtained using different bimetallic systems during both target compounds degradation (section 4.1.1), and also to compare the reactivity of TCE reduction using different pH (2 and 11) (section 4.1.1.1), ii) influence of different additive metals loadings into iron nanoparticles, prepared by displacement plating, to obtain the maximum reactivity during TCE and *cis*-DCE degradation and compare with rate constant at the same unamended iron loading used and to determine the generalized bimetallic trend of the bimetals used, as well the chlorinated ethylenes reactivity trend (section 4.1.2) iii) influence of each additive metal salt solution toward TCE and *cis*-DCE, to better understand the reactivity on bimetallic systems (section 4.1.3).

4.1.1. Influence of unamended-iron loading for chlorinated ethylenes reduction

A pseudo-first order kinetic (eq. 4) was applied to both TCE and *cis*-DCE degradation to test the reactivity of zero-valent iron reductant mass loading (100 to 500 mg iron toward TCE and 200 to 600 mg toward *cis*-DCE), containing 50 mM Tris at pH 7 under anaerobic conditions.

Aqueous chlorinated ethylenes concentrations were quantified directly using the target compound calibration curve. Values of rate constant (k_{obs}) for contaminant degradation were achieved from plots of the natural logarithm of the compound concentration versus time. The next figure shows an example of how the k_{obs} was achieved for all different unamended iron loadings tested for both TCE and *cis*-DCE during degradation (figure 12).

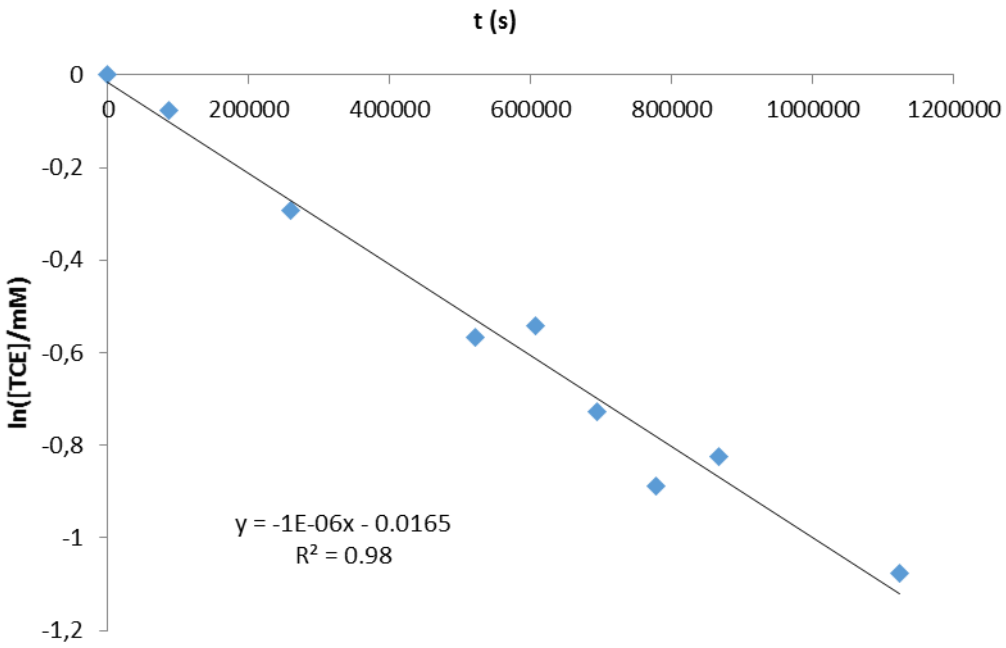

Figure 12: Plot of the natural log of TCE concentration vs time for 200 mg iron at pH 7.

Batch experiments with *cis*-DCE revealed a nonlinear relationship between k_{obs} and the iron loading tested, wherein, k_{obs} kept nearly constant over the increasing iron mass loading and is generally smaller than k_{obs} for TCE (figure 13). The experiments with TCE show an initial increase of the rate constant, followed by a stabilization and, finally, further decrease.

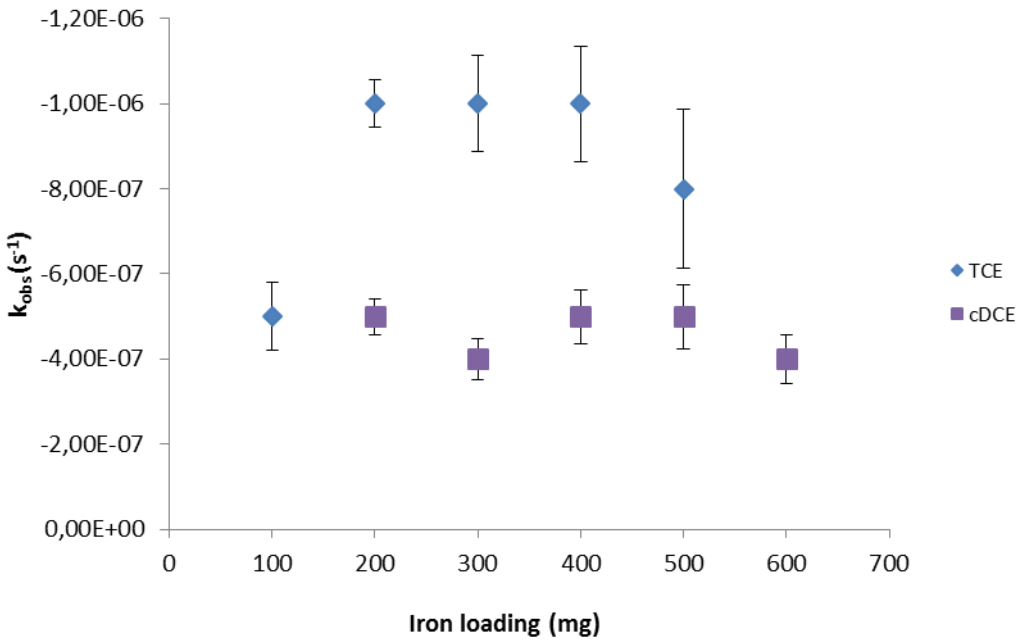

Figure 13: Influence of iron loading on k_{obs} for TCE and cis-DCE degradation (uncertainties represent 95% confidence intervals).

Several studies have shown a linear relationship between rate constant and metal loading, although some studies indicate discordant results, suggesting that the reaction rate may not be proportional (nonlinear relationships) [27]. Arnold and Roberts 2000 reported a directly proportional constant to metal loading over a limited range (0 to 0.5 g per 160 mL), in which a possible explanation was inefficient mixing at higher metal loadings [26]. Cwiertny and Roberts 2005, regarding the 1,1,1-TCA degradation, reported a nonlinear relationship between rate constant and the granular iron mass loading [64]. However, they were able to obtain a linear relationship when reduction seemed to be mass-limited but, again, when tested under various experimental conditions, reported rate constants decreasing on the same order of magnitude of the increasing loading [64]. Similarly, Song and Carraway 2005 reported a 1,1,1-TCA reduction in which it was linear with increasing iron loading (between 0.01 to 0.05 g per 124 mL) [82], as well, Matheson and Tratnyek 1994, toward carbon tetrachloride using unbuffered granular iron [83] and Shih *et al.* 2011, during the hexachlorobenzene reduction with nanoscale zero valent iron [84]. Xie and Cwiertny 2013 suggest that the nonlinear dependence of rate constants on reductant loading is due to a system variable that limits the reactive surface area to a greater extent at high reductant loading [50].

Thus, the results herein, may be explained by the fact that iron reactivity increases linearly at low loadings and at high loadings it is already reached the apparent plateau [64], especially for the reactivity of the iron toward TCE which are also in accordance with Xie and Cwiertny 2013.

Relatively to the reactivity trend, the figure 13 also shows that it increases with increasing chlorination, i.e., TCE > *cis*-DCE. Therefore, the results here obtained are consistent if it is assumed that the reactivity should increase with increasing reduction potential whereby the degradation occurred under thermodynamic control, and due to DCE be a poorer electron acceptor than TCE [26, 29, 85]. Likewise, the results herein obtained are also in accordance with Song and Carraway 2005, that notice that the reactivity toward chlorinated ethanes and ethenes, increases with increasing chlorination, wherein the reactivity was higher for compounds with chlorine atoms more localized on a single carbon [82].

4.1.1.1. Influence of the pH during reductive dechlorination with unamended iron

As an additional experiment, the pH influence during TCE degradation under anaerobic conditions was tested, using two different loadings (125 and 250 mg) at low and high pH (2 and 11). Data obtained are plotted as a function of the natural logarithm of TCE concentration versus time on figure 14.

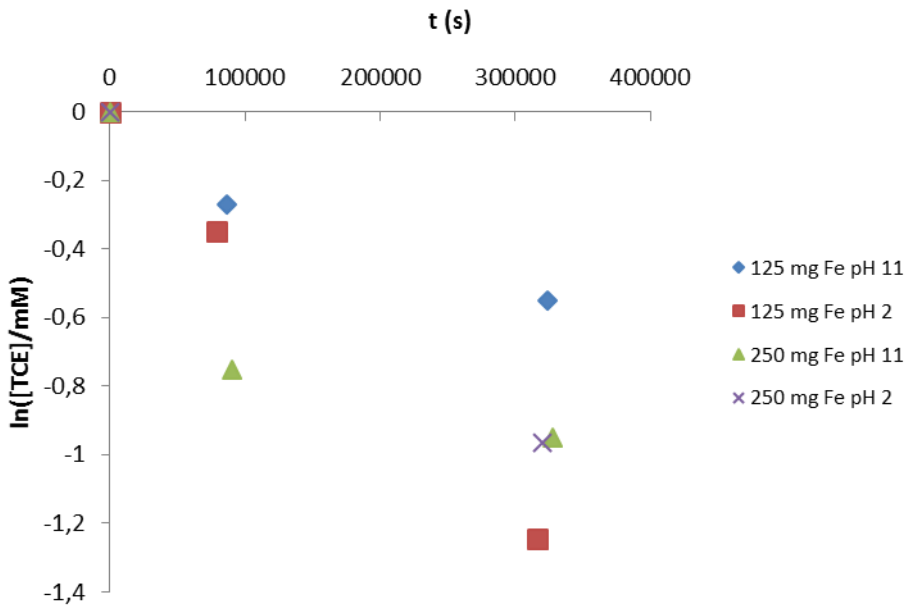

Figure 14: Plot of the natural log of TCE concentration vs time using two different loadings (125 and 250 mg) at pH 2 and pH 11.

Considering the different pH tested toward 125 mg iron, it is noticed a greater variation of the concentration at lower pH than high pH, whereby the degradation is faster at lower pH. Toward 250 mg iron, after approximately the same time, the degradation is nearly the same regarding the different pH tested. Likewise, considering the different iron loading tested toward pH 11, when used more amount of iron (250 mg) the degradation was faster, however, at pH 2 is observed an opposite trend of degradation. Noticing that when used a higher iron loading, TCE degradation is faster being in accordance, as expected, since it was performed with higher amount of Fe available and, therefore, larger surface area.

The redox potential is extremely useful insofar it allows to predict the relative quantities of oxidized and reduced elements in water, especially at a specific pH, by using Nernst equation. The Nernst equation relates the standard potential (E^0) and the activities of the chemical species involved in the cell reaction through the potential generated by an electrochemical cell [86, 87, 88], as:

eq. 9 $$E = E^0 - 2.303\frac{R\,T}{n\,F}\log[H^+]$$ [86]

where E is the half-cell reduction potential (V), R is the universal gas constant (8.314472 J K^{-1} mol^{-1}), T is the temperature (K), n is the number of moles of electrons transferred in the half-

reaction and *F* is the Faraday constant (9.64853399×10^4 C mol^{-1}) [86]. Thereafter, considering the reduction potentials at pH 2 (*E* = - 0,499 V) and 11 (*E* = - 0,765 V), without the influence of others reagents or compounds, it would be expected a faster degradation at pH 11.

However, as mentioned above, the iron corrosion is accelerated at lower pH owing to the greater availability of electrons from the iron core, whereas at high pH due to release OH^- ions during oxidation, the iron reactivity decreases [31], which explains the faster degradation at lower pH. The results here are in accordance with Chen *et al.* 2001 that verified during TCE reduction the reaction rate constant and also noticed that the iron corrosion decreased with pH [89]. As well as, Liu and Lowry 2006 that reported when decreased pH from 8.9 to 6.5, the reaction rate constant of TCE degradation doubled [90] and Shih *et al.* 2011 which described favorable acidic conditions toward hexachlorobenzene transformation by nanoscale zero-valent iron, with decreasing pH from 9.2 to 3.2 and rate constants from 0.052 to 0.12 h^{-1} [91].

4.1.2. Influence of iron-based bimetallic reductants for chlorinated ethylenes degradation

In order to obtain the maximum reactivity during TCE degradation and to compare the rate constant at the same unamended iron loading used, were tested Pd, Pt, Ni, Co, Au and Cu different loadings (Pd, Pt, Au and Cu at 2, 4, 10, 20, 30, 40 and 60 mM and Co and Ni at 20, 40, 100, 200, 300, 400, 600, 800 and 1000 mM) into iron nanoparticles by displacement plating. For Co and Ni are used higher loadings due to the fact of Cwiertny *et al.* 2006 during elemental mapping those bimetals reductants had failed to reveal particles deposited onto iron surface [56].

A pseudo-first-order rate constants of TCE degradation was applied in the same manner as described in the section 4.1.1, to test the reactivity of different additive metals loading toward 200 mg iron reactions, containing 50 mM Tris at pH 7, under anaerobic conditions. The compilation data are shown in figure 15 for Au/Fe, Pd/Fe, Pt/Fe and Cu/Fe and figure 16 for Ni/Fe and Co/Fe. Data obtained are plotted as a function of metal additive concentration toward of 200 mg unamended iron.

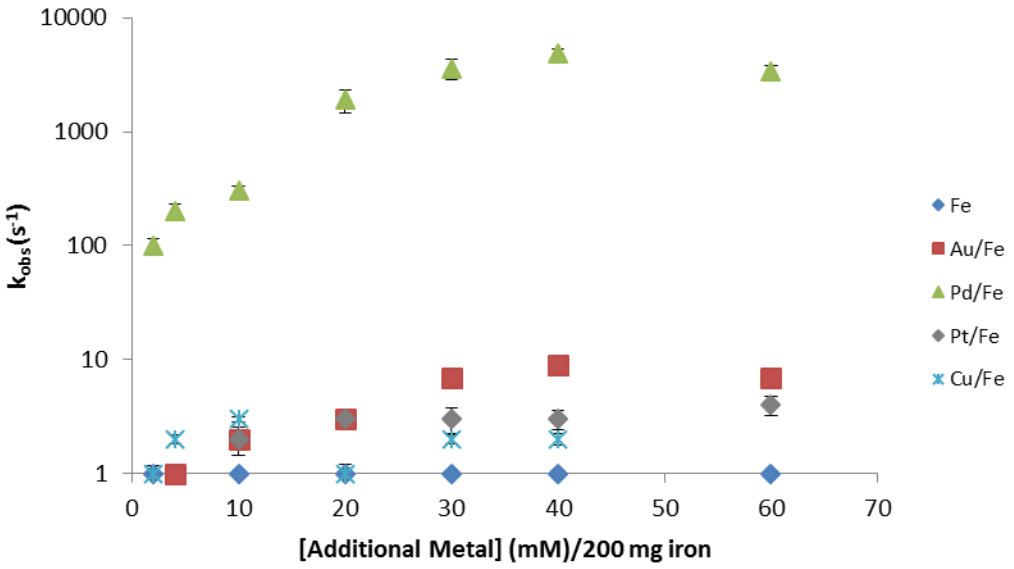

Figure 15: Values of k_{obs} for TCE reduction, on logarithmic scale, as a function of additive metals (Au, Pd, Pt and Cu) concentration toward 200 mg iron, comparing with k_{obs} for TCE reduction by unamended iron (200 mg, k_{obs} = -1.00 x 10^{-6} s^{-1}) (uncertainties represent 95% confidence intervals; if no bars are visible, they are smaller than the symbol).

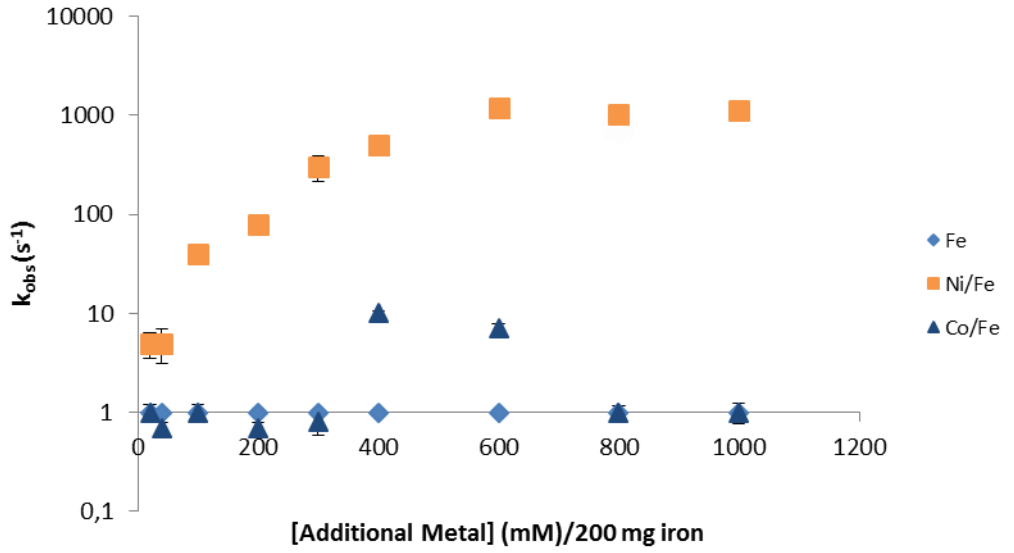

Figure 16: Values of k_{obs} for TCE reduction, on logarithmic scale, as a function of additive metals (Ni and Co) concentration toward 200 mg iron comparing with rate constant for TCE reduction by unamended iron (200 mg, k_{obs} = -1.00 x 10^{-6} s^{-1}) (uncertainties represent 95% confidence intervals; if no bars are visible, they are smaller than the symbol).

Pd/Fe, Ni/Fe, Au/Fe, Pt/Fe and Cu/Fe, generally shown an increased k_{obs} for higher concentrations of additive metal during TCE reduction and are greater than the rate constants of 200 mg unamended iron. Thus, relative reactivity of TCE reduction by iron-based bimetallic reductants, seems to be: Pd/Fe > Ni/Fe >> Au/Fe > Pt/Fe > Cu/Fe >> Co/Fe ≥ Fe. However, Co/Fe failed to exert a visible influence on rate constant. At small and higher concentrations of the metal additive applied tested, it shows similar or inhibited TCE reduction rates, comparing with unamended iron, and only at 400 and 600 mM toward 200 mg iron exhibited an increase of the k_{obs}.

To test the reactivity of different additive metals loading during *cis*-DCE degradation under anaerobic conditions, were performed similar experiments to those mentioned above (Pt, Au and Cu at 2, 4, 10, 20, 30 and 60 mM, Pd at 2, 4, 10, 20, 30, 40 and 60 mM and Co and Ni at 20, 40, 100, 200, 300, 400 and 600 mM) toward 200 mg iron reactions, containing 50 mM Tris at pH 7, prepared by displacement plating.

Figure 17, figure 18, and figure 19, show a pseudo-first-order rate constants of *cis*-DCE degradation plotted as a function of metal additive concentration toward 200 mg unamended iron, results of data compilation, also treated as the same manner as above. The first one shows the degradation rate using Au/Fe, Pt/Fe and Cu/Fe, the second one using Pd/Fe, and figure 19 for Ni/Fe and Co/Fe.

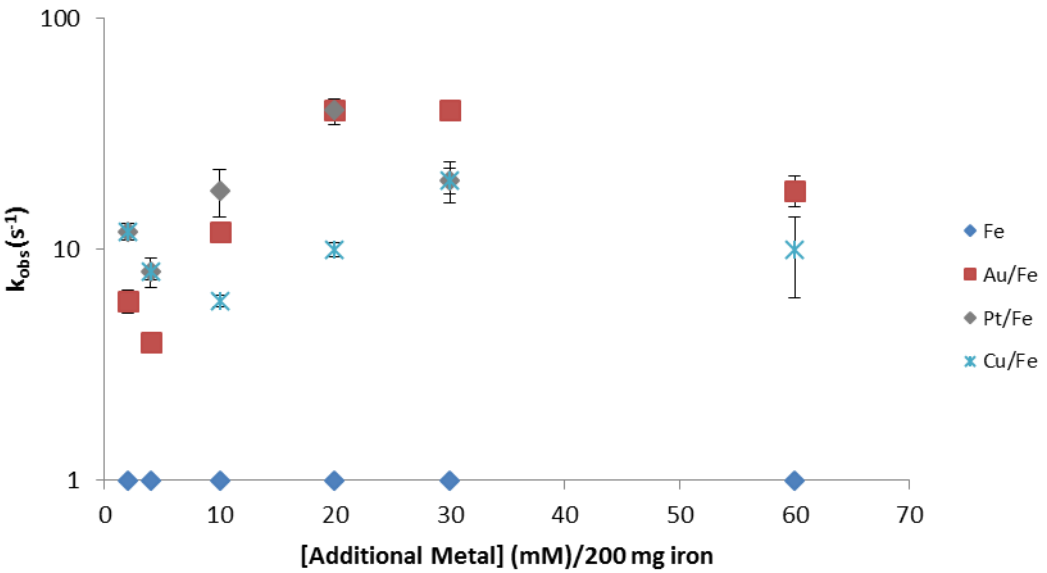

Figure 17: Values of k_{obs} for *cis*-DCE reduction , on logarithmic scale, as a function of additive metals (Au, Pt and Cu) concentration toward 200 mg iron, comparing with k_{obs} for cis-DCE reduction by unamended iron (200 mg, k_{obs} = -5.00 x 10^{-7} s^{-1}) (uncertainties represent 95% confidence intervals; if no bars are visible, they are smaller than the symbol).

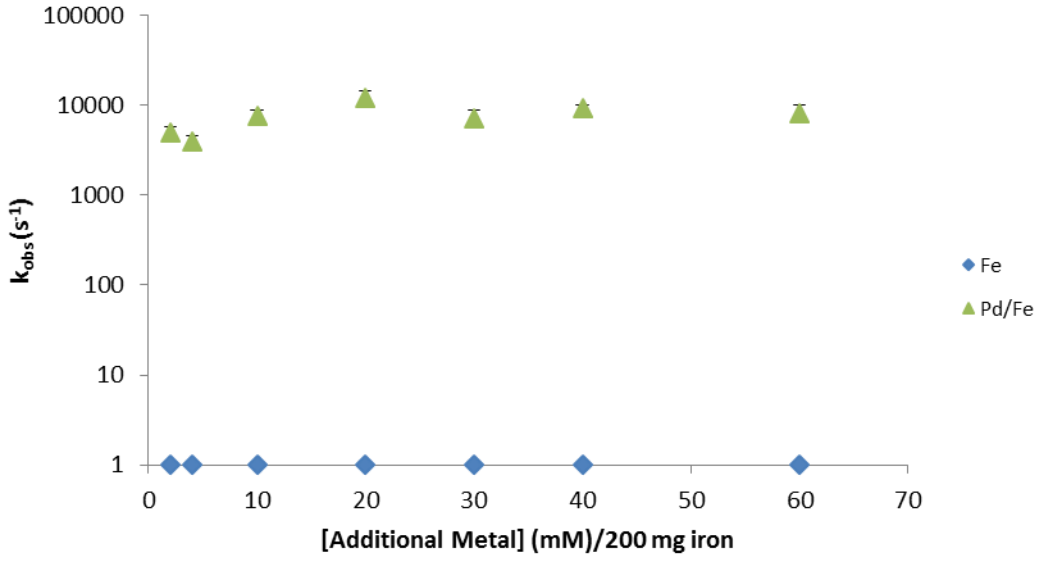

Figure 18: Values of k_{obs} for *cis*-DCE reduction, on logarithmic scale, as a function of palladium concentration toward 200 mg iron, comparing with k_{obs} for cis-DCE reduction by unamended iron (200 mg, k_{obs} = -5.00 x 10^{-7} s^{-1}) (uncertainties represent 95% confidence intervals; if no bars are visible, they are smaller than the symbol).

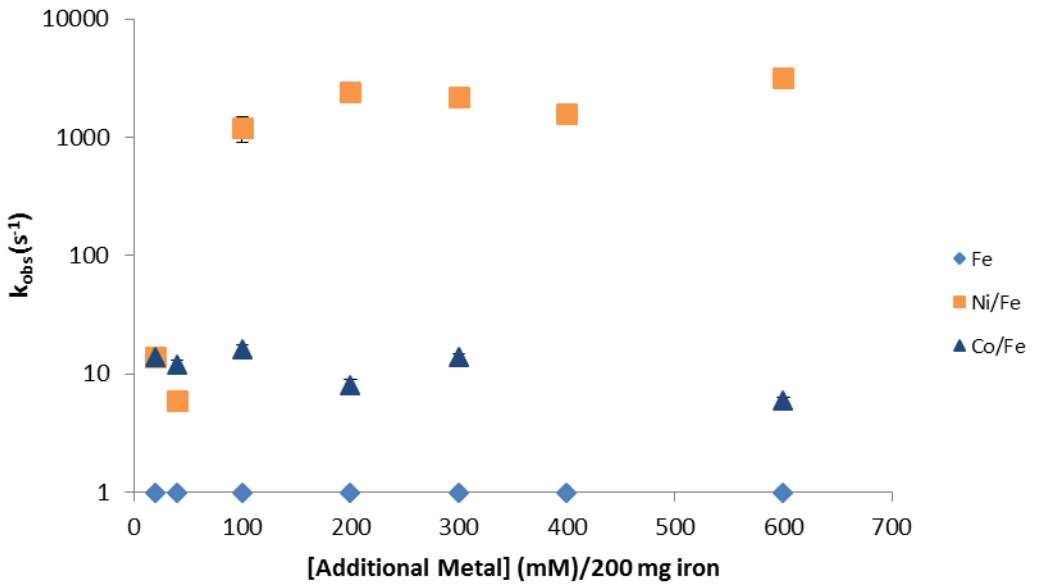

Figure 19: Values of k_{obs} for *cis*-DCE reduction, on logarithmic scale, as a function of additive metals (Ni and Co) concentration toward 200 mg iron comparing with k_{obs} for cis-DCE reduction by unamended iron (200 mg, k_{obs} = -5.00 x 10^{-7} s^{-1}) (uncertainties represent 95% confidence intervals; if no bars are visible, they are smaller than the symbol).

In general, all the bimetals increased the *cis*-DCE degradation rate constants when compared with the rate constants of 200 mg unamended iron. The relative reactivity of *cis*-DCE using bimetals, appears to be slightly different than the relative reactivity towards TCE: Pd/Fe >> Ni/Fe >> Au/ Fe > Pt/Fe > Cu/Fe ≈ Co/Fe > Fe.

When compared, it is noticed that Pd/Fe was without doubt the bimetal more reactive, following by Ni/Fe. Other studies also reported, during *cis*-DCE degradation with bimetallic reductants that Pd/Fe was more reactive than Ni/Fe, following by Pt/Fe [44]. Likewise, Ni/Fe was faster during PCE degradation comparing with Cu/Fe and Co/Fe [61] or during TCE dechlorination by Pd, Pt, Ru and Au, which followed the order of Pd/Fe >> Ru/Fe > Pt/Fe > Au/Fe [92] and, for example, during 1,1,1-TCA reduction, Ni/Fe and Pd/Fe had similar reactivity [56].

However, as reported by Cwiertny *et al.* 2006, displacement plating is able to produce a heterogeneous metallic overlayer on iron even though the elemental maps suggested they are similar, especially on Pd/Fe, Pt/Fe, Au/Fe and Cu/Fe, differing from Co/Fe and Ni/Fe systems, in which they confirmed the existence of Co and Ni particles in the near-surface region of the

reductants [56, 65]. May be for that reason that the considerable difference herein observed toward relative reactivity of the bimetals, despite of slightly differences of each additional metal, this reason cannot fully explain the reactivity trend. As Cwiertny *et al.* 2006 and Chao *et al.* 2012 reported, the results herein are also inconsistent with the galvanic couple formation, for example, whereupon Pd/Fe does not have a comparable reactivity to Au/Fe and Pt/Fe and they usually behave in similar manner in aqueous systems [56, 93].

With all this results is possible to assume that generally merely small amounts of additive metals applied onto Fe^0 are enough to cause an increased reactivity, which is in accordance with described by Xie and Cwiertny 2013. They also mentioned that toward such behavior, it implied the 1,1,1,2-TeCa reduction on the Pd deposited surface and when tested the same degradation with higher amount of palladium plated onto iron, observed a parabolic dependence between reductant loading and rate constant, suggesting multiple mechanisms for the transformation dependents on the reductant loading and additive metals coverage [50]. Somehow, the results herein support this hypothesis of multiple mechanisms for the transformation, especially when looking at figure 15 and figure 16 showing TCE rate constants toward Pd/Fe and Ni/Fe reduction, it is evident a clear parabolic behavior. However, there is no enough indications to support and generalize this hypothesis, as is the contrasting case of Co/Fe (figure 15).

It is also noticed that comparing rate constants of TCE and *cis*-DCE, the last one was more reactive towards all the bimetals reductants tested, in contrast to previously results with unamended iron. Likewise, the bimetals reductants toward *cis*-DCE degradation tend to reach the apparent plateau at lower concentration, comparing with TCE reduction. Zhang *et al.* 1998 also reported for both Fe and Pd/Fe the trend: PCE > TCE > *cis*-DCE > VC, consistent with the redox potentials [49], however, it does not agree with the results herein obtained. This difference herein observed on the reactivity may be explained by the adsorbed or absorbed atomic hydrogen associated with the additional metal, which causes somewhat altered reactivity toward chlorinated ethylenes. However, so far no evidences to support this hypothesis has been clearly found.

4.1.3. Influence of metals salt solution toward chlorinated ethylenes

To verify that iron function as primary source on the degradation of TCE and *cis*-DCE (control experiments), experiments in absence of unamended iron, iron-based bimetals and under anaerobic conditions were carried out (data shown on attachments: figure 24 to 35). In this reactions is expected no degradation of chlorinated compound due to the absence of a reductant or electron donor by which is responsible for the transformation [56]. However, the obtained results failed to the extent that the plots, generally, demonstrate an increase or decrease of the concentration, when was expected a constant behavior.

In the cases in which is observed a decrease concentration one possible explanation could be due to adsorption of the chlorinated ethylenes from water. This scenario would be expected once the experiments were carried out with headspace, however, in some point of the relevant experimental time scales the concentration should stabilize [94]. Even though, during sampling over a long monitoring period, losses can occur due to build-up of overpressure in the reaction vials.

On the other hand, when tested the behavior of palladium salt solution, the samples were withdraw over the same times scales than 10 mM palladium on 200 mg iron for both TCE and *cis*-DCE. In this case, especially for *cis*-DCE, may had not be enough time for complete dissolution of the compound and to stabilize after adding the salt solution.

However, there is no apparent reason to explain these results and this reactions should be repeated by changing some conditions, namely, i) free of headspace and ii) withdraw samples for longer time scales.

4.2. Isotope analysis

As reported above, CSIA is a powerful tool that permits the separation of organic analytes from mixtures and the determination of a target element in their individual stable isotope ratios. Experiments of TCE reductive dechlorination by unamended iron (200 mg) and iron-based bimetal reductants (Au, Pt, Cu at 60 mM and Co at 600 mM toward 200 mg iron), prepared by displacement plating, containing 50 mM Tris at pH 7 under anaerobic conditions, were performed in order to i) determine intermediates and products partitioning to compare between the different reductants (section 4.2.1), ii) determine carbon isotope fractionation

according to the Rayleigh equation, with the purpose of acquire evidence toward TCE degradation by different reductants (section 4.2.2) and iii) with dual isotope approach, to obtain additional information about the reaction mechanism toward the given slopes of the dual element isotope plots and determine chlorine and hydrogen isotope enrichment factors (section 4.2.3).

4.2.1. Influence on intermediates and product partitioning by different metal reductants

To determine TCE, intermediates and degradation products during TCE degradation, gas concentrations were quantified using Henry's Law constants [95, 96]. The next figure (figure 20 A and B) shows an example of TCE degradation in one batch experiment and its products over time by Co/Fe reductant. The lower panel is a zoom of the upper panel, without TCE, ethene, ethane and mass balance (the remaining data is shown in attachments: figure 36 to 48). In all experiments were achieved less than 40% reduction of TCE and were observed pronounced mass balance deficits that may result from losses during sampling due to build-up of overpressure in the reaction vials over a long monitoring period.

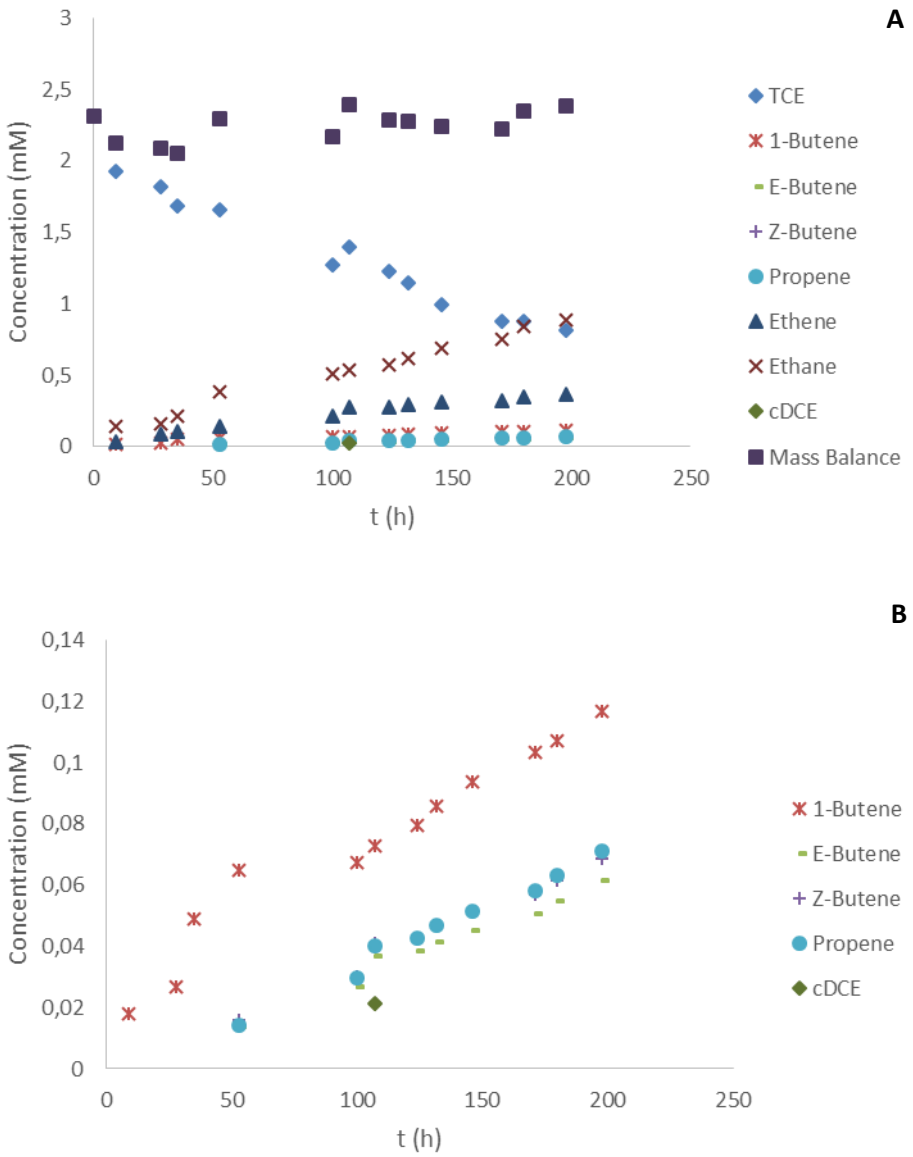

Figure 20: Degradation of TCE and its products over time in isotope experiments toward Co/Fe reductant (reaction 2) (A and B: Panel B is a zoom of Panel A without TCE, Ethene, Ethane and Mass Balance).

As mentioned above, all experiments altered TCE to favor the formation of dehalogenated products and, generally, were detected ethene and ethane, as major products at last sampling point. In unamended iron and Au/Fe reductants, ethene prevailed over ethane, while in the remaining reductants, it was observed the reverse. The three butene isomers (1-butene, *E*-butene and *Z*-butene), propene and propane were also detected in minor traces,

although in Pt/Fe and Cu/Fe experiments no propane was detected. Also, on Co/Fe experiments was possible to detect and quantify small amounts of *cis*-DCE during TCE degradation.

Similarly Han *et al.* 2016 verified during TCE dechlorination by Pd/Fe nanoparticles detection of ethane and ethene as the major products (90% and 7.2%, respectively) and no traces of DCE or VC, while for TCE reduction by monometallic iron nanoparticles, identified ethene and C_4 products as the major end products [62]. Likewise, Elliott and Zhang 2001 described that after complete degradation of TCE by Pd/Fe nanoparticles, the major end products were ethene and ethane, and by unamended iron was only ethene [97]. The results herein are also in agreement with Arnold and Roberts 2000 which reported that ethene may be formed by hydrogenolysis through vinyl chloride and, therefore, over *cis*-DCE, or by β-elimination pathway through acetylene due to production of major coupling products, such as C_3 and C_4 hydrocarbons [26]. On the other hand, the results may also suggest simultaneous hydrogenolysis and β-elimination (as parallel) as in accordance with Audí-Miró *et al.* 2013 [13].

4.2.2. Isotope fractionation according to the Rayleigh equation

Enrichment factors for carbon of unamended iron and iron-based bimetallic reductants during TCE degradation were determined according to the Rayleigh equation (eq. 6) to acquire evidence toward the target compound degradation by different reductants.

The next figure (figure 21) shows the Rayleigh plot for carbon with results of data compilation from duplicate experiments and from sacrificial batch experiments, for both unamended iron and bimetals systems (Au/Fe, Pt/Fe, Co/Fe and Cu/Fe) tested.

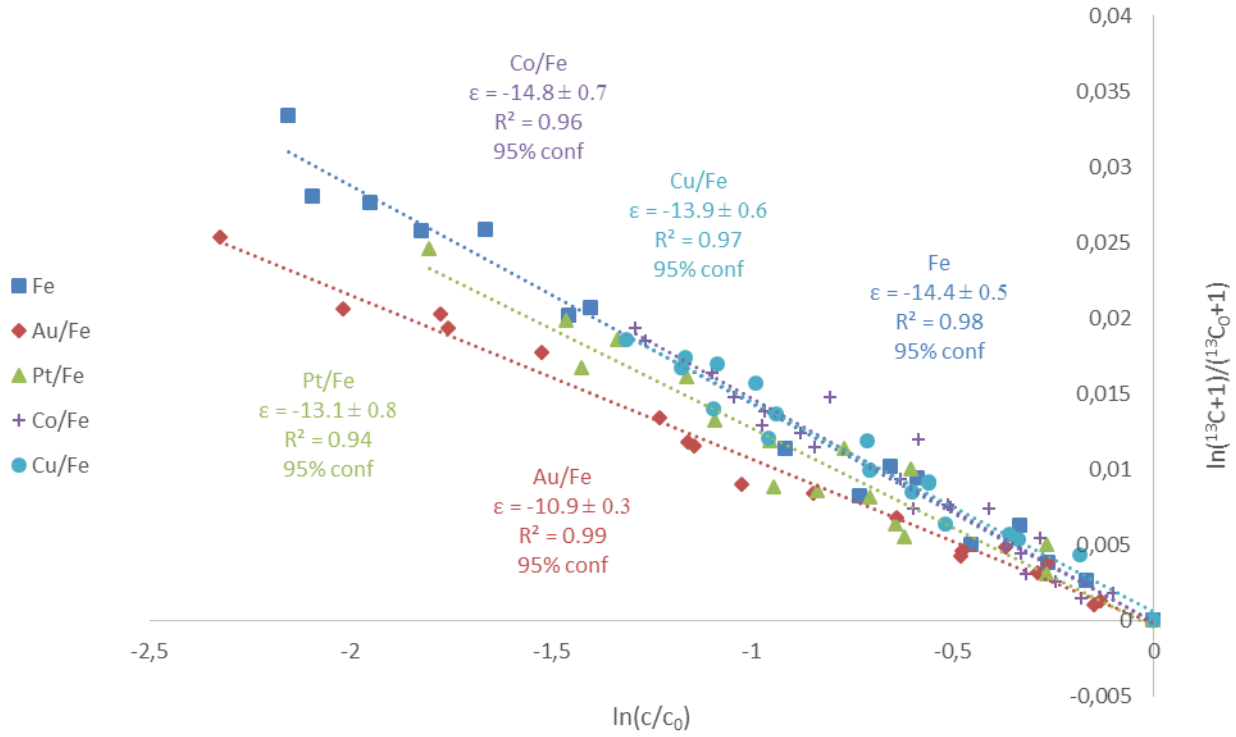

Figure 21: Rayleigh plot for C during TCE reduction by nanoparticles of zero valent iron and iron-based bimetals (Au/Fe, Pt/Fe, Co/Fe and Cu/Fe) (uncertainties for given ε are 95% confidence intervals).

Enrichment in ^{13}C for the first step of the degradation was observed in all experiments, confirming carbon fractionation and TCE degradation by unamended iron and bimetals tested. The highest enrichment factor value obtained was toward Co/Fe (ε = -14.8 ± 0.7), followed by unamended iron nanoparticles (ε = -14.4 ± 0.5‰), Cu/Fe (ε = -13.9 ± 0.6‰), Pt/Fe (ε = -13.1 ± 0.8‰) and Au/Fe (-10.8 ± 0.3‰), respectively.

Interestingly, this trend is the opposite of that obtained previously on section 4.1.2 regarding to the influence of iron-based bimetallic reductants for TCE degradation. These results show variable extent of isotope fractionation on TCE transformation. Although the type of iron used for all experiments was the same, C enrichment factors may diversify. For example, Elsner *et al.* 2008 chosen two different types of iron to simulate different methods of synthesis. With Fe^{BH} (produced by reduction of dissolved Fe^{II} by $NaBH_4$) obtained ε_C = -23.5‰ and with Fe^{H2} (by goethite and hematite reduction with H_2 gas at 200-600˚C) acquired an enrichment factor from -20.9‰ to -26.5‰ [79]. Nevertheless, according to Audí-Miró *et al.*

2013, several studies had reported carbon enrichment factors ranging from -8.6‰ to -27‰ [13], suggesting that not only the type of iron may have some influence, but also the different systems used for degradation of TCE.

On the other hand, all the reductants tested revealed similar enrichment factors on the initial reaction step, despite the slightly lower value of Au/Fe (ε_C = -10.8‰). Han *et al.* 2016 during TCE dechlorination by fresh Fe and Pd/Fe nanoparticles, reported carbon enrichment factors of -15.6‰ and -1.4‰, respectively [62]. When compared these values with the values herein obtained for bimetals reductants, they are not in accordance and it is visible a big discrepancy. They mentioned that ε_C toward bimetal nanoparticles is characteristically small and may be due to the fact of the facilitated bond-breaking on Pd surface [62]. In fact, palladium (and nickel) plated onto iron exhibits much higher reactivity than any of the other additional metals herein tested, as verified above on section 4.1.2. However, such values cannot be directly compared due to de fact of one element enrichment factors do not be typical of the intrinsic isotope effects on the reaction and masking effects may be the reason of decreased enrichment trends to an unknown degree [22].

In contrast, comparing the values herein acquired for unamended iron nanoparticles, with Han *et al.* 2016 and taken into account the range mentioned above, the values are consistent, even though slightly different. Moreover, the high variability of carbon enrichment factors reported in several studies can be explained by rate-limiting steps owing to high reactivity of the metal, in which exhibit small or no isotope fractionation [98].

4.2.3. Dual isotope approach

Dual element isotope plots are a powerful tool to obtain additional information about the reaction mechanism once only analyzing individual isotope effects can be problematic. In the following figure is present the proportion of Cl isotope fractionation to C isotope fractionation (2D-CSIA) during TCE degradation.

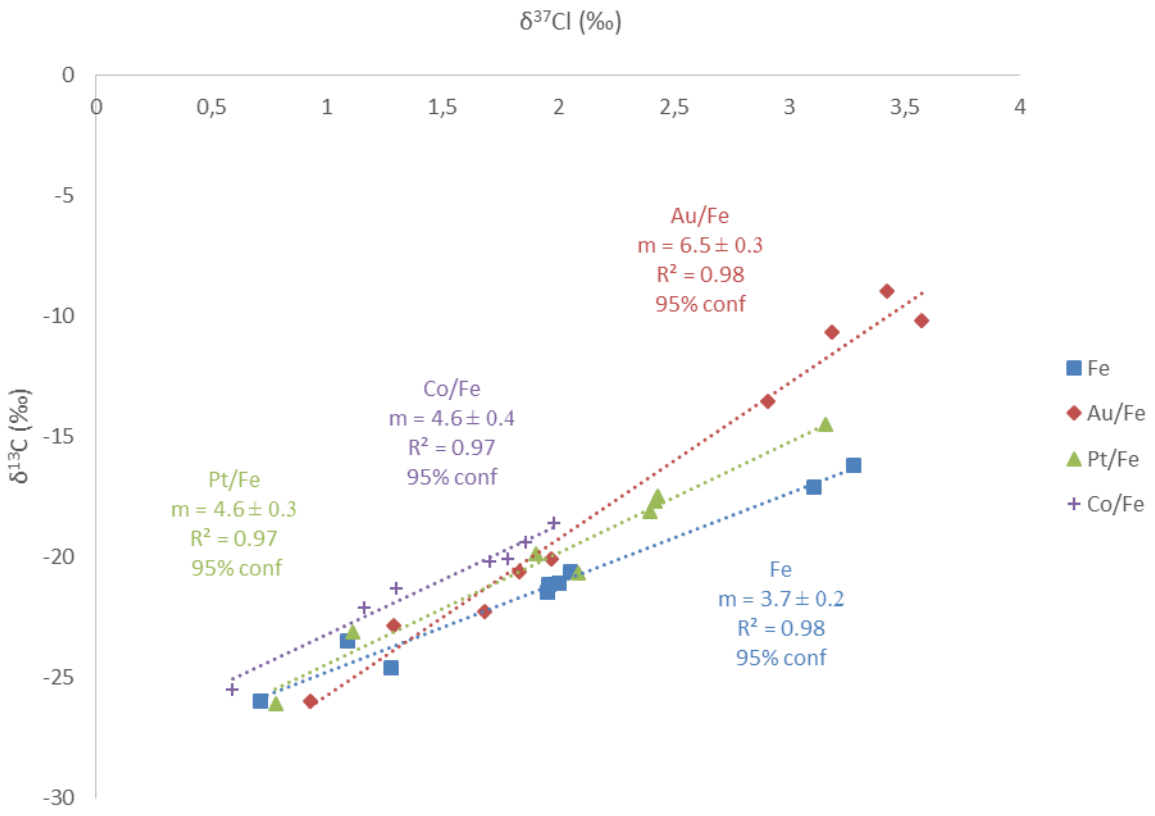

Figure 22: Dual isotope plot of $\delta^{13}C$ versus $\delta^{37}Cl$ during TCE degradation in the additional experiments (uncertainties for given slopes are 95% confidence intervals).

Generally, the reductants show a linear relation between $\delta^{13}C$ and $\delta^{37}Cl$ and, somehow, also show a parallel trend. TCE transformation by Au/Fe is highlighted by having the most discrepant and, therefore, higher slope of 6.5 ± 0.3. In contrast, the reduction by unamended iron, Pt/Fe and Co/Fe showed a very close slope of 3.7 ± 0.2, 4.6 ± 0.3 and 4.6 ± 0.4, respectively.

Different slopes are the result of the difference in ε_C and ε_{Cl} values for each reductant obtained above. Usually, these different results points out for different mechanisms associated [21]. For example, Cretnik *et al.* 2013 compared the dual element slopes toward cobalamine (m = 3.9), cobaloxime (m = 6.1) and dehalogenating bacteria (m = 3.4), and hypothesized that TCE transformation with cobaloxime may have a different rate-determining step [22]. On the other hand, Palau *et al.* 2014 obtained $\delta^{13}C$ vs $\delta^{37}Cl$ slopes of 1.5 and 0.33 for 1,1,1-TCA degradation by Fe^0 and using hydrolysis/dehydrohalogenation, emphasizing the potential of this methodology to identify abiotic degradation pathways once, despite of the distinctly

different slopes obtained, both reaction pathways involve cleavage of a C-Cl bond in the initial reaction step [98].

Therefore, with the results herein obtained, it is suggested that the degradation mechanism for the first reaction step of TCE by Au/Fe may be different. In addition, the reduction by Au/Fe showed that chlorine isotope effects are smaller than carbon, whereas degradation by the others reductants has a stronger chlorine isotope effect.

In this study was also used another approach to determine enrichment factors for chorine and hydrogen: by 2D-CSIA plots. Therefore, considering the follow equation:

eq. 10 $$\frac{\Delta\delta^{13}C}{\Delta\delta^{37}Cl} \approx \frac{\varepsilon_C}{\varepsilon_{Cl}}$$ [99]

where $\Delta\delta^{13}C$ and $\Delta\delta^{37}Cl$ are the differences in carbon and chlorine isotope ratios between time *t* and zero, the equation demonstrates that the slope of dual element plots (in this case $\delta^{13}C$ vs $\delta^{37}Cl$) should correspond to the ratio of ε_C and ε_{Cl} [99]. Thus, by using the provided slope above is possible to obtain ε_{Cl} for all reductants.

Although the different approach to obtain the enrichment factor, chlorine fractionation was also observed by the enrichment in ^{37}Cl for all experiments tested through TCE transformation. Fe, Co/Fe and Pt/Fe achieved the most pronounced chlorine enrichment factor values of -4.0‰, -3.2‰ and -2.7‰, respectively, while Au/Fe obtained the lower value of -1.7. Chlorine isotope effects are expected to be lower than isotope effects for carbon due to its larger relative mass difference between heavy and light isotopes [98]. Moreover, the calculated chlorine enrichment factors also supports the discussed above, i.e., the degradation by Au/Fe has a weakest chlorine isotope effect on the first reaction step.

Other studies, namely Audí-Miró *et al.* 2013 achieved ε_{Cl} = -2.6‰ on TCE transformation with ZVI [13] and Sakaguchi-Söder *et al.* 2007 determined -2.4‰ during the reductive dechlorination of TCE in a batch experiment using zero-valent iron [100]. When comparing these last mentioned with the ε_{Cl} values of Pt/Fe, Co/Fe and Fe reductants obtained, the values are a little high but closest, while Au/Fe has a much lower value for the same step.

The figure below shows the proportion of C isotope fractionation to H isotope fractionation (2D-CSIA) during TCE degradation.

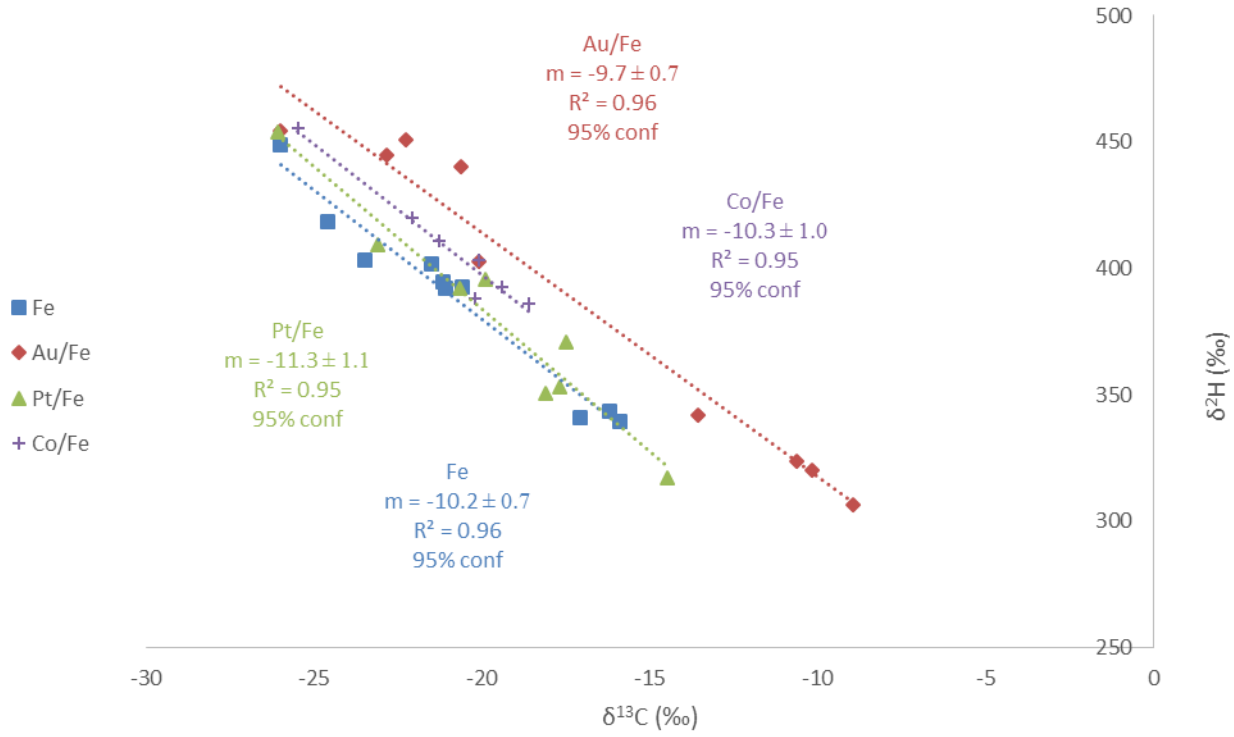

Figure 23: Dual isotope plot of δ^2H versus $\delta 1^3C$ during TCE degradation in the additional experiments (uncertainties for given slopes are 95% confidence intervals).

Generally, the reductants show a parallel trend, however, do not show a precise linear relation between δ^2H and $\delta^{13}C$, as comparing with the dual isotope plot of $\delta^{13}C$ versus $\delta^{37}Cl$. Here, the slopes are also slightly similar. The first step of TCE transformation by Pt/Fe, Co/Fe, unamended iron and Au/Fe resulted in the slopes of -11.3 ± 1.1, -10.2 ± 0.7, -10.3 ± 1.0 and -9.7 ± 0.7, respectively. Different slopes also result from the difference in ε_H and ε_C values for each reductant obtained above. As reported in several studies [21, 101], an inverse isotope effect is observed. Depletion of δ^2H for all reductants are the result of the strong steric restrictions of the hydrogen atom during protonation of TCE throughout its degradation.

As mentioned above, hydrogen enrichment factors for the first step of the degradation were also calculated through 2D-CSIA plot. Here, unamended iron obtained the higher ε_H value of 158.8‰, Co/Fe with 150.9‰, and lastly, 142.0‰ toward Pt/Fe, while the hydrogen enrichment factor by Au/Fe was 105.3‰. This obtained results are once again an evidence that support the possibility of different mechanism throughout the initial step of TCE degradation,

by the large discrepancy in the hydrogen enrichment factors toward Au/Fe, comparing with remaining reductants evaluated in this section.

To the authors' knowledge, no dual isotope plot of $\delta^{2}H$ versus $\delta 1^{3}C$ during TCE degradation toward zero valent iron nanoparticles nor iron-based bimetals reductants, therefore, no comparison can be performed.

Moreover, with such evidences from the slope of the dual isotope plot of $\delta^{13}C$ versus $\delta^{37}Cl$ and carbon, chlorine and hydrogen enrichment factors it is assumed that the first step of TCE degradation by Au/Fe is different. However, it remains to discriminate the possible mechanisms herein involved. Therefore, looking at the results discussed on section 4.2.1, the only intermediate detected and quantified during TCE degradation was *cis*-DCE by Co/Fe reductant. Considering that Co/Fe, Pt/Fe and unamended iron have the same mechanism involved for the first reaction step, even it was not possible to detect and quantify the same intermediate with both Pt/Fe and Fe reductants, it cannot be directly assumed that no *cis*-DCE was formed throughout TCE degradation. In fact, as discussed on section 4.1.2, it was found that *cis*-DCE was more reactive than TCE towards all the bimetals reductants tested, whereby vinyl chloride can also be more reactive than *cis*-DCE by the same conditions and, thus, explain why this compound was not detected. In addition, thereafter the first reaction step, it remains unclear whether the degradation continues through β-elimination or hydrogenolysis for each reductant. As a consequence, it is possible to assume that TCE may undergo preferably by hydrogenolysis toward Pt/Fe, Co/Fe and Fe reductants on the first step, while with Au/Fe, TCE reduction goes preferably by β-elimination for the same step.

5. Conclusion

The general aim of this study was to evaluate the reductive dechlorination of TCE and *cis*-DCE by zero-valent iron and iron-based bimetallic reductants, using the kinetics and 2D compound specific isotope effects of the degradation as approach.

The main conclusions derived from the study of kinetics were:

- TCE reductive dechlorination confirmed to be faster at low pH by unamended iron nanoparticles.
- Generally the bimetal reductants tested (Pd/Fe, Ni/Fe, Au/Fe, Pt/Fe, Cu/Fe and Co/Fe) revealed to increase the reactivity of chlorinated ethylenes (TCE and *cis*-DCE) degradation, when compared with unamended iron nanoparticles, and merely small amounts of the additional metal are enough to increase the reactivity.
- Palladium confirmed to be the additional metal more reactive, followed by nickel, on both chlorinated ethylenes tested.
- Similar trends for the bimetallic reductants during chlorinated ethylenes degradation but different reactivities were obtained: Pd/Fe >> Ni/Fe >> Au/ Fe > Pt/Fe > Cu/Fe ≈ Co/Fe > Fe throughout TCE degradation, while Pd/Fe > Ni/Fe >> Au/Fe > Pt/Fe > Cu/Fe >> Co/Fe ≥ Fe for *cis*-DCE.
- *cis*-DCE revealed to be more reactive than TCE toward bimetal reductants, but when used only iron nanoparticles, TCE is more reactive.
- No apparent elucidation was confirmed to explain the high reactivity on bimetals systems, nevertheless, it is supported the hypothesis of the galvanic cell formation do not play a role on the degradation.

Regarding to the isotope analysis the main conclusions were:

- Ethene and ethane were confirmed to be the major products of TCE reductive dechlorination by iron nanoparticles and iron-based bimetallic reductants (Au/Fe, Pt/Fe, Cu/Fe and Co/Fe), while C_3 and C_4 compounds revealed as the minor products.
- The hypothesis of simultaneous hydrogenolysis and β-elimination (as parallel) throughout TCE reduction is supported.

- TCE degradation on the first reaction step by Au/Fe undergoes preferably by β-elimination, whereas the reduction by unamended iron, Pt/Fe and Co/Fe goes preferably by hydrogenolysis for the same step.

Overall, the study of kinetics allowed to evaluate the reactivity of different reductants during TCE and *cis*-DCE reductive dechlorination and 2D-CSIA proved to be a good tool, in order to take a step forward, to acquire more knowledge on the degradation mechanism of TCE toward different iron-based bimetallic reductants. Therefore, more laboratory experiments would be necessary to better understand the role of the additional metal plays on the mechanism of chlorinated ethylenes degradation.

6. Experimental Section

All of the experiments were performed in the Institute of Groundwater Ecology of the Helmholtz Zentrum München, Germany.

6.1. Chemicals

Iron nanopowder (40-60 nm, 99%, Aldrich) and the following additional metal salts were used to generate bimetallic reductants: copper(II) chloride dehydrate (99%, Merck), cobalt(II) chloride hexahydrate (99%, Merck) gold(III) chloride trihydrate (99,9%, Aldrich), potassium hexachloroplatinate(IV) (98%, Aldrich), potassium hexachloropalladate(IV) (99%, Aldrich), nickel(II) chloride hexahydrate (98%, Merck). The metal salt solutions, buffer solution of 50 mM Tris (Trizima base, 99,9%, Sigma) and 1 M HCl (hydrochloric acid fuming, 37%, Carl Roth) and 1 M NaOH (sodium hydroxide, 98%, Sigma Aldrich) were deoxygenated by sparging (1 h/L) with N_2 before used.

All solutions were stored within an anaerobic chamber (95% N_2/5% H_2 atmosphere) until use as well TCE (98%, Merck) and *cis*-DCE (98%, Merck).

6.2. Kinetics

6.2.1. Preparation of bimetallic reductants

The preparation of bimetallic reductants was preformed based on the method used by Cwiertny *et al.* 2006 [56], adapted to this study. Briefly, in an anaerobic chamber, before the displacement plating, were added 3 mL of water to 200 mg of iron nanoparticles. The iron nanoparticles in suspension were acid-wash pretreated by adding 0.3 mL of 1M HCl, for a few seconds to remove surface oxides and increase the iron surface area, and added 1M NaOH to neutralize. The displacement plating was accomplished by adding 3 mL of a metal additive salt solution to the acid-washed and water-rinsed iron, following by stirring by hand for 5 to 10 min, providing necessary time to proceed to completion for Pd, Pt, Cu and Au and to reach equilibrium for the Ni and Co. For Ni and Co, the range used was of 20 mM to 1000 mM whereas for Pd, Pt, Cu and Au the range was of 2 mM to 60 mM.

The slurry was immediately used.

6.2.2. Experiments with unamended iron reductants (Control experiments)

The experiments with unamended iron were carried out to simulate the conditions of displacement plating of bimetallic reductants. The iron nanoparticles in suspension were acid-wash, pretreated with 1M HCl for a few seconds and the same amount of 1M NaOH was added. The slurry was immediately used.

Experiments in the absence of unamended iron and iron-based bimetals were also carried out with salt solution of each metal (10 mM for Au, Cu, Pt and Pd and 100 mM for Ni and Co).

6.2.3. Batch experimental procedure

The experiments were conducted in 40 mL vials sealed with Screw-Cap Mininert Valves (Supleco), within an anaerobic chamber at room temperature. The vials were covered with aluminum foil to avoid photolytic oxidation of chlorinated ethylenes and were put in a magnetic stirrer to preserve maximum contact between the nanoparticles and the contaminants.

All the 40 mL vials were filled with 30 mL of deoxygenated water containing 50 mM Tris at pH 7 (pH values correspond to the solution pH prior to move to within of the anaerobic chamber). The pH was adjusted by using 1M solutions of HCl or NaOH. Subsequently, were added 6 µL TCE or 5 µL *cis*-DCE and were stirred for approximately 24h to allow the complete dissolution. The reactors were initially free of headspace after added the bimetallic reductants or unamended iron. In the experiments, in absence of unamended iron and bimetals (control experiments), only was added 3 mL of salt solution of each metal, leaving headspace.

Over the relevant experimental time scales, 1 mL samples were withdrawn from the reactors through the Minninert valve and were immediately frozen.

In the cases that the experimental times scales were too short, 20 mL deoxygenated H_2O containing 50 mM Tris at pH 7 were added to 40 mL vials. Consequently, were added 4 µL TCE or 3.4 µL *cis*-DCE to the vials and were stirred for 24h. After the bimetallic reductants addition and, over the relevant experimental time scales, were withdrawn 0,1 mL samples from

the headspace of the reaction bottles through the Minninert valve by a Pressure-Lok® Analytical Syringe (VICL) with sideport taper needle and immediately analyzed.

6.2.4. Kinetic modeling

To investigate the metal additives rate constants for the degradation of TCE and *cis*-DCE, concentrations were determined from experimental time course data using linear regression methods, accordingly with equation 4. The accuracy of the concentration was determined by calibration curves of the chlorinated ethylenes standards.

6.2.5. Gas chromatography

The samples were analyzed by gas chromatography (GC) coupled to a mass spectrometer (MS) (Agilent 7890A) equipped with a 30 m VOCOL column, 0.25 μm inner diameter. The temperature program was of 50˚C (3 min), increasing at 10˚C/min to 80˚C (2 min) and 30˚C/min to 180˚C (2 min). The carrier gas was helium at 1.6 mL/min flow rate. This temperature program allowed separation of the chlorinated ethylenes.

1 mL frozen samples were unfrozen and of which 300 μL were transferred to an autosampler vial and subsequently analyzed. The remaining sample was frozen again. In the cases that the samples were withdraw through the headspace, the analysis was done by direct injection.

The standards to the calibration curves were analyzed in identical manner.

6.3. Isotope analysis

6.3.1. Concentration and Carbon Isotope analysis

6.3.1.1. Preparation of bimetallic reductants

In an anaerobic chamber, before the displacement plating, were added 6 mL water to 400 mg iron nanoparticles. The iron nanoparticles in suspension were acid-wash pretreated by adding 0.6 mL of 1M HCl and adding the same amount of 1M NaOH. The displacement plating was accomplished by adding 6 mL of a metal additive salt solution (600 mM for Co and 60

mM for Pt, Au and Cu) to the acid-washed and water-rinsed iron, following by stirring by hand for 5 to 10 min. In the case of the unamended iron were added 6 mL H_2O to the acid-washed and water-rinsed iron.

The slurry was immediately used.

6.3.1.2. Batch experimental procedure

The experiments were conducted in duplicate in 40 mL vials sealed with Screw-Cap Mininert Valves, within an anaerobic chamber at room temperature, which were put in a magnetic stirrer and covered with aluminum foil.

Initially was prepared a 60 mL vial filled up with 60 mL deoxygenated H_2O containing 50 mM Tris at pH 7 and 18 µL TCE, that stirred approximately 24h. Subsequently, in the 40 mL vials were added 6.6 mL of iron or bimetal slurry (prepared immediately before) and filled with 15 mL of the solution with TCE of the 60 mL vial, leaving 18.4 mL of headspace.

Samples were taken from the headspace of the reaction bottles through the Minninert valve by a Pressure-Lok® Analytical Syringe (0.5 mL for concentration analysis and 0.2 mL to 1 mL to carbon isotope analysis), at the relevant experimental time scales. Headspace sampling from the same bottle for concentration and carbon isotope measurements were performed sequentially and immediately analyzed to obtain values at the same time point, whereas the duplicate was sampled and analyzed right afterwards.

6.3.1.3. Concentration and carbon isotope analysis

Analysis of compound concentrations was performed on a gas chromatograph coupled to a mass spectrometer (GC-MS) equipped with a 60 m Q-PLOT column, 0.25 mm inner diameter, using helium as the carrier gas at 1,6 mL/min flow rate. The temperature program used was of 40˚C (9 min), increasing at 15˚C/min to 53˚C (2.7 min), at 13˚C/min to 134˚C (3.3 min) and at 20˚C/min to 200˚C (23 min). This temperature program allowed separation of the chlorinated ethylenes and chlorinated ethylenes byproducts.

Carbon isotope analysis of TCE and their byproducts were conducted on a GC-C-IRMS system (Thermo Scientific) consisting of a Trace GC, equipped with a 60 m Q-PLOT column, 0.25 mm inner diameter, connected to a MAT 253 IRMS through a GC/C III combustion

interface, by injection of headspace samples. The GC temperature program used was 35˚C (9 min), increasing at 15˚C/min to 53˚C (2.7 min), at 13˚C/min to 134˚C (3.3 min) and at 10˚C/min to 200˚C (13 min), using helium as the carrier gas. Standards were measured daily for calibration in a manner identical.

6.3.2. Concentration, Carbon, Chlorine and Hydrogen Isotope analysis (additional experiments)

6.3.2.1. Preparation of bimetallic reductants

The bimetallic reductants were prepared in a manner identical to described above at 6.3.1.1 section.

6.3.2.2. Batch experimental procedure

The experiments were conducted in nine 8 mL vials, covered with aluminum foil and put in a magnetic stirrer, within an anaerobic chamber, where the vials were prepared at the same starting points but were sacrificed at different times, over the relevant experimental time scales.

Firstly, was prepared a 60 mL vial filled up with 60 mL of deoxygenated H_2O containing 50 mM Tris at pH 7 and 20 μL TCE. After it stirred for approximately 24h, in the 8 mL vials were added 1 mL of slurry bimetal (prepared immediately before) and filled with 5 mL of the solution with TCE, of the 60 mL vial, prepared above.

Samples were taken in an identical manner as described above at section 6.3.1.2, although for chlorine isotope measurements, liquid samples were withdrawn from the reactors through the Minninert valve and were immediately frozen (0.3 mL). Headspace sampling were performed for concentration and carbon isotope and instantly analyzed to obtain values at the same time point. For hydrogen isotope measurements, the vials were immediately frozen and stored assuming the same conditions.

6.3.2.3. Concentration and Dual Element isotope analysis

Analysis of compound concentrations and carbon isotope analysis were performed in an identical manner as described above at section 6.3.1.3.

Chlorine isotope analysis was carried out on a GC-IRMS system (Thermo Scientific) consisting of a Trace GC that was connected to a MAT 253 IRMS with dual inlet system *via* a heated transfer line. The gas chromatograph was equipped with a 30 m VOCOL column, 0.25 mm inner diameter. The GC temperature program used was 70˚C (2 min), increasing at 10˚C/min to 100˚C (3 min) and at 60˚C/min to 172˚C (1.2 min). Standards were measured for calibration in an identical manner.

Hydrogen isotope analysis was accomplished by using a purge and trap Teledyne-Tekmar XPT concentrator (Teledyne-Tekmar) coupled to an Agilent 6890 GC and a Deltaplus XL CF-IRMS (ThermoFinnigan) equipped with a chromium reduction (R) system. The gas chromatograph was equipped with a 30 m VOCOL column, 0.25 mm inner diameter. The GC temperature program used was 50˚C (12 min), increasing at 25˚C/min to 80˚C (2 min) and at 30˚C/min to 180˚C (3 min).

7. References

1. Dunlap, R. E. and Jorgenson, A. K. Environmental problems. George Ritzer. *The Wiley-Blackwell Encyclopedia of Globalization.* Blackwell Publishing Ltd, 2012.

2. *Lenntech BV* . [Online] [Cited: 08 21, 2016.] http://www.lenntech.com/environmental-problems.htm.

3. *The relationship between land use and groundwater resources and quality.* Lerner, D. N. and Harris, B. Land Use Policy, 2009, Vols. 26S: S265-S273.

4. Fried, J. J. Groundwater Pollution. V. T. Chow. *Developments in Water Science.* Elsevier, 1975.

5. [Online] [Cited: 08 21, 2016.] http://www.groundwater.org/get-informed/groundwater/contamination.html.

6. *Review of risk from potential emerging contaminants in UK groundwater.* Stuart, M., Lapworth, D., Crane, E. and Hart, A. Science of the Total Environment, 2012, Vols. 416: 1-21.

7. *Emerging organic contaminants in groundwater: A review of sources, fate and occurrence.* Lapworth, D. J., Baran, N., Stuart, M. E. and Ward, R. S. Environmental Pollution, 2012, Vols. 163: 287-303.

8. *Abiotic degradation of chlorinated ethanes and ethenes in water.* Tobiszewski, M. and Namieśnik, J. Environmental Science and Pollution Research, 2012, Vols. 19: 1994–2006.

9. *Vitamin B12-mediated hydrodechlorination of dichloromethane by bimetallic Cu/Al particles.* Huang, C., Lo, S. and Lien, H. Chemical Engineering Journal, 2015, Vols. 273: 413-420.

10. *Electrocatalytic properties of transition metals toward reductive dechlorination of polychloroethanes.* Huang, B., Isse, A. A., Durante, C., Wei, C. and Gennaro, A. Electrochimica Acta, 2012, Vols. 70: 50-61.

11. *Establishing the trichloroethene dechlorination rates of palladium-based catalysts and iron-based reductants.* Li, S., Fang,Y., Romanczuk, C. D., Jin, Z., Li, T. and Wong, M. S. Applied Catalysis B: Environmental, 2012, Vols. 125: 95-102.

12. The Priority List of Hazardous Substances. [Online] Agency for Toxic Substances and Disease Registery . [Cited: 08 28, 2016.] https://www.atsdr.cdc.gov/spl/.

13. *Cl and C isotope analysis to assess the effectiveness of chlorinated ethene degradation by zero-valent iron: Evidence from dual element and product isotope values.* Audí-Miró, C., Cretnik, S., Otero, N., Palau, J., Shouakar-Stash, O., Soler, A. and Elsner, M. Applied Geochemistry, 2013, Vols. 32: 175–183.

14. Stroo, H. F. and Ward, C. H.. *In Situ Remediation of Chlorinated Solvent Plumes.* Springer Science & Business Media, 2010.

15. *Review of Abiotic Degradation of Chlorinated Solvents by Reactive Iron Minerals in Aquifers.* He, Y. T., Wilson, J. T., Su, C. and Wilkin, R. T. Groundwater Monitoring & Remediation, 2015, Vols. 35(3): 57–75.

16. Jong, F.M.W. , Posthuma-Doodeman, C.J.A.M. and Verbruggen, E.M.J. *Ecotoxicologically based environmental risk limits for several volatile aliphatic hydrocarbons.* National Institute for Public Health and the Environment, 2007.

17. *Dechlorination mechanism of 2,4-dichlorophenol by Ni/Fe nanoparticles in the presence of humic acid.* Wo, J., Zhang, Z. and Xu, X. Journal of Zhejiang University Science A, 2009, Vols. 10(1): 121-126.

18. Heck, K. N. *Developing gold-based nanostructures to study catalytic reactions in water.* PhD diss., Texas: Rise University, 2009.

19. Miró, C. A. *Compound Specific Isotope Analysis (13C, 37Cl, 2H) to trace induced attenuation of chlorinated organic contaminants in groundwater.* PhD diss., Barcelona : Universitat de Barcelona, 2014.

20. Velimirovic, M. *Use of injectable Fe-based particles for in-situ treatment of contaminated groundwater.* PhD diss., Belgium: Universiteit Antwerpen, 2013.

21. *3D-CSIA: Carbon, Chlorine, and Hydrogen Isotope Fractionation in Transformation of TCE to Ethene by a Dehalococcoides Culture.* Kuder, T., Breukelen, B. M., Vanderford, M. and Philp, P. Environmental Science & Technology, 2013, Vol. 47: 9668−9677.

22. *Reductive Dechlorination of TCE by Chemical Model Systems in Comparison to Dehalogenating Bacteria: Insights from Dual Element Isotope Analysis (13C/12C, 37Cl/35Cl).*

Cretnik, S., Thoreson, K. A., Bernstein, A., Ebert, K., Buchner, D., Laskov, C., Haderlein, S., Shoukar-Stash, O., Kliegman, Sarah., McNeill, K. and Elsner, M. Environmental Science & Technology, 2013, Vol. 47: 6855−6863.

23. *Dechlorination of chloroethylenes by cob(I)alamin and cobalamin model complexes.* Kliegman, S. and McNeill, K. The Royal Society of Chemistry, 2008, Vols. Dalton Transactions: 4191-4201.

24. *Iron nanoparticles for environmental clean-up: recent developments and future outlook.* Yan, W., Lien, H., Koel, B. E. and Zhang, W. Environmental Science: Processes & Impacts, 2013, Vols. 15: 63–77.

25. *Nanoscale zero valent iron and bimetallic particles for contaminated site remediation.* O'Carroll, D., Sleep, B., Krol, M., Boparai, H. and Kocur, C. Advances in Water Resources, 2013, Vols. 51: 104–122.

26. *Pathways and Kinetics of Chlorinated Ethylene and Chlorinated Acetylene Reaction with Fe(0) Particles.* Arnold, W. A. and Roberts, A. L. Environmental Science & Technology, 2000, Vols. 34: 1794-1805.

27. *Pathways of Chlorinated Ethylene and Chlorinated Acetylene Reaction with Zn(0).* Arnold, W. A. and Roberts, A. L. Environmental Science & Technology, 1998, Vols. 32: 3017-3025.

28. Ju, X. *Reductive Dehalogenation of Gas-phase Trichloroethylene using Heterogeneous Catalytic and Electrochemical Methods.* PhD diss., Arizona: University of Arizona, 2005.

29. *Hydrodechlorination of Trichloroethylene to Hydrocarbons Using Bimetallic Nickel-Iron Nanoparticles.* Schrick, B., Blough, J. L., Jones, A. D. and Mallouk, T. E. Chemistry of Materials, 2002, Vols. 14: 5140-5147.

30. Lim, D. *Density functional theory studies on the relative reactivity of chloroethenes on zerovalent iron.* PhD diss., Michigan: University of Michigan, 2008.

31. *Measuring the reactivity of commercially available zero-valent iron nanoparticles used for environmental remediation with iopromide.* Schmid, D., Micic, V., Laumann, S. and Hofmann, T. Journal of Contaminant Hydrology, 2015, Vols. 181: 36–45.

32. *Synthesis of granular activated carbon/zero valent iron composites for simultaneous adsorption/dechlorination of trichloroethylene.* Tseng, H., Su, J. and Liang, C. Journal of Hazardous Materials, 2011, Vols. 192: 500– 506.

33. *Zero-Valent Iron Nanoparticles for Abatement of Environmental Pollutants: Materials and Engineering Aspects.* Li, X., Elliott, D. W. and Zhang, W. Critical Reviews in Solid State and Materials Sciences, 2006, Vols. 31(4): 111-122.

34. *Adsorption–dechlorination of 2,4-dichlorophenol using two specified MWCNTs-stabilized Pd/Fe nanocomposites.* Xu, J., Sheng, T., Hu, Y., Baig, S. A., Lv, X. and Xu, X. Chemical Engineering Journal, 2013, Vols. 219: 162-173.

35. *Influence of the Oxidizing Species on the Reactivity of Iron-Based Bimetallic Reductants.* Cwiertny, D. M., Bransfield, S. J. and Roberts, A. L. Environmental Science & Technology, 2007, Vols. 41: 3734-3740.

36. *Methods for characterizing the fate and effects of nano zerovalent iron during groundwater remediation.* Shi, Z., Fan, D., Johnson, R. L., Tratnyek, P. G., Nurmi, J. T., Wu, Y. and Williams, K. H. Journal of Contaminant Hydrology, 2015, Vols. 181: 17-35.

37. McPherson, A. W., Goltz, M. N. and Agrawal, A. Pollutant Degradation by Nanoscale Zero Valent Iron (nZVI): Role of Polyelectrolyte Stabilization and Catalytic Modification on nZVI Performance. R. Doong and et al. *Interactions of Nanomaterials with Emerging Environmental Contaminants.* Washington, DC : American Chemical Society, 2013.

38. Sogaard, E. G. *Chemistry of Advanced Environmental Purification Processes of Wate: Fundamentals and Applications.* Poland : Elsevier, 2014.

39. *Nanotechnology and in Situ Remediation: A Review of the Benefits and Potential Risks.* Karn, B., Kuiken, T. and Otto, M. Environ Health Perspect, 2009, Vols. 117(12): 1813-1831.

40. *The limitations of applying zero-valent iron technology in contaminants sequestration and the corresponding countermeasures: The development in zero-valent iron technology in the last two decades (1994e2014).* Guan, X., Sun, Y., Qin, H., Li, J., Lo, I. M., He, D. and Dong, H. Water Research, 2015, Vols. 75: 224-248.

41. *Evaluating TCE Abiotic and Biotic Degradation Pathways in a Permeable Reactive Barrier Using Compound Specific Isotope Analysis.* Lojkasek-Lima, P., Aravena, R., Shouakar-Stash,

O., Frape, S. K., Marchesi, M., Fiorenza, S. and Vogan, J.. Ground Water Monitoring & Remediation, 2012, Vols. 32(4): 53-62.

42. *Characterization and Properties of Metallic Iron Nanoparticles: Spectroscopy, Electrochemistry, and Kinetics.* Nurmi, J. T., Tratnyek, P. G., Sarathy, V., Baer, D. R., Amonette, J. E., Pecher, K., Wang, C., Linehan, J. C., Matson, D. W., Penn, R. L. and Driessen, M. D.. Environmental Science & Technology, 2005, Vols. 39: 1221-1230.

43. *Degradation of Chlorinated Phenols by Zero Valent Iron and Bimetals of Iron: A Review.* Gunawardana, B., Singhal, N. and Swedlund, P. Environmental Engineering Research, 2011, Vols. 16(4): 187-203.

44. Cwiertny, D. M. *Mechanistic investigations of granular iron and iron-based bimetallic reductants for treatment of organohalide pollutants.* PhD diss., Maryland: The Johns Hopkins University, 2005.

45. Powell, R. M., Puls, R. W., Blowes, D. W., Vogan, J. L., Gillham, R. W., Powell, P. D., Schultz, D., Landis, R. and Sivaec, T. *Permeable Reactive Barrier Technologies for Contaminant Remediation.* Environmental Protection Agency, 1998.

46. *Reductive dechlorination of TCE by zero valent bimetals.* Kim, Y-H. and Carraway, E. R. Environmental Technology, 2003, Vols. 24: 69-75.

47. *Long-Term Performance of Zero-Valent Iron Permeable Reactive Barriers: A Critical Review.* Henderson, A. D. and Demond, A. H. Environmental Engineering Science, 2007, Vols. 24(4): 401-423.

48. *Nanoscale zero-valent iron: Future prospects for an emerging water treatment technology.* Crane, R.A. and Scott, T.B. Journal of Hazardous Materials, 2012, Vols. 211– 212: 112– 125.

49. *Treatment of chlorinated organic contaminants with nanoscale bimetallic particles.* Zhang, W., Wang, C. and Lien, H. Catalysis Today, 1998, Vols. 40: 387 - 395.

50. *Chlorinated Solvent Transformation by Palladized Zerovalent Iron: Mechanistic Insights from Reductant Loading Studies and Solvent Kinetic Isotope Effects.* Xie, Y. and Cwiertny, D. M. Environmental Science & Technology, 2013, Vol. 47: 7940−7948.

51. Reisner, D. E. and Pradeep, T. *Aquananotechnology: Global Prospects.* CRC Press, New York, 2014.

52. *Bimetallic nickel–iron nanoparticles for groundwater decontamination: Effect of groundwater constituents on surface deactivation.* Han, Y. and Yan, W. Water Research, 2014, Vols. 66: 149-159.

53. *Review on nano zerovalent iron (nZVI): From synthesis to environmental applications.* Stefaniuk, M., Oleszczuk, P. and Ok, Y. S. Chemical Engineering Journal, 2015.

54. *Nanoalloys: From Theory to Applications of Alloy Clusters and Nanoparticles.* Ferrando, R., Jellinek, J. and Johnston, R. L. Chemical Reviews, 2008, Vols. 108(3): 845-910.

55. *Bimetallic Fe nanoparticles: Recent advances in synthesis and application in catalytic elimination of environmental pollutants.* Liu, W-J., Qian, T-T. and Jiang, H. Chemical Engineering Journal, 2014, Vols. 236: 448–463.

56. *Exploring the influence of granular iron additives on 1,1,1-trichloroehtane reduction.* Cwiertny, D. M., Bransfield, S. J., Livi, K. J. T., Fairbrother, D. H. and Roberts, A. L. Environmental Science & Technology, 2006, Vols. 40: 6837-6843.

57. *Optimization of nano-scale nickel/iron particles for the reduction of high concentration chlorinated aliphatic hydrocarbon solutions.* Barnes, R. J., Riba, O., Gardner, M.N., Scott, T. B., Jackman, S. A. and Thompson, I. P.. Chemosphere, 2010, Vols. 79: 448–454.

58. *Dechlorination of Pentachlorophenol by Zero Valent Iron and Modified Zero Valent Irons.* Kim, Y-H. and Carraway, E. R. Environmental Science & Technology, 2000, Vols. 34: 2014-2017.

59. Zhang, W. *Nanoscale Bimetallic Particles for In Situ Remediation.* Environmental Protection Agency: Lehigh University, 2006.

60. *Catalytic reductive dechlorination of p-chlorophenol in water using Ni/Fe nanoscale particles.* Zhang, W., Quan, X. and Zhang, Z. Journal of Environmental Sciences, 2007, Vols. 19: 362–366.

61. *Effect of metal ions and humic acid on the dechlorination of tetrachloroethylene by zerovalent iron.* Doong, R. and Lai, Y. Chemosphere, 2006, Vols. 64: 371-378.

62. *Trichloroethene hydrodechlorination by Pd-Fe bimetallic nanoparticles: Solute-induced catalyst deactivation analyzed by carbon isotope fractionation.* Han, Y., Liu, C., Horita, J. and Yan, W. Applied Catalysis B, 2016, Vols. Environmental 188: 77–86.

63. Bard, A. J., Parsons, R. and Jordan, J. *Standard Potentials in Aqueous Solution.* New York and Basel: Marcel Dekker, Inc., 1985.

64. *On the Nonlinear Relationship between kobs and Reductant Mass Loading in Iron Batch Systems.* Cwiertny, D. M. and Roberts, A. L. Environmental Science & Technology, 2005, Vols. 39(22): 8948-8957.

65. *Influence of copper loading and surface coverage on the reactivity of granular iron toward 1,1,1-trichloroethane.* Bransfield, S. J., Cwiertny, D. M., Roberts, A. L. and Fairbrother, D. H. Environmental Science & Technology, 2006, Vols. 40:1485-1490.

66. Upadhyay, S. K. *Chemical Kinetics and Reaction Dynamics.* India : Springer, 2006.

67. *Effects of iron surface pretreatment on sorption and reduction kinetics of trichloroethylene in a closed batch system.* Lin, C. J. and Lo, S-L. Water Research, 2005, Vols. 39: 1037–1046.

68. Grob, R. L. and Barry, E. F. *Modern Practice of Gas Chromatography. Pennsylvania:* John Wiley & Sons, 2004.

69. Engewald, W. and Dettmer-Wilde, K. Theory of Gas Chromatography. Katja Dettmer-Wilde and Werner Engewald. *Practical Gas Chromatography.* Germany: Springer, 2014.

70. Pavia, D. L. *Introduction to Organic Laboratory Techniques: A Small Scale Approach.* United States of America: Cengage Learning, 2005.

71. LibreTexts. Gas Chromatography. [Online] National Science Foundation, 03 13, 2015. [Cited: 08 30, 2016.] http://chem.libretexts.org/Core/Analytical_Chemistry/Instrumental_Analysis/Chromatography/Gas_Chromatography.

72. *Simultaneous Determination of Chlorinated Ethenes and Ethene in Groundwater Using Headspace Solid-Phase Microextraction with Gas Chromatography.* Ziv-El, M., Kalinowski, T., Krajmalnik-Brown, R. and Halden, R. U. Journal of Chromatographic Science, 2014, Vols. 52:137–142.

73. *Current challenges in compound-specific stable isotope analysis of environmental organic contaminants.* Elsner, M., Joachmann, M. A., Hofstetter, T. B., Hunkeler, D., Bernstein, A., Schmidt, T. C. and Schimmelman, A. Analytical and Bioanalytical Chemistry, 2012, Vols. 403: 2471-2491.

74. *Satble isotope fractionation to investigate natural transformation mechanisms of organic contaminants: principles, prospects and limitations.* Elsner, M. Journal of Environmental Monitoring, 2010, Vols. 12: 2005-2031.

75. *Compound-Specific Hydrogen Isotope Analysis of Heteroatom-Bearing Compounds via Gas Chromatography−Chromium-Based High-Temperature Conversion (Cr/HTC)−Isotope Ratio Mass Spectrometry.* Renpenning, J., Kümmel, S, Hitzfeld, K., L., Schimmelmann, A. and Gehre, M. Analytical Chemistry, 2015, Vol. 87: 9443−9450.

76. *Evaluating Chlorine Isotope Effects from Isotope Ratios and Mass Spectra of Polychlorinated Molecules.* Elsner, M. and Hunkeler, D. Analytical Chemistry, 2008, Vols. 80: 4731–4740.

77. *C, Cl and H compound-specific isotope analysis to assess natural versus Fe(0) barrier-induced degradation of chlorinated ethenes at a contaminated site.* Audí-Miró, C., Cretnik, S., Torrentó, C., Rosell, M., Shouakar-Stash, O., Otero, N., Palau, J., Elsner, M. and Soler, A. Journal of Hazardous Materials, 2015, Vols. 299: 747-754.

78. *Carbon isotope fractionation during reductive dechlorination of TCE in batch experiments with iron samples from reactive barriers.* Schüth, C., Bill, M., Barth, J. A. C., Slater, G. F. and Kalin, R. M. Journal of Contaminant Hydrology, 2003, Vols. 66: 25-37.

79. *Identifying Abiotic Chlorinated Ethene Degradation: Characteristic Isotope Patterns in Reaction Products with Nanoscale Zero-Valent Iron.* Elsner, M., Chartrand, M., VanStone, N., Couloume, G. L. and Lollar, B. S. Environmental Science & Technology, 2008, Vols. 42: 5963-5970.

80. *Isotopic fractionation during reductive dechlorination of trichloroethene by zero-valent iron: influence of surface treatment.* Slater, G. F., Lollar, B. S., King, R. A. and O'Hannesin, S. Chemosphere, 2002, Vols. 49: 587–596.

81. Geiger, C. L., Carvalho-Knighton, K., Novaes-Card, S., Maloney, P. and DeVor, R. A Review of Environmental Applications of Nanoscale and Microscale Reactive Metal Particles. C. L. Geiger and K. Carvalho-Knighton. *Environmental Applications of Nanoscale and Microscale Reactive Metal Particles.* Washington, DC : American Chemical Society, 2010.

82. *Reduction of Chlorinated Ethanes by Nanosized Zero-Valent Iron: Kinetics, Pathways, and Effects of Reaction Conditions.* Song, H. and Carraway, E. R. Environmental Science & Technology, 2005, Vols. 39: 6237-6245.

83. *Reductive Dehalogenation of Chlorinated Methanes by Iron Metal.* Matheson, L. J. and Tratnyek, P. G. Environmental Science & Technology, 1994, Vols. 28: 2045-2053.

84. *Reduction of hexachlorobenzene by nanoscale zero-valent iron: Kinetics, pH effect, and degradation mechanism.* Shih, Y., Hsu, C. and Su, Y. Separation and Purification Technology, 2011, Vols. 76: 286-274.

85. *Catalytic hydrodechlorination of chlorinated ethenes by nanoscale zero-valent iron.* Song, H. and Carraway, E. R. Applied Catalysis B, 2008, Vols. 78: 53–60.

86. Rieger, P.H. *Electrochemistry.* United States of America: Springer Science & Business Media, 1993.

87. Company, R. M. *Handbook of Ground Water Development.* Califormia: John Wiley & Sons, 1990.

88. Minear, R. *Inorganic Species, Part 1.* New York: Elsevier, 2012.

89. *Effects of pH on dechlorination of trichloroethylene by zero-valent iron.* Chen, J-L., Al-Abed, S. R., Rayan, J. A. and Li, Z. Journal of Hazardous Materials, 2001, Vols. B83: 243–254.

90. *Effect of Particle Age (Fe0 Content) and Solution pH On NZVI Reactivity: H2 Evolution and TCE Dechlorination.* Liu, Y. and Lowry, G. V. Environmental Science & Technology, 2006, Vols. 40: 6085-6090.

91. *Reduction of hexachlorobenzene by nanoscale zero-valent iron: Kinetics, pH effect,and degradation mechanism.* Shih, Y., Hsu, C. and Su, Y. Separation and Purification Technology, 2011, Vols. 76: 268–274.

92. *Dechlorination of trichloroethylene in aqueous solution by noble metal-modified iron.* Lin, C. J., Lo, S. L. and Liou, Y. H. Journal of Hazardous Materials, 2004, Vols. B116: 219–228.

93. *Degradation of trichloroethylene using iron, bimetals and trimetals.* Chao, K-P., Ong, S. K., Fryzek, T., Yuan, W. and Braida, W. Journal of Environmental Science and Health, 2012, Vols. 47: 1536–1542.

94. Diffen LLC. *Absorption vs Adsorption.* [Online] [Cited: 09 03, 2016.] http://www.diffen.com/difference/Absorption_vs_Adsorption.

95. *Henry's Law Constant for Trichloroethylene between 10 and 95 °C.* Heron, G., Christensen, T. H. and Enfield, C. G. Environmental Science & Technology, 1998, Vols. 32: 1433-1437.

96. *Compilation of Henry's law constants (version 4.0) for water as solvent.* Sander, R. Atmospheric Chemistry and Physics, 2015, Vols. 15: 4399-4981.

97. *Field Assessment of Nanoscale Bimetallic Particles for Groundwater Treatment.* Elliott, D. W. and Zhang, W-X. Environmental Science & Technology, 2001, Vols. 35: 4922-4926.

98. *Carbon and Chlorine Isotope Analysis to Identify Abiotic Degradation Pathways of 1,1,1-Trichloroethane.* Palau, J., Shouakar-Stash, O. and Hunkeler, D. Environmental Science & Technology, 2014, Vol. 48: 14400−14408.

99. *Carbon and Chlorine Isotope Fractionation during Aerobic Oxidation and Reductive Dechlorination of Vinyl Chloride and cis-1,2-Dichloroethene.* Abe, Y., Aravena, R., Zopfi, J., Shouakar-Stash, O., Cox, E., Roberts, J. D. and Hunkeler, D. Environmental Science & Technology, 2009, Vols. 43: 101–107.

100. *Monitoring and evaluation of dechlorination processes using compound-specific chlorine isotope analysis.* Sakaguchi-Söder, K., Jager, J., Grund, H., Matthäus, F. and Schüth, C. Rapid Communications In Mass Spectrometry, 2007, Vols. 21: 3077-3084.

101. *Stable hydrogen, carbon and chlorine isotope measurements of selected chlorinated organic solvents.* Shouakar-Stash, O., Frape, S. K. and Drimmie, R. J. Journal of Contaminant Hydrology, 2003, Vols. 60: 211– 228.

8. Attachments

8.1. Influence of metals salt solution toward chlorinated ethylenes

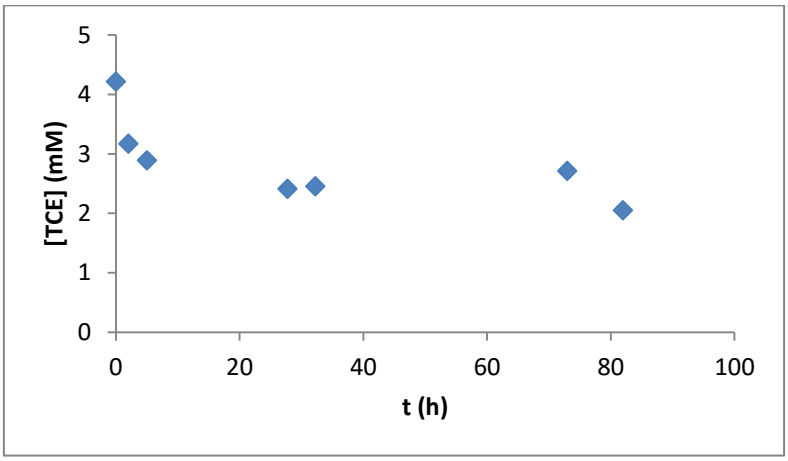

Figure 24: Plot of TCE concentration vs time for gold salt solution.

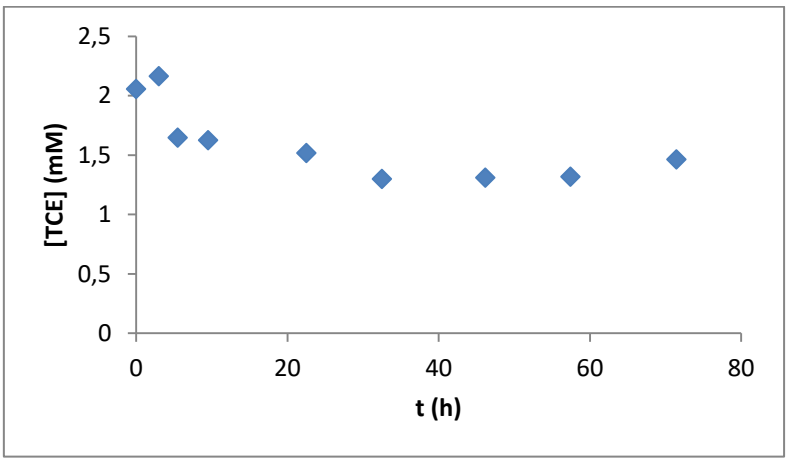

Figure 25: Plot of TCE concentration vs time for platinum salt solution.

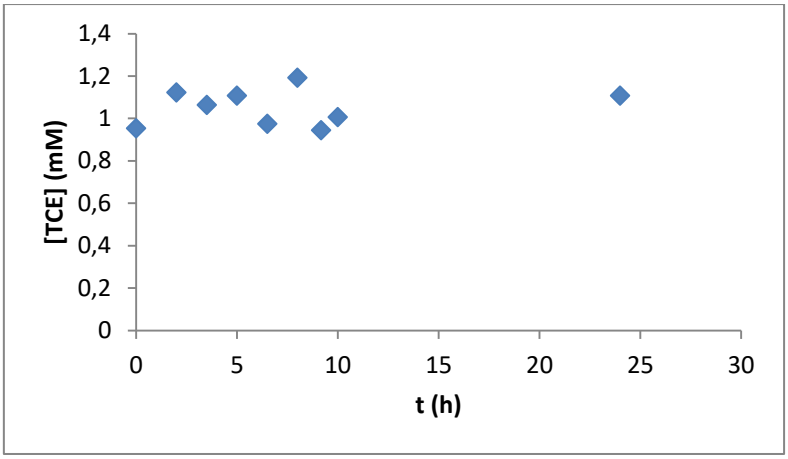

Figure 26: Plot of TCE concentration vs time for cobalt salt solution.

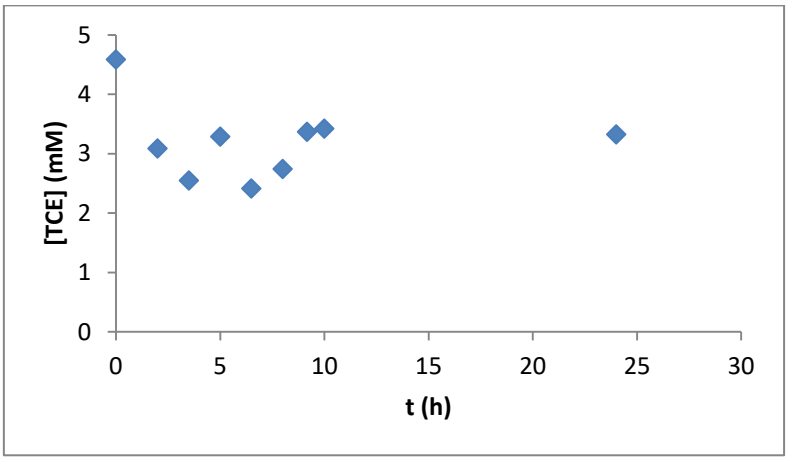

Figure 27: Plot of TCE concentration vs time for copper salt solution.

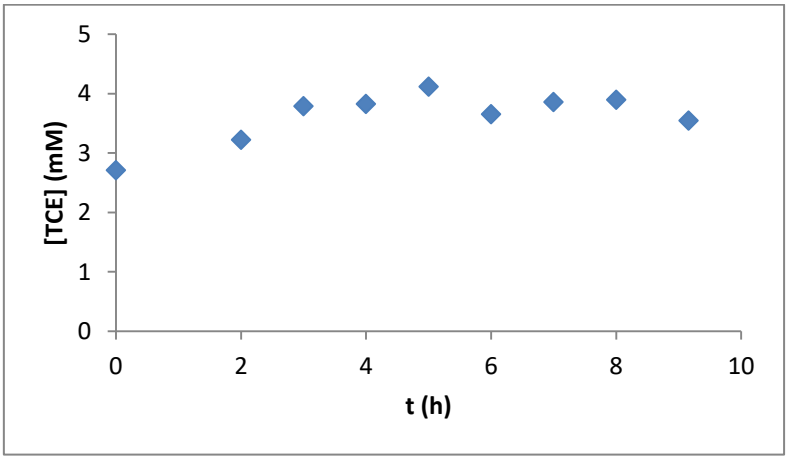

Figure 28: Plot of TCE concentration vs time for nickel salt solution.

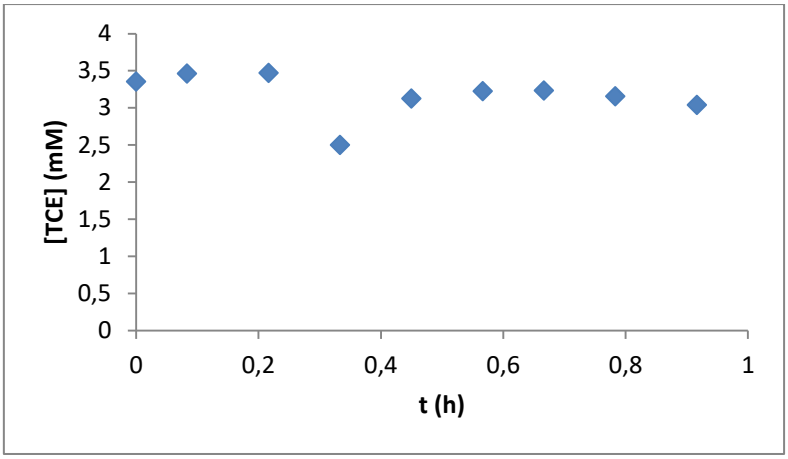

Figure 29: Plot of TCE concentration vs time for palladium salt solution.

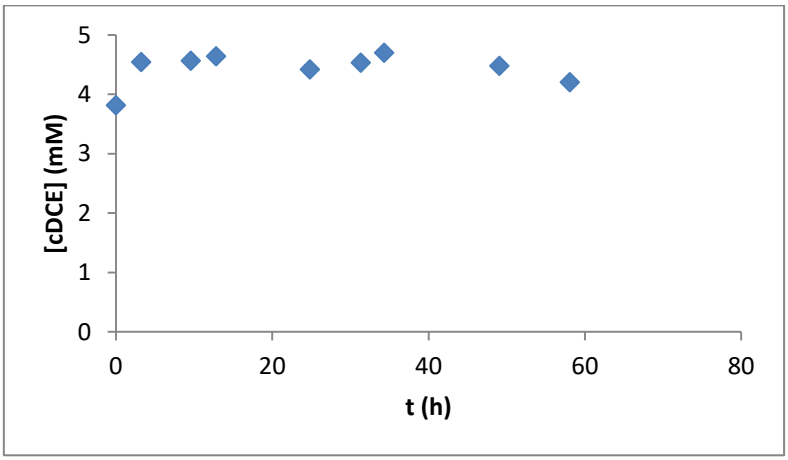

Figure 30: Plot of *cis*-DCE concentration vs time for gold salt solution.

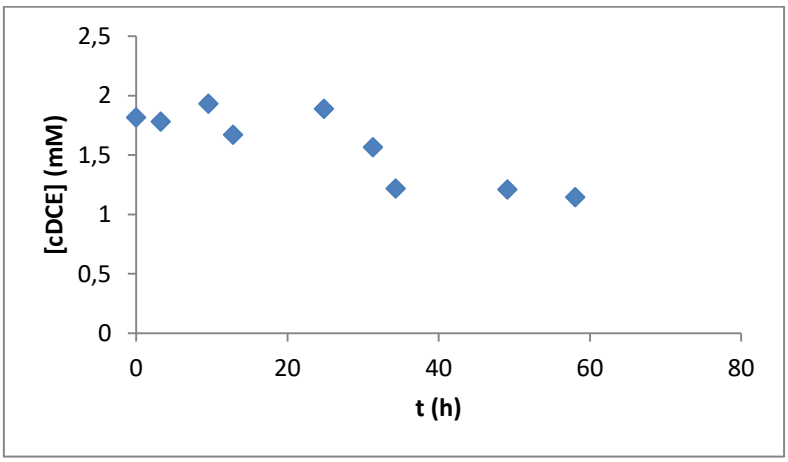

Figure 31: Plot of *cis*-DCE concentration vs time for platinum salt solution.

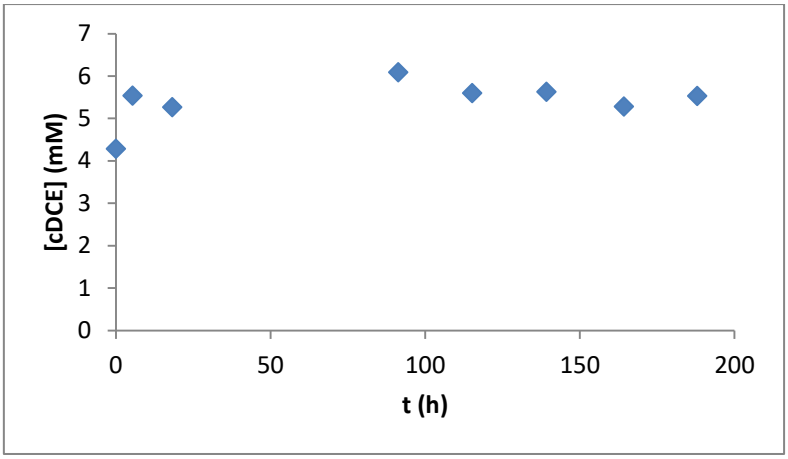

Figure 32: Plot of *cis*-DCE concentration vs time for cobalt salt solution.

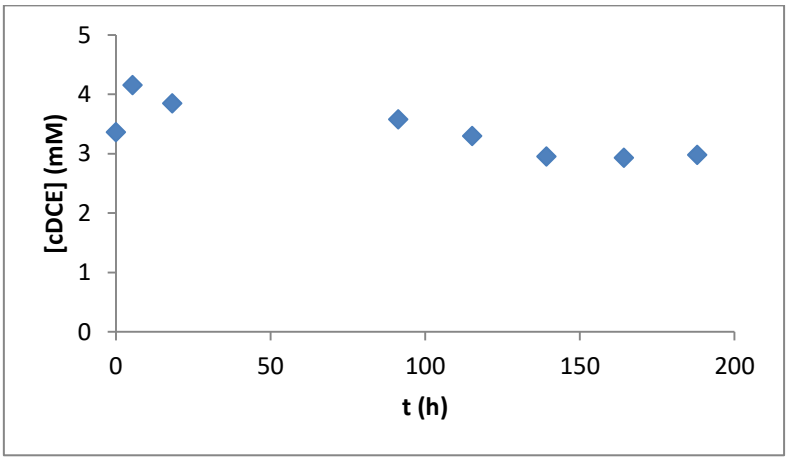

Figure 33: Plot of *cis*-DCE concentration vs time for copper salt solution.

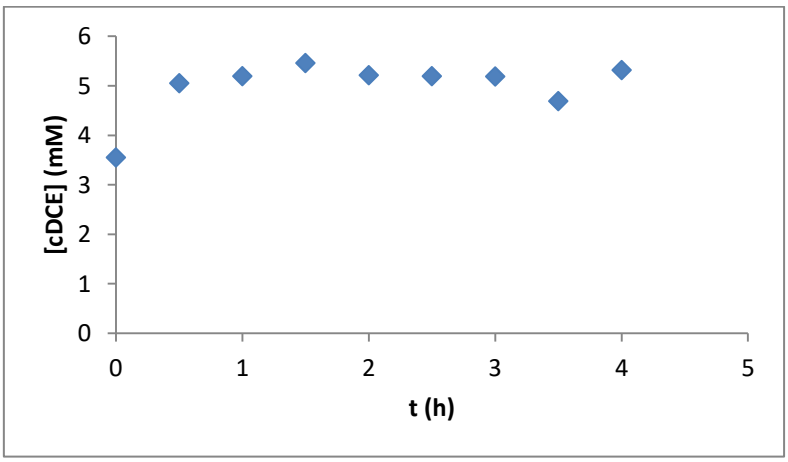

Figure 34: Plot of *cis*-DCE concentration vs time for nickel salt solution.

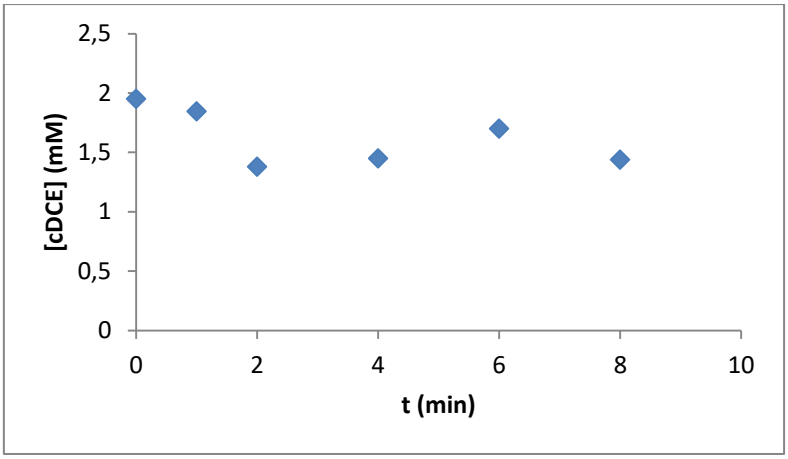

Figure 35: Plot of *cis*-DCE concentration vs time for palladium salt solution.

8.2. Influence on product partitioning by different reductants

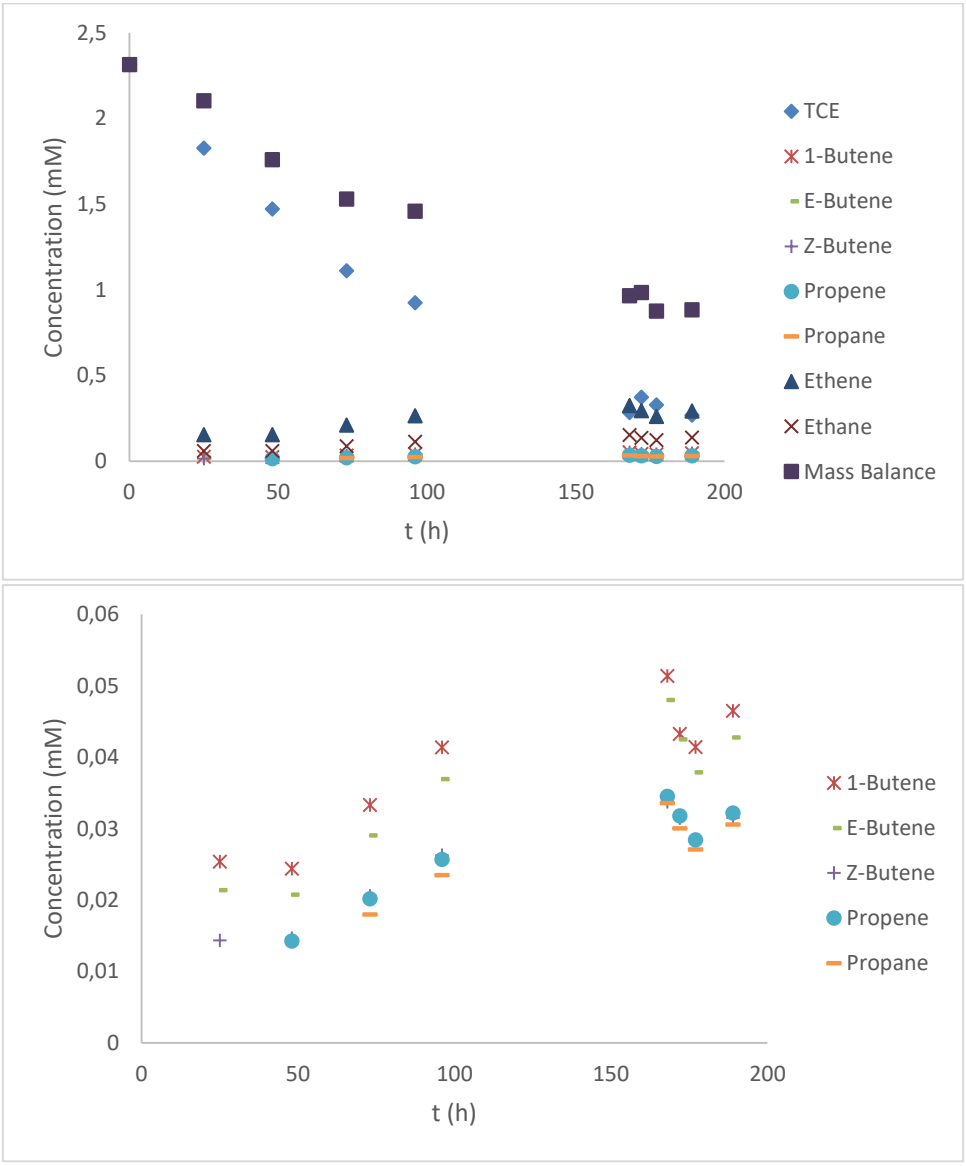

Figure 36: Degradation of TCE and its products over time toward unamended iron reductant in isotope experiments (reaction 1) (A and B: Panel B is a zoom of Panel A without TCE, Ethene, Ethane and Mass Balance).

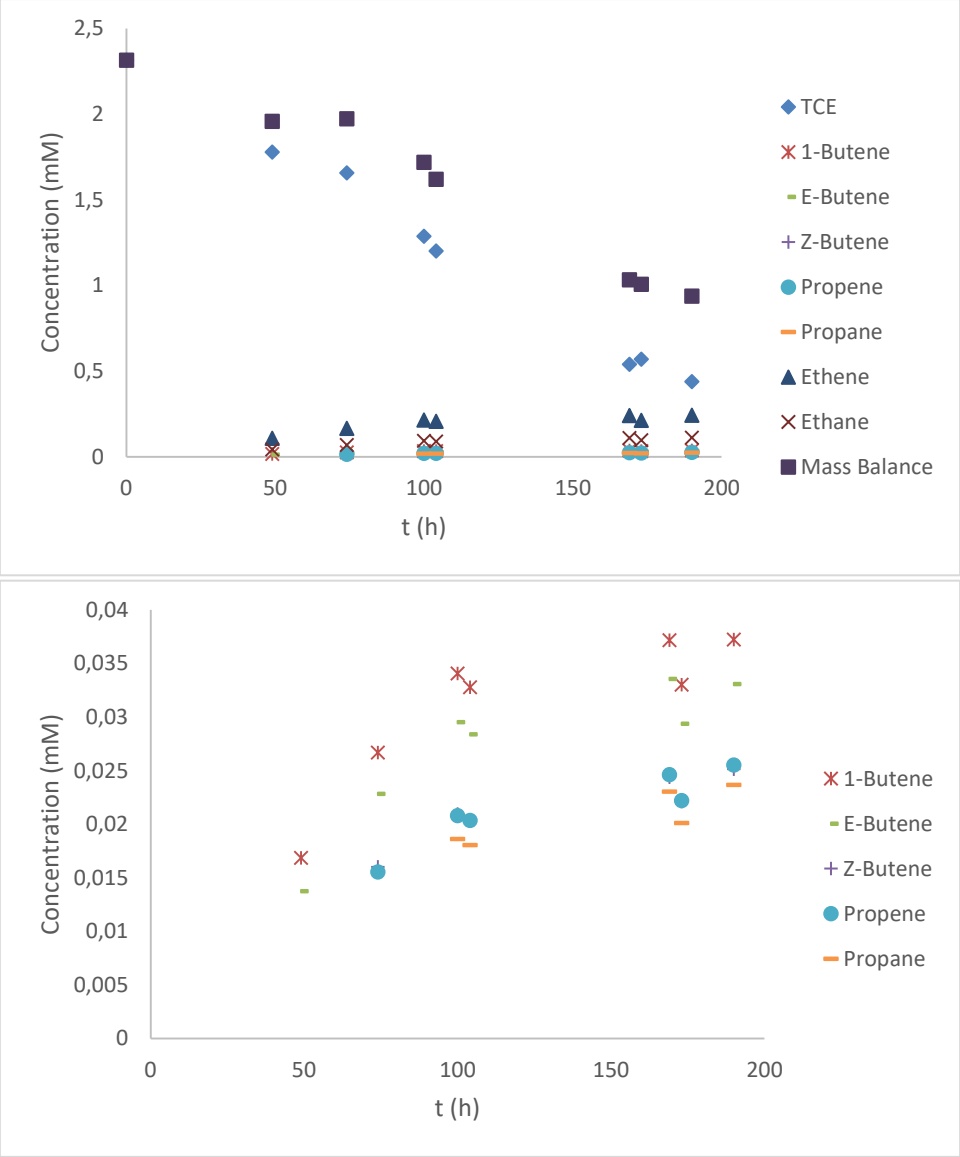

Figure 37: Degradation of TCE and its products over time toward unamended iron reductant in isotope experiments (reaction 2) (A and B: Panel B is a zoom of Panel A without TCE, Ethene, Ethane and Mass Balance).

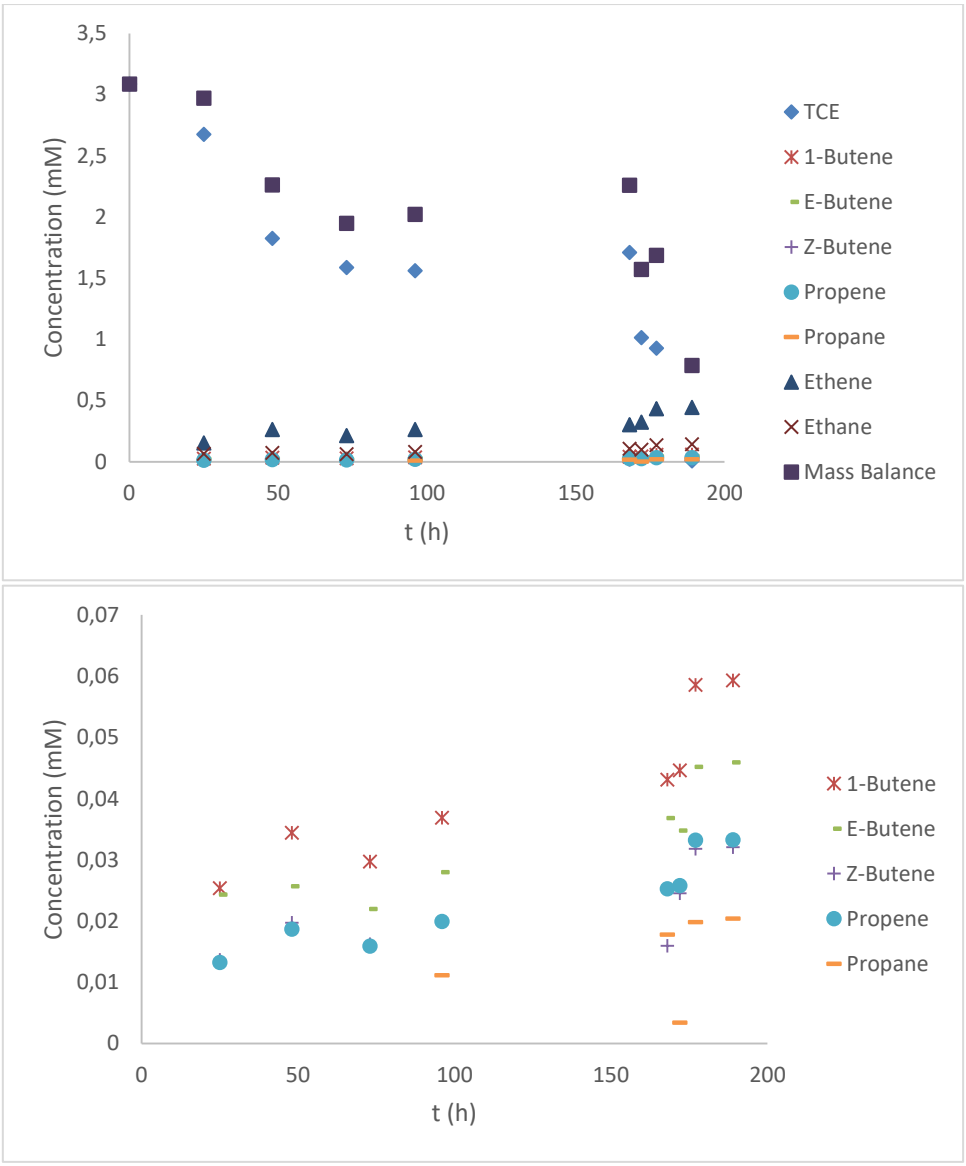

Figure 38: Degradation of TCE and its products over time toward unamended iron reductant in isotope experiments (additional experiments) (A and B: Panel B is a zoom of Panel A without TCE, Ethene, Ethane and Mass Balance).

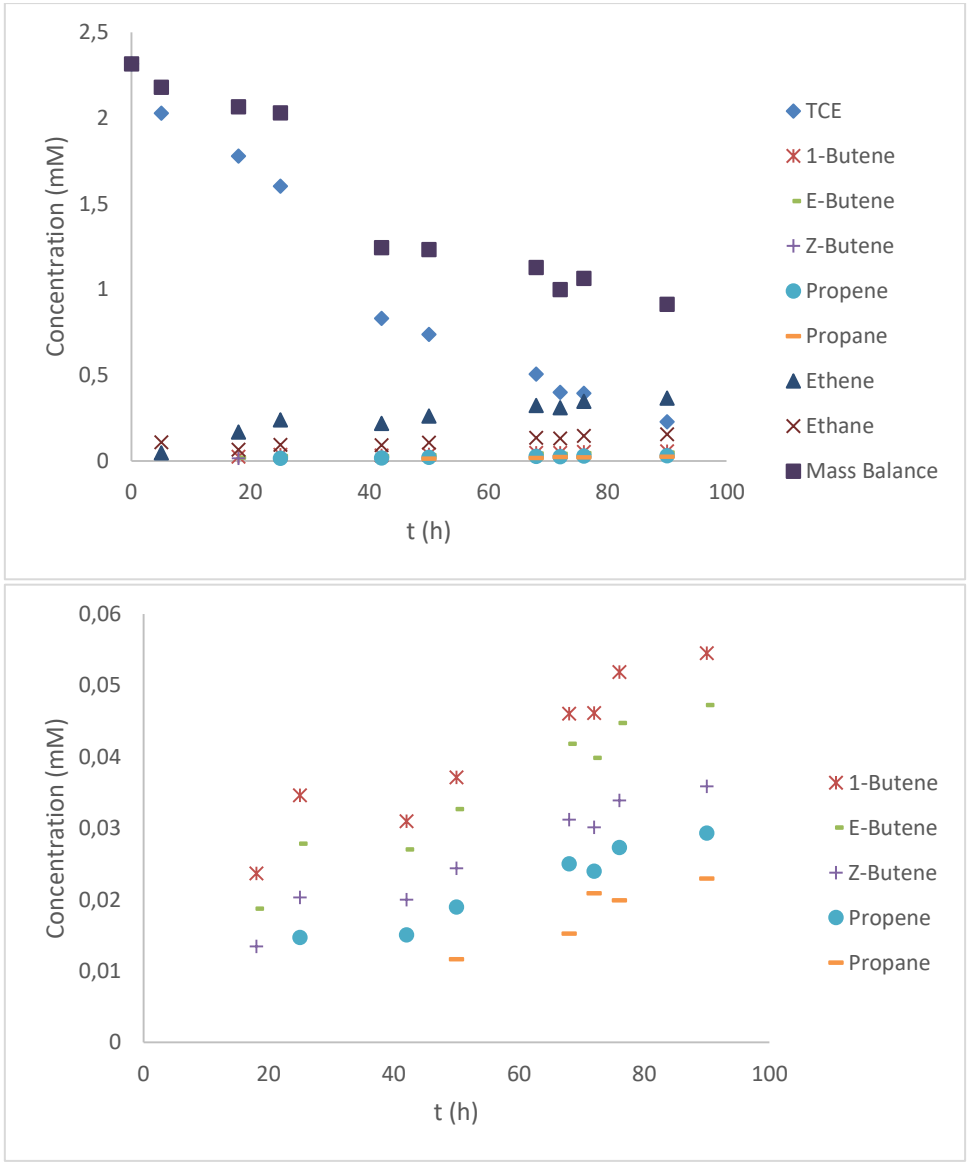

Figure 39: Degradation of TCE and products over time toward Au/Fe reductant in isotope experiments (reaction 1) (A and B: Panel B is a zoom of Panel A without TCE, Ethene, Ethane and Mass Balance).

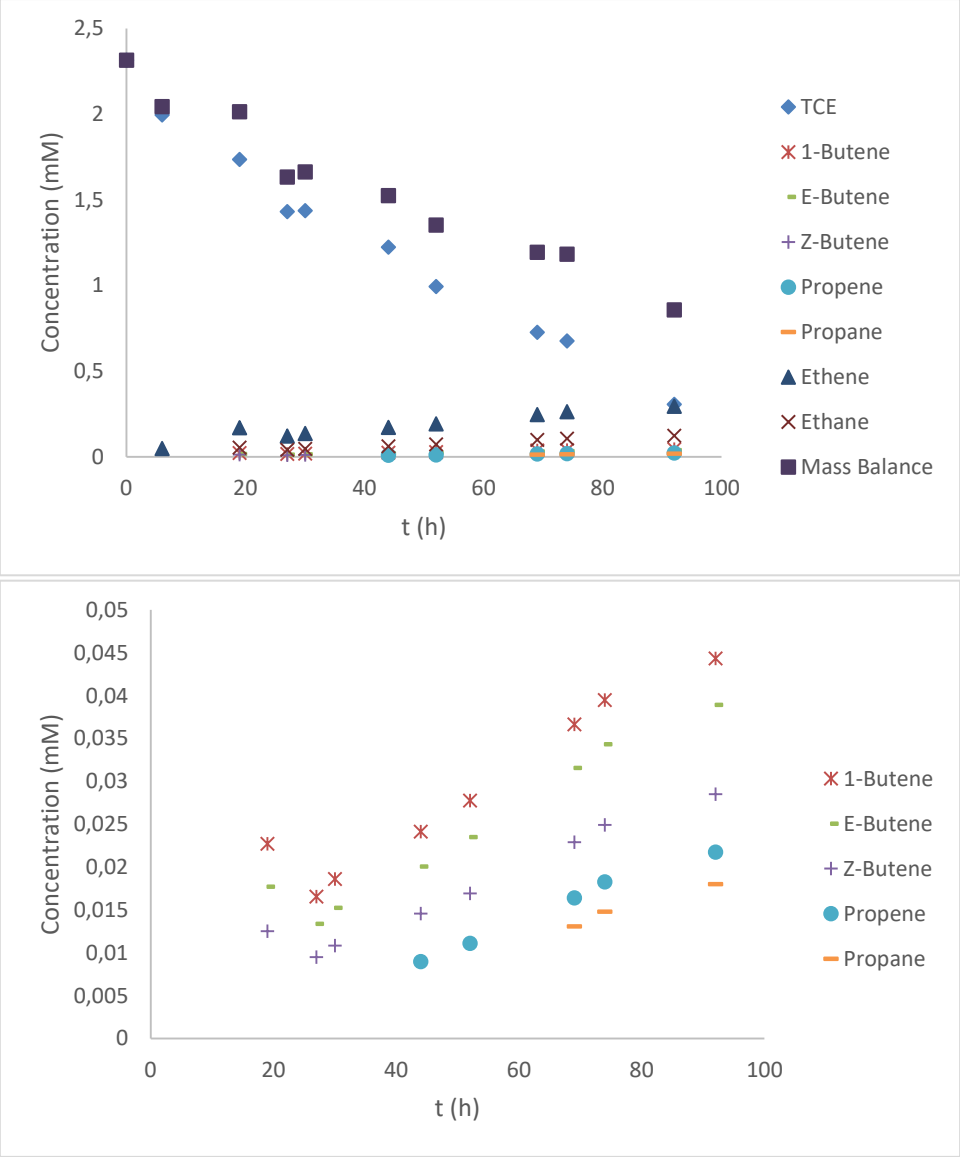

Figure 40: Degradation of TCE and products over time toward Au/Fe reductant in isotope experiments (reaction 2) (A and B: Panel B is a zoom of Panel A without TCE, Ethene, Ethane and Mass Balance).

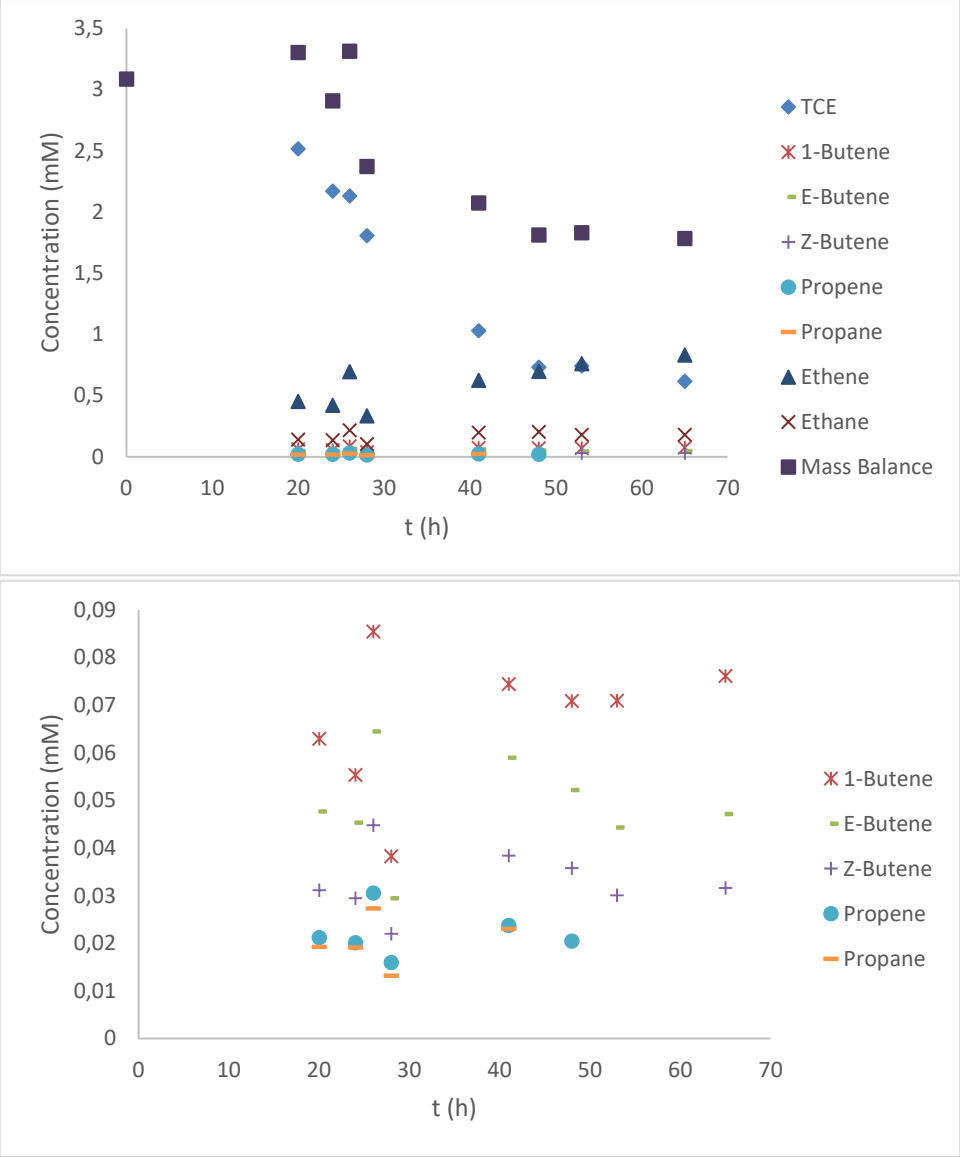

Figure 41: Degradation of TCE and products over time toward Au/Fe reductant in isotope experiments (additional experiments) (A and B: Panel B is a zoom of Panel A without TCE, Ethene, Ethane and Mass Balance).

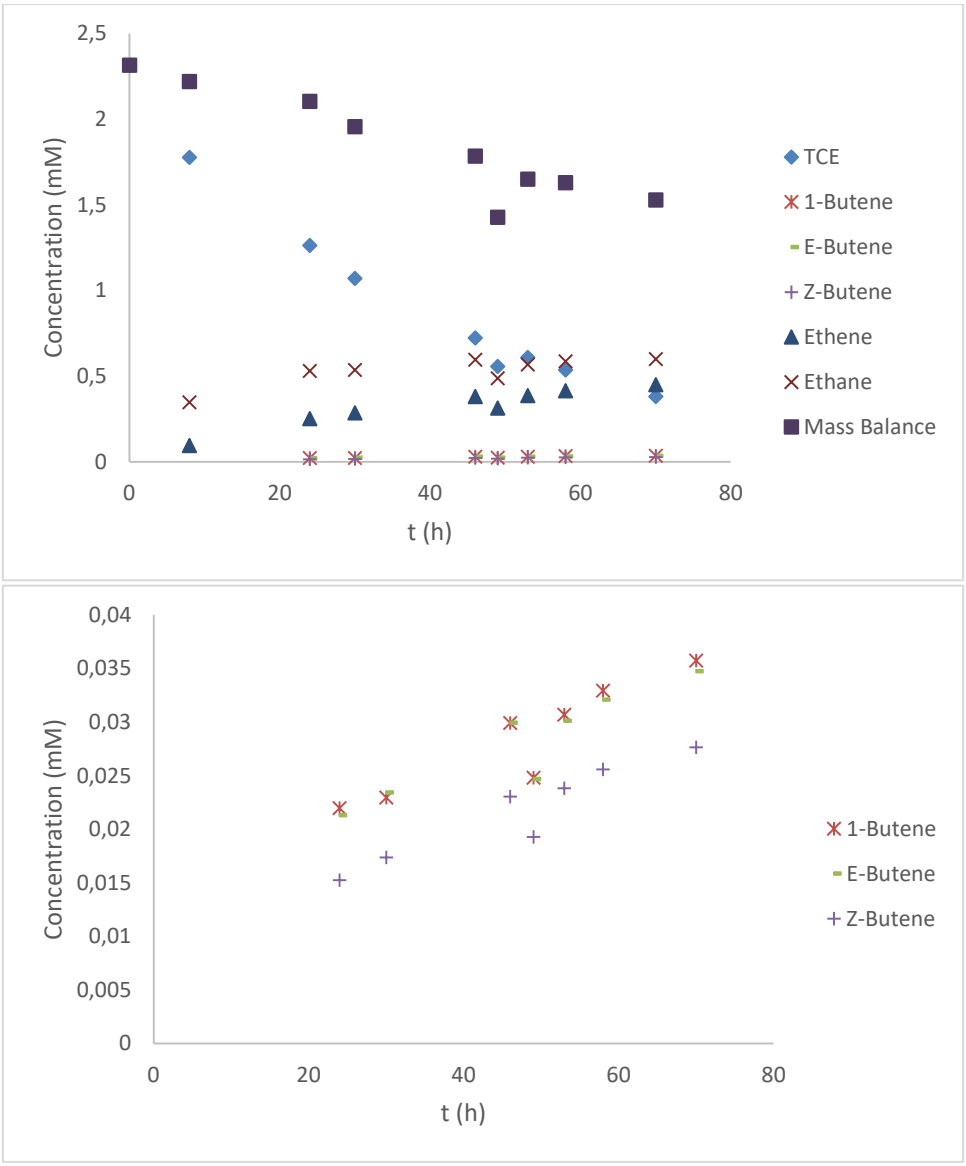

Figure 42: Degradation of TCE and its products over time toward Pt/Fe reductant in isotope experiments (reaction 1) (A and B: Panel B is a zoom of Panel A without TCE, Ethene, Ethane and Mass Balance).

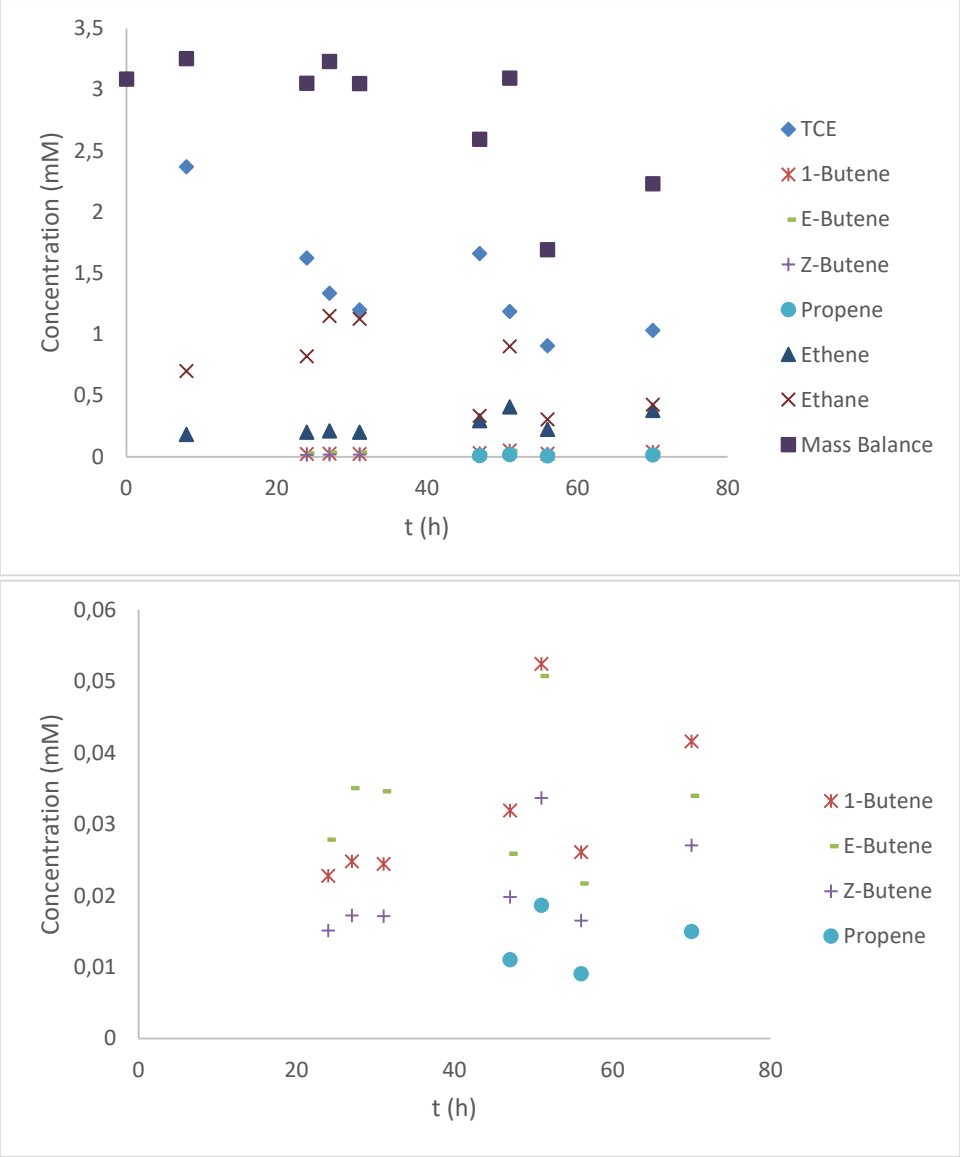

Figure 43: Degradation of TCE and its products over time toward Pt/Fe reductant in isotope experiments (additional experiments) (A and B: Panel B is a zoom of Panel A without TCE, Ethene, Ethane and Mass Balance).

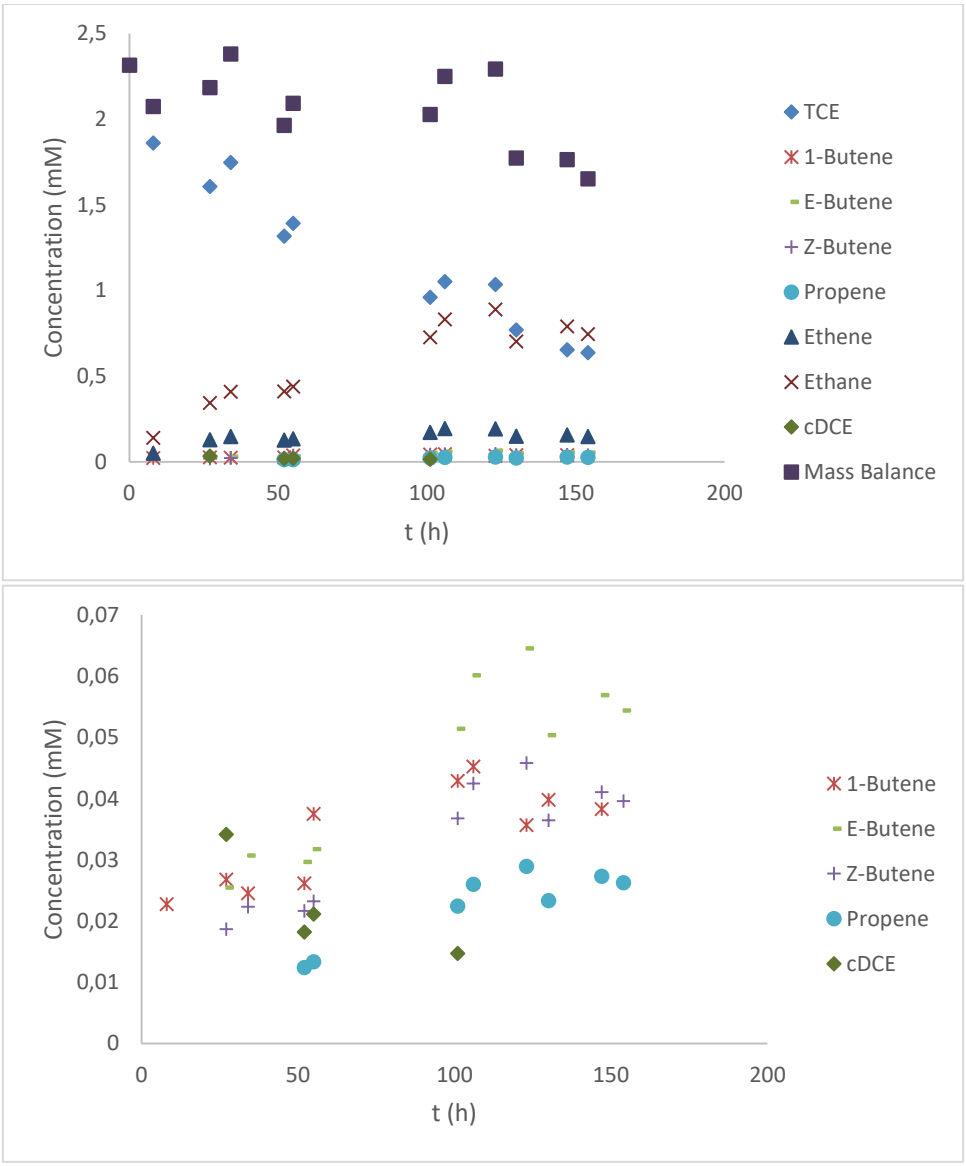

Figure 44: Degradation of TCE and its products over time in isotope experiments toward Co/Fe reductant (reaction 1) (A and B: Panel B is a zoom of Panel A without TCE, Ethene, Ethane and Mass Balance).

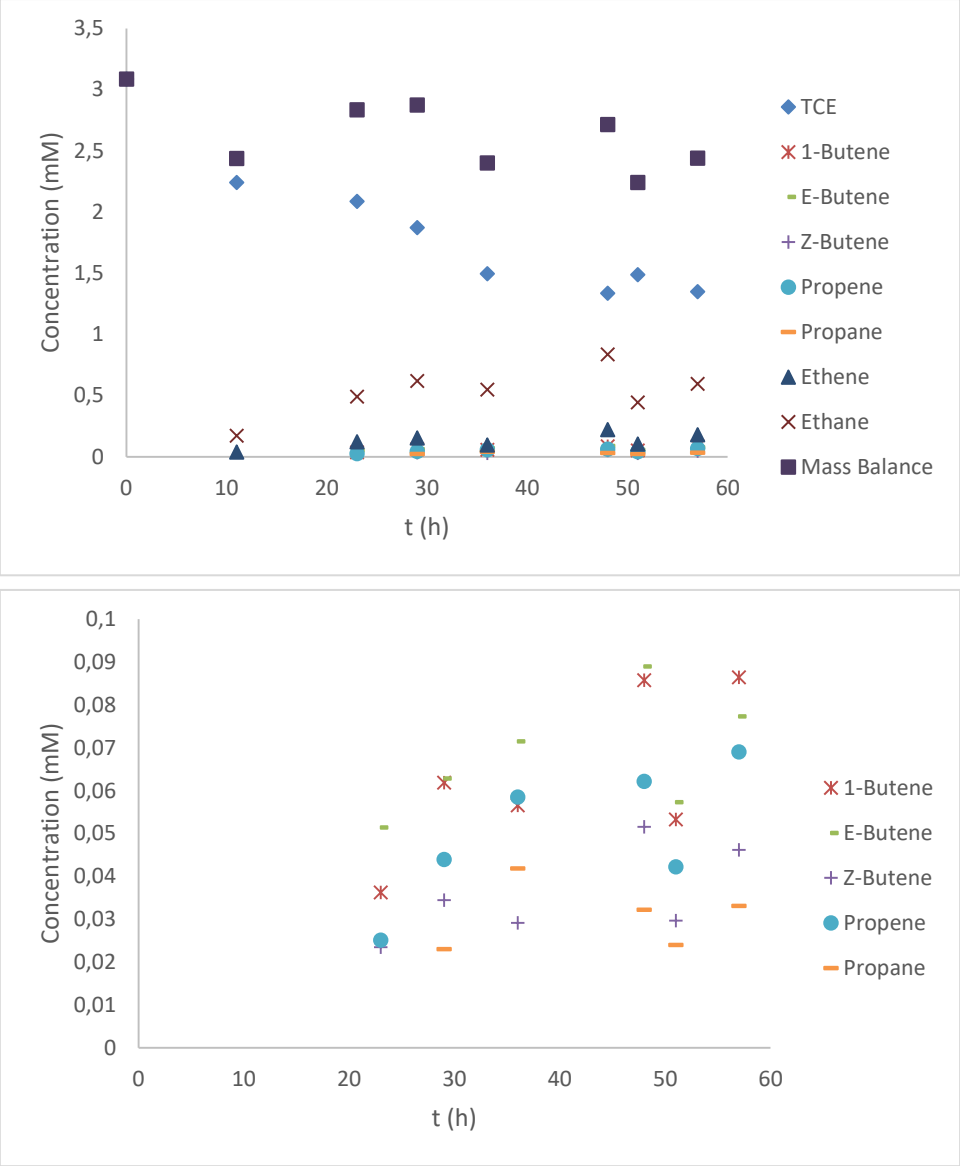

Figure 45: Degradation of TCE and its products over time toward Co/Fe reductant in isotope experiments (additional experiments) (A and B: Panel B is a zoom of Panel A without TCE, Ethene, Ethane and Mass Balance).

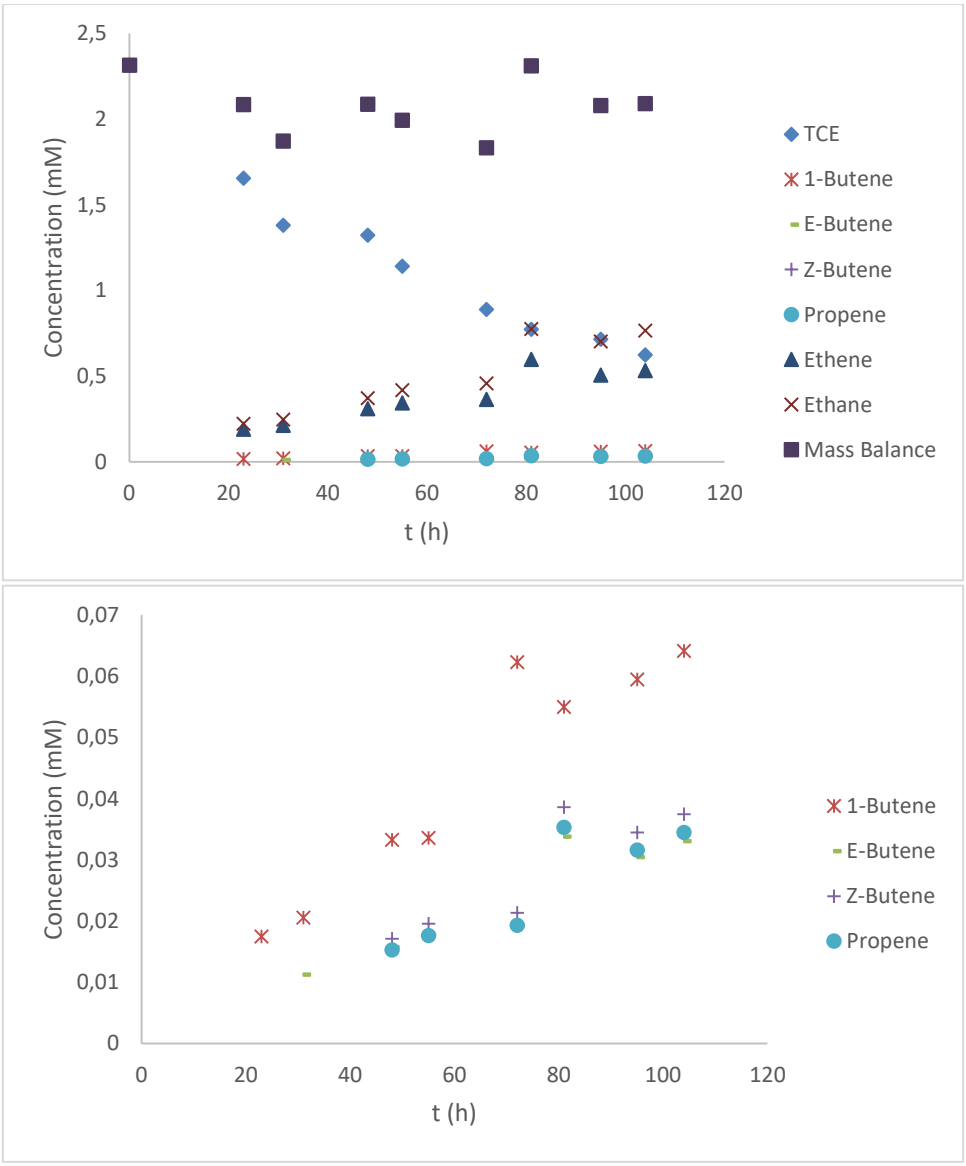

Figure 46: Degradation of TCE and its products over time in isotope experiments toward Cu/Fe reductant (reaction 1) (A and B: Panel B is a zoom of Panel A without TCE, Ethene, Ethane and Mass Balance).

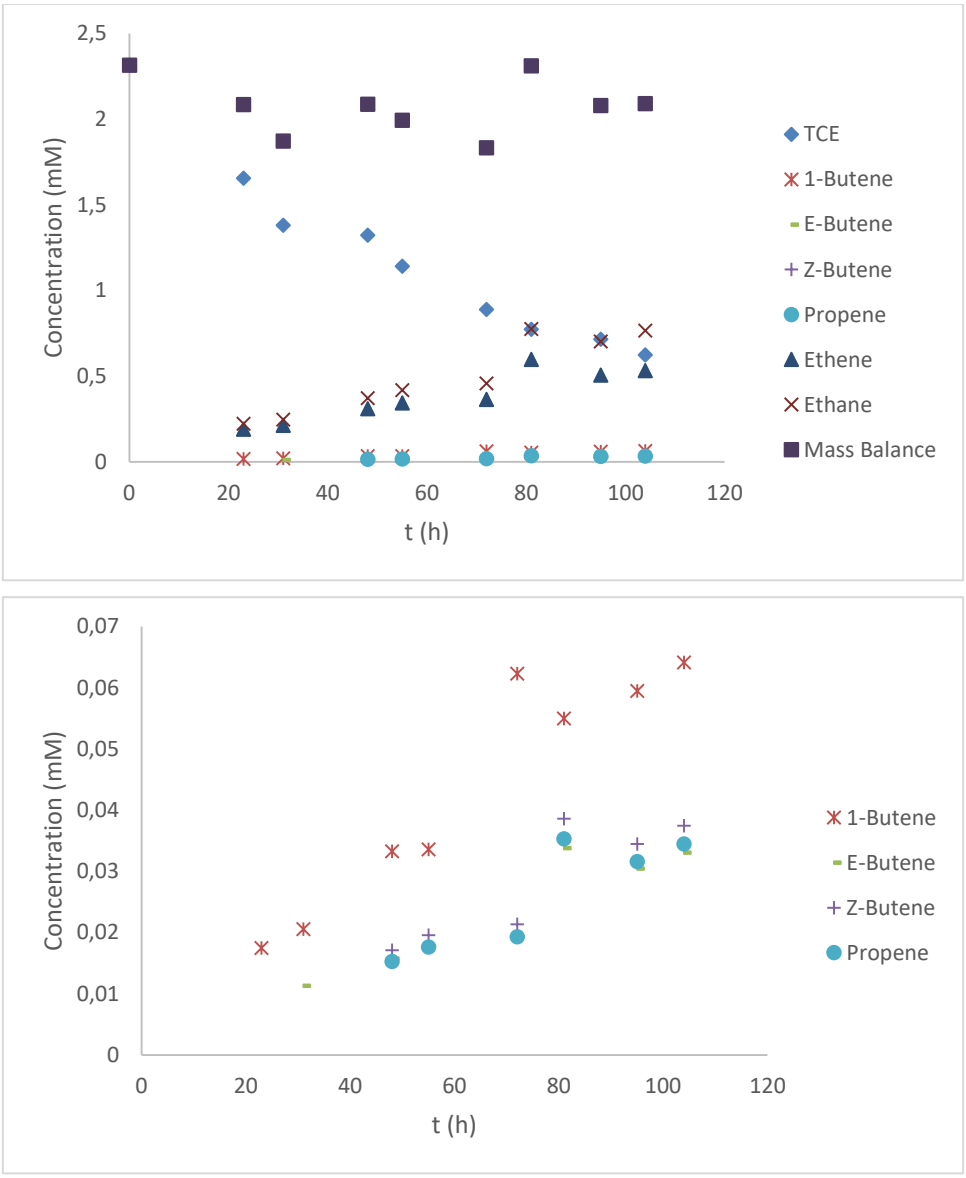

Figure 47: Degradation of TCE and its products over time in isotope experiments toward Cu/Fe reductant (reaction 2) (A and B: Panel B is a zoom of Panel A without TCE, Ethene, Ethane and Mass Balance).

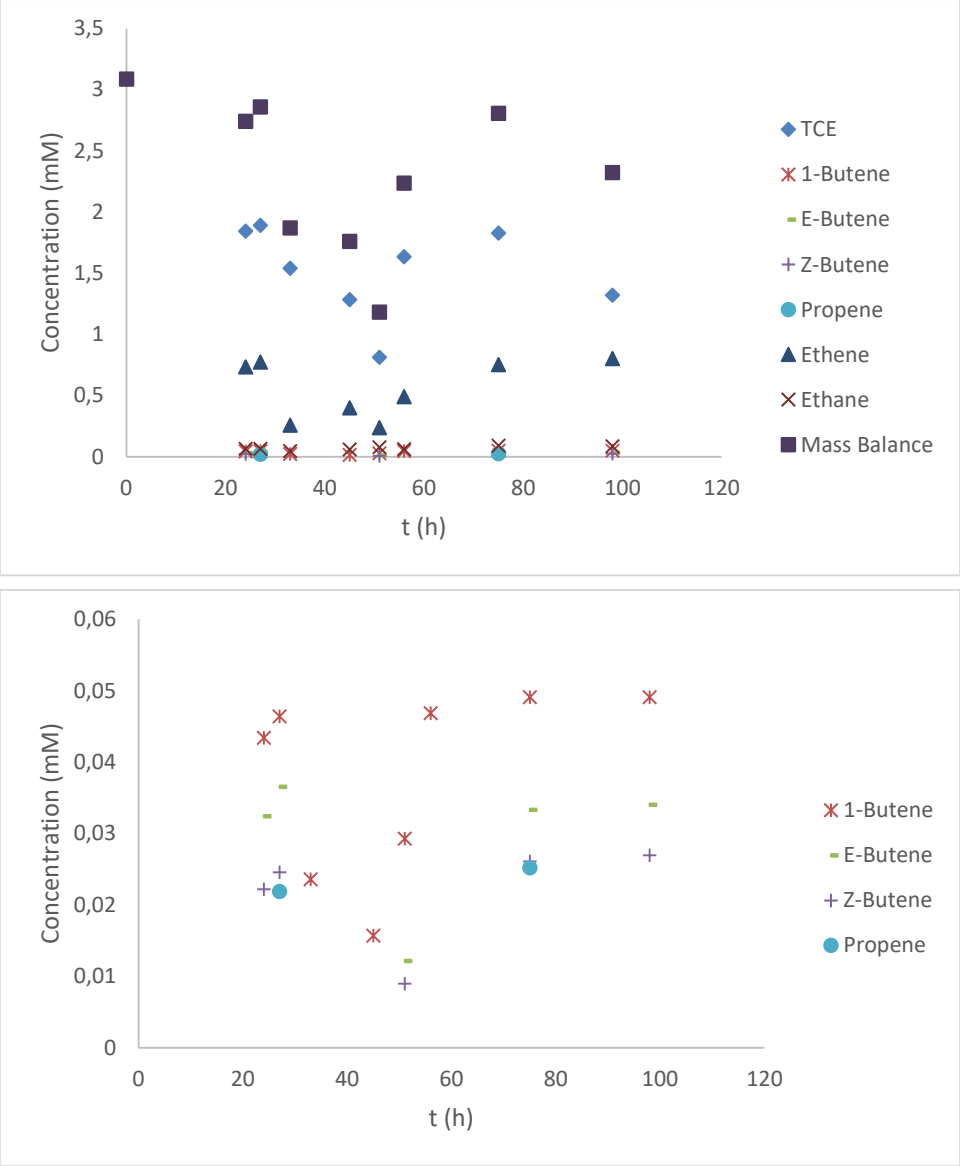

Figure 48: Degradation of TCE and its products over time toward Cu/Fe reductant in isotope experiments (additional experiments) (A and B: Panel B is a zoom of Panel A without TCE, Ethene, Ethane and Mass Balance).